A Biologically-Inspired Whole-Body Motion Control (WBMC) System for Humanoid Robots

Federico Lorenzo Moro

University of Genoa, Italy

Istituto Italiano di Tecnologia (IIT)

A thesis submitted for the degree of

Doctor of Philosophy (Ph.D.)

April 2014

Thesis Supervisors:

Dr. Nikos G. Tsagarakis
Senior Researcher
Department of Advanced Robotics
Istituto Italiano di Tecnologia (IIT)

Prof. Darwin G. Caldwell
Director
Department of Advanced Robotics
Istituto Italiano di Tecnologia (IIT)

To Maddalena, my soon wife-to-be

Acknowledgements

I would like to first thank all the people who helped and supported me during these three years, making the work presented in this dissertation possible. I am grateful for having had the big chance to meet and work with so many valuable researcher. From each of them I have learned something.

A huge thanks goes out to Michael Gienger and Ambarish Goswami. Since the beginning they showed me they believed in what I was doing, and stayed on my side through all the process. I always could feel their support and friendship. Many are the things I learned from them, and even more are those I still have to learn. If I can be satisfied with the results we got with the WBMC System it is mainly thanks to Michael and Ambarish.

Thanks to Nikos Tsagarakis and Darwin Caldwell for their guidance and advising, and for giving me the chance to work on a topic I proposed, always providing me everything I needed to do it at my best.

Thanks to Alessio Margan for his extraordinary work to optimize the C-code of the WBMC System: it is only thanks to him if the period of the control cycle is below $1ms$.

Thanks to the EPFL friends, Alexander Spröwitz, Alexandre Tuleu, Massimo Vespignani, and Auke Ijspeert, for accepting to work with us on the horse kMPs, and for helping a lot with the tests with the Cheetah-Cub robot.

Thanks to all the great people I met at the EU project meetings of AMARSI and WALK-MAN, particularly my friends from Bielefeld.

Thanks to Matteo Laffranchi, Jody Saglia, Nikos Karavas, Juan Alejandro Castaño, and Silvia Ivaldi for been good friends more than colleagues, and to all the people in the Humanoids & Human Centred Mechatronics Lab I was so lucky to work with in the last years.

Many thanks to Mum and Dad, and to all my family for always supporting me in any possible way, and to Maddalena, simply for always being on my side.

Abstract

In the past 20 years humanoid robots have made impressive improvements in the performance of non-trivial individual tasks such as walking, climbing stairs, manipulating objects etc., but when the scenario involves multiple complex actions and interactions, humans still far outperform even the most sophisticated robots. This inability to combine multiple diverse tasks to solve more complex problems limits the use of robots in real world applications. Whole-Body Control longs to fill this gap, exploiting the entire body capabilities to execute individual and simultaneous tasks.

The work presented in this dissertation aims to advance the fast evolving state-of-the-art in Whole-Body Control, and to achieve this goal two main research directions were investigated. Firstly, a thorough analysis of human motion was performed, in order to better understand how humans can successfully handle composite tasks. Based on the experience gained through this analysis, the lesson learned was applied to synthesize a novel attractor-based *Whole-Body Motion Control (WBMC)* System, that presents a further step towards having robots be capable of operating in the real world.

The analysis of human motion led to the identification of the so-called *kinematic Motion Primitives (kMPs)* for both periodic and discrete movements. The kMPs are defined as invariant waveforms underlying human motion, and can combine to produce more complex movements that simultaneously achieve both discrete and periodic tasks.

The periodic kMPs were employed to generate by reconstruction a human-like walking for COMAN, the COmpliant huMANoid robot. The stable, dynamic, kMPs-based walking gait was then scaled in frequency, and it will be shown that "walking in the resonance" can be beneficial in terms

of energy efficiency (15% of the energy required to track the kMPs-based trajectories is provided by the springs).

The work on the kMPs was further extended to quadrupeds, with the identification of horse kMPs that describe walking, trotting, and galloping gaits. Horse-like trajectories for each of the three gaits were generated and applied to Cheetah-Cub, a small-size quadruped robot. A gait transition strategy was also proposed and successfully tested on the robot.

The attractor-based Whole-Body Motion Control (WBMC) system was developed based on two specific features arising from the experience gained with the kMPs: *simplicity* and *modularity*.

The proposed, novel WBMC System combines several unique concepts. Firstly, a computationally efficient gravity compensation algorithm for floating-base systems was derived. Secondly, a novel balancing approach was proposed, which exploits a set of fundamental physical principles from rigid multi-body dynamics, such as the overall centroidal linear and angular momentum, the joint momentum, which is a quantity that had been rarely used to control humanoid robots, as well as a minimum effort formulation. Thirdly, a set of *attractors* was used to implement both balance and movement features such as to avoid joint limits or to create end-effector movements. Superposing several of these attractors allows the generation of complex whole-body movements in order to perform different tasks simultaneously. The modular structure of the proposed control system easily allows extensions.

The presented concepts have been validated both in simulations, and on the 29-dofs compliant torque-controlled humanoid robot COMAN, and the WBMC has proven robust to the unavoidable model errors.

Contents

List of Figures

List of Tables

1

Introduction

With growing research interest in humanoid robotics, robots have become increasingly proficient in performing many different, non-trivial tasks, such as running, jumping, climbing stairs, and manipulating objects. In most cases, however, each of these tasks is addressed individually, and this imposes a fundamental limitation on the use of robots in the real world. While humans may occasionally be outperformed by robots in a single task, they are vastly more capable of adapting and combining behaviors to solve multiple different tasks. This flexibility allows humans to generalize their knowledge, and to successfully perform tasks that they have never explicitly faced before. This also opens the door for simultaneous execution of multiple tasks.

1.1 Objectives and Motivation

To address these constraints, Whole-Body Control Systems have been proposed as a promising research direction. They represent a wide range of complex movement skills in the form of low-dimensional task descriptors which are projected on to the robot's

actuators, thereby exploiting the full capabilities of the entire body.

The work presented in this thesis aims to contribute by reducing the gap that still divides robots from humans when achieving whole-body, simultaneous, complex tasks. To achieve this goal, two research directions were investigated, one ideally sequencial to the other, and both finalized to the same ultimate objective:

- First, a thorough analysis of human motion was performed, to understand better how humans can successfully handle composite tasks that, possibly, they have never explicitly met before. This research lead to the identification of the so-called *kinematic Motion Primitives (kMPs)*.
- Based on the experience of this analysis, the lesson learned was applied to synthesize a novel attractor-based *Whole-Body Motion Control (WBMC)* System, that may present a further step towards having robots capable of operating in the real world.

The work on the kMPs led to satisfactory results, that served not only as a inspiration for a more thorough development of a WBMC System, but also allowed a direct application in generating human-like walking for the COMAN robot, and the extensions that followed.
The attractor-based WBMC System was developed based in particular on two features arising from the experience with the kMPs:

- *simplicity:* few, easy, very generic rules that are sufficient to perform any task
- *modularity:* a scalable, modular structure formed by unitary stand-alone modules

The topics of the research described in this dissertation still present several open

questions, and this made it possible to actively contribute to progress the state-of-the-art.

1.2 Contributions

The main contributions of this dissertation are the following:

- the kinematic Motion Primitives (kMPs), a set of invariant waveforms underlying human motion, were identified for both periodic and discrete motions. It was shown that periodic kMPs and discrete kMPs can combine to produce more complex motions that are a combination of discrete and periodic movements;
- the kMPs of periodic motions were used to generate a human-like gait that was tested on the COMAN robot. COMAN could perform a valid, stable, dynamic walk, with knees straightening to within 5° of straight;
- the kMPs-based trajectories were scaled in frequency to vary in a range from 0.5Hz to 1.25Hz. It was shown that when the robot "walks in resonance" (i.e., the gait frequency is close to one of the main resonance frequencies of the mechanism) the springs contribute about 15% of the work required to track the reference trajectories, by storing and releasing elastic energy;
- the work on the kMPs was further extended to quadrupeds, with the identification of horse kMPs that describe walk, trot, and gallop gaits. Horse-like trajectories for each of the three gaits were generated and applied to a small-size quadruped robot. A gait transition strategy was also proposed and successfully tested on the robot;

- a complete attractor-based Whole-Body Motion Control (WBMC) system was developed, where the attractors are defined as "atomic control modules that affect the state of the robot driving it towards a more preferred one", and where each controlled task is associated with an attractor;
- a computationally efficient gravity compensation model for floating-base systems was derived;
- inspired by a basic definition of equilibrium, the balance of the robot was guaranteed by controlling the effort of the robot, joint momentum, and the linear and angular momenta about its CoM;
- the proposed approach was successfully validated both in simulation and with a real torque-controlled robot, COMAN.

1.2.1 Related Publications

The following is a list of published works that are related to the topics presented in this dissertation:

2013 Journal Papers

Moro et al [2013c]

F.L. Moro, N.G. Tsagarakis, D.G. Caldwell

"Walking in the Resonance with the COMAN Robot with Trajectories based on Human Kinematic Motion Primitives (kMPs)"

Autonomous Robots

Moro et al [2013b]

F.L. Moro, A. Spröwitz, A. Tuleu, M. Vespignani, N.G. Tsagarakis, A.J. Ijspeert, D.G. Caldwell

"Horse-Like Walking, Trotting and Galloping derived from Kinematic Motion Primitives (kMPs) and their Application to Walk/Trot Transitions in a Compliant Quadruped Robot"

Biological Cybernetics, 107(3), pp. 309-320

Video: http://www.youtube.com/watch?v=zJF_-2Rbaxo

Conference Papers

Moro et al [2013a]

F.L. Moro, M. Gienger, A. Goswami, N.G. Tsagarakis, D.G. Caldwell

"An Attractor-based Whole-Body Motion Control (WBMC) System for Humanoid Robots"

IEEE-RAS International Conference on Humanoid Robots (Humanoids), Atlanta, Georgia, USA

Video: http://www.youtube.com/watch?v=MxFuXWzi6lg

2012

Journal Papers

Moro et al [2012b]

F.L. Moro, N.G. Tsagarakis, D.G. Caldwell

"On the kinematic Motion Primitives (kMPs) - theory and application"

Frontiers in Neurorobotics, 6(10), pp. 1-18

Conference Papers

Moro et al [2012c]

F.L. Moro, N.G. Tsagarakis, D.G. Caldwell

"The kinematic Motion Primitives (kMPs) of periodic motions, discrete motions, and motions that are a combination of discrete and periodic movements"

Cognitive Neuroscience Robotics (CNR) Workshop at the IEEE/RSJ International Conference on Intelligent Robots and Systems (IROS), Vilamoura, Algarve, Portugal

Moro et al [2012a]

F.L. Moro, N.G. Tsagarakis, D.G. Caldwell

"Efficient Human-Like Walking for the COmpliant huMANoid COMAN based on Kinematic Motion Primitives (kMPs)"

IEEE International Conference on Robotics and Automation (ICRA), Saint Paul, Minnesota, USA

2011

Conference Papers

Moro et al [2011]

F.L. Moro, N.G. Tsagarakis, D.G. Caldwell

"A Human-like Walking for the Compliant Humanoid COMAN based on CoM Trajectory Reconstruction from Kinematic Motion Primitives"

IEEE-RAS International Conference on Humanoid Robots (Humanoids), Bled, Slovenia

Video: http://www.youtube.com/watch?v=bnlCAZLhHz0

1.3 Thesis Outline

The organization of this dissertation is as follows. Chapter 2 reports on the state-of-the-art of both Motor Control in humans and animals, and Whole-Body Control of humanoid robots. The COMAN robot is also presented. The work related to the kinematic Motion Primitives (kMPs) is then described in Chapter 3, with all its research extensions, while Chapter 4 describes the implementation of the proposed attractor-based Whole-Body Motion Control (WBMC) System. A discussion follows in Chapter 5, and some final remarks can be found in Chapter 6.

2

Background and Related Work

The nature of the work presented in this dissertation is intrinsically interdisciplinary. It starts from the analysis of biological systems (humans and animals), touching disciplines like neuroscience and biology, to develop a motion control system for robots. This Chapter presents a survey of related works in the literature, and for convenience is divided in three sections. First, an analysis of the state-of-the-art in Motor Control is presented in Section 2.1. Following, Section 2.2 describes the fast evolving research area of Whole-Body Control, with some notes on balancing. Finally, Section 2.3 presents COMAN, the COmpliant huMANoid that was used as experimental platform for testing the proposed Whole-Body Motion Control (WBMC) System.

2.1 Motor Control in Humans and Animals

Humans are capable of performing an impressive variety of motions including locomotion, manipulation, and coordination between simultaneous locomotion with manipulation, with the control of these motions not being trivial. The way this complexity is

handled is still an open problem that researchers on Motor Control investigate.

In the early 20th century Brown proposed the theory of Central Pattern Generators (CPG) [Brown, 1911, 1912] as a possible interpretation: it was hypothesized that open-loop signals are produced in the spinal cord and sent to the limbs to produce motion. A first experimental validation was provided by Wilson [1961] with experiments on a locust in flight. Since that time, evidence has arisen for the presence of CPG in vertebrate animals. Lampreys, particularly, have been extensively studied to investigate the presence of CPG [Ayers et al, 1983]. Further studies extended this research to mammalians [Dimitrijevic et al, 1998; Kiehn and Butt, 2003].

Related to CPG is the research that led to the identification of *primitives* as the basis of human/animal motion. Among the many works in this field are Tresch et al [1999]; Mussa-Ivaldi and Bizzi [2000]; D'Avella et al [2003]; Poggio and Bizzi [2004]; Ivanenko et al [2004, 2005]; Bizzi et al [2008]; Lacquaniti et al [2012], where Motor Primitives were extracted from EMG signals. Dominici et al [2011] showed that these primitive patterns are present even in new born babies, and remain unvaried through development until adulthood. Motor Primitives represent evidence of an underlying CPG reflected on to the muscle level.

Other related works are Santello et al [1998], that shows how to reduce the complexity of the grasping motion of a human hand by identifying a set of synergies, and Hollands et al [2007], that applied a Principal Component Analysis (PCA) to the Cartesian trajectories of tracked points on the body of subjects performing a dancing motion.

CPG and primitives were traditionally associated with cyclic motions only [Delcomyn, 1980; Grillner, 1985; Marder and Bucher, 2001]. Valuable researches on discrete motions include Soechting and Lacquaniti [1981]; Hollerbach and Flash [1982]; Atke-

son and Hollerbach [1985]; D'Avella and Lacquaniti [2013], that studied hand reaching movements. The works of Grillner [2006]; Ronsse et al [2009] extended CPG to include both periodic and discrete movements. In the work of Schaal et al [2004], Van Mourik and Beek [2004], Hogan and Sternad [2007], Sternad [2008], Dégallier Rochat and Ijspeert [2010], and Dégallier Rochat et al [2011] it is possible to find important contributions to the on-going discussions around the possibility of describing both periodic and discrete motions by means of a unified theory.

An alternative interpretation comprising both discrete and periodic movements was proposed by Giszter et al [1993]. In this case primitives are not represented as signals, but as force fields. Experiments on frogs validated this theory.

The outcomes of all these brilliant works of analysis have several potential applications. They can be useful in the field of neuromotor rehabilitation, performance enhancement for athletes, or in the reproduction of natural behaviors in artificial systems, i.e., robots. Prominent examples of biologically-inspired control systems for robots include Collins and Richmond [1994]; Fukuoka et al [1999, 2003]; Billard and Ijspeert [2000]; Fujii et al [2002]; Ijspeert et al [2002]; Witte et al [2003]; Ishii et al [2004]; Son et al [2006]; Cappelletto et al [2006, 2007]; Degallier et al [2008]; Righetti and Ijspeert [2008]; Rutishauser et al [2008]; Liu et al [2009]; Kulic et al [2012]; Sugimoto et al [2012]. A comprehensive overview of this class of methods can be found in Schaal [2007]; Ijspeert [2008]; Dégallier Rochat and Ijspeert [2010].

Mimicry is considered by many in the robotics community as a way to reduce the gap between the performance of robots and the humans/animals they take inspiration from, both for hardware/design, and software/control.

2.2 Whole-Body Control of Humanoid Robots

The literature in this area is vast, and two main directions have emerged. *Inverse kinematics* concepts utilize kinematic redundancy resolution [Nakamura, 1991]; [Kajita et al, 2003b]; [Gienger et al, 2005, 2008, 2010]; [Toussaint et al, 2007], and are particularly popular due to their compatibility with velocity-controlled robots. More recently, torque-controlled humanoid robots have become available [Stephens and Atkeson, 2010]; [Moro et al, 2011]; [Ott et al, 2012]; [Herzog et al, 2013]. Control concepts based on various *inverse dynamics* formulations allow to implement whole-body controllers utilizing the dynamic equations of motion. A prominent example is the so-called operational space control [Khatib, 1987], that was extended to control the whole-body of humanoid robots and tested in simulation [Sentis and Khatib, 2005, 2006, 2010]; [Sentis, 2007, 2010]. An excellent survey on such methods is given in Peters et al [2008]. The authors of Righetti et al [2011]; Mistry and Righetti [2011]; Saab et al [2013] have further extended this formulation proposing improved contact models. A comprehensive comparative analysis of the solutions adopted can be found in Del Prete [2013]. Other brilliant examples of Whole-Body Control solutions have been recently presented by Berenson et al [2009]; Lengagne et al [2013].

More recently, whole-body motion concepts from the computer graphics domain have emerged. Other than in inverse dynamic formulations, these methods represent unilateral constraints such as the contact and friction properties explicitly, and make use of quadratic programming techniques to solve for the joint torques. While they have been applied to problems in the computer graphics domain [Abe et al, 2007]; [Wensing and Orin, 2013], the high computational demands make it still hard to apply them to real-time control systems.

Humanoids, and more in general legged robots, differ from industrial robots in the fact they do not present a fixed base. This on the one hand represents their main strength, as it guarantees a potentially infinite working space, on the other hand it introduces the complex problem of balancing. For this reason, one of the most important decisions to take when designing a Whole-Body Control is to define how to guarantee a stable balance.

The most widely used criterion to evaluate the dynamic stability of a robot is to verify the location of the projection of the Zero-Moment Point (ZMP) Vukobratovic and Borovac [2004] on the ground plane. The stability area is delimited by the feet in contact with the ground. Among the many examples of robots driven by ZMP-based trajectories are Sheridan [1966]; Mitobe et al [2000]; Kagami et al [2002]; Kajita et al [2003a]; Nagasaka et al [2004]; Kajita et al [2006]; Morisawa et al [2007]; Kaynov et al [2009]; Sugihara [2009]. Other methods for legged locomotion based on ground references can be found in [Popovic et al, 2005].

Linear and angular momenta about the center of mass (CoM), i.e., the *centroidal momentum*, play a key role in balancing. Examples of momentum-based control systems are Kajita et al [2003b]; Goswami and Kallem [2004]; Ugurlu and Kawamura [2010]; Lee and Goswami [2012]; Wensing et al [2013]. A comprehensive theoretical study on the centroidal momentum has been recently presented by Orin et al [2013].

2.3 COMAN: the COmpliant huMANoid

Robots in the near future are supposed to be capable to operate in the real world. This includes dynamic environments, and interaction with humans. A common trend in robot design is to make use of compliant actuation elements [Brooks et al, 1998]; [Edsinger-

Gonzales and Weber, 2004]; [Torres-Jara, 2005]; [Iwata and Sugano, 2009]; [Grebenstein et al, 2011], mostly for safety reasons, but also for increased energy efficiency [Vanderborght et al, 2006]; [Jafari et al, 2011]. In Ugurlu et al [2012] it is shown that compliance can also be used to improve the performance of robots executing explosive motions.

The experimental platform used to validate the control system presented in this dissertation is one of the few humanoid robots with intrinsically compliant actuators, and because of this feature was named COmpliant huMANoid (COMAN).

COMAN, which is based on a prototype of the legs developed for the iCub robot [Tsagarakis et al, 2007a,b, 2011, 2013], is being developed within the AMARSI European project, which aims to achieve a qualitative jump toward rich motor behavior in robotic systems, rigorously following a systematic approach in which novel mechanical systems with passive compliance, control, and learning solutions will be integrated.

With regards to mechanical systems with passive compliance the goal is [Tsagarakis et al, 2011]:

- to reduce the distinction between plant and controller, that is typical in traditional control engineering, to fully exploit complex body properties,
- to simplify perception, control, and learning, and to explore how compliance can be exploited for safer human robot interaction, reduced energy consumption, simplified control, and faster and more aggressive learning.

2.3.1 A First Prototype of COMAN's Lower Body

A first prototype of the lower body of COMAN (15 dofs: 6 per leg, and 3 for the waist) was used for the experiments described in Chapter 3 (Figure 2.1(b)). Each leg has two

series elastic actuation (SEA) units, which are placed at the knee flexion and the ankle dorsiflexion joints (Figure 2.1(a)). The actuation structure used in COMAN is based on a compliant actuation unit developed in Tsagarakis et al [2009]. More details on the actuator will be provided in Section 2.3.3.

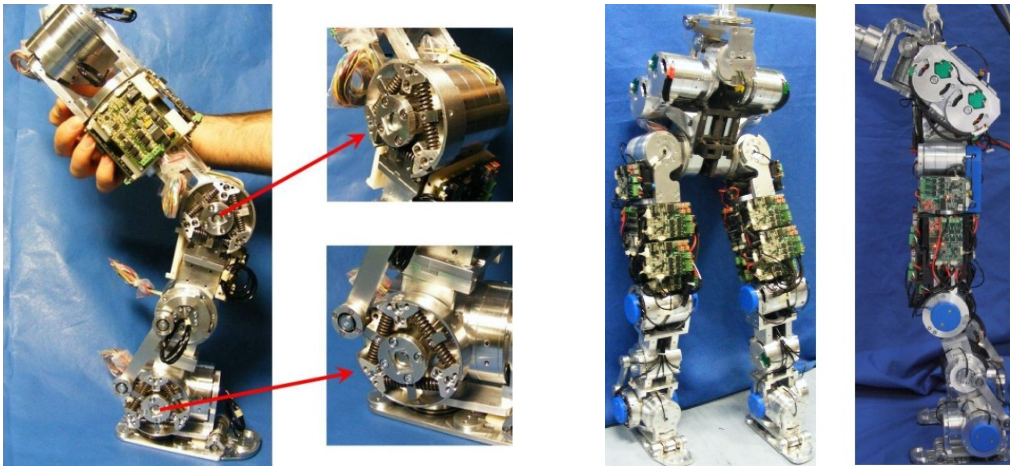

(a) (b)

Figure 2.1: a) The right leg of COMAN, with details of the compliant joints, and b) the prototype of the lower body of the COMAN robot that were used to experimentally test the gait generated by reconstruction from kMPs

2.3.2 The Full-Body COMAN Robot

This first prototype served as a basis to develop a new full-body version of COMAN. This is the version of COMAN currently in use at IIT, and it was employed as test platform for the experiments on the Whole-Body Motion Control (WBMC) System that will be described in Chapter 4.

The size of the COMAN humanoid robot approximates the dimensions of a 4 year old child (Figure 2.2). The height of COMAN from the foot to the center of the neck

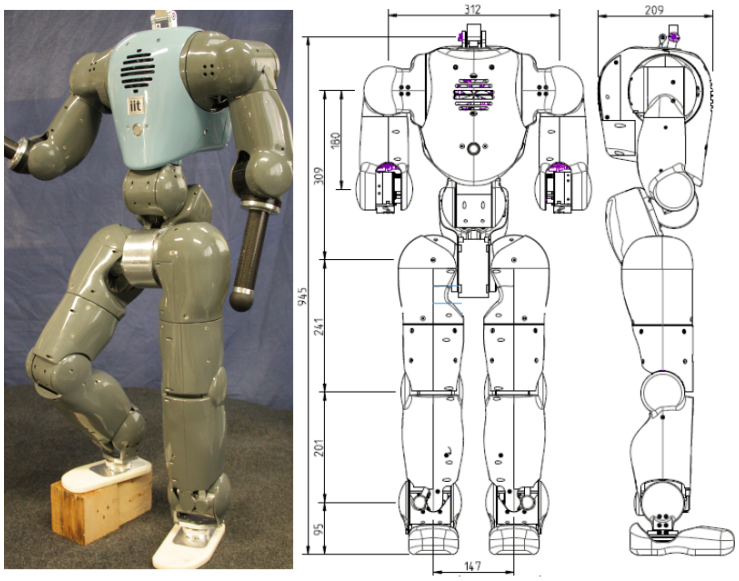

Figure 2.2: The full-body COmpliant huMANoid COMAN, all dimensions are in (mm)

is 945*mm*. The width and depth at the hip are 147*mm* and 110*mm*, respectively, and the distance between the centers of the shoulders is 312*mm*. The total weight of the robot is 31.2*kg* with the legs and the waist module weighting 18.5Kg, and the torso and the arms weighting 12.7Kg. COMAN body has 25 dofs in total. Each leg has 6 dofs: 3 dofs at the hip, 1 dof at the knee level, and 2 dofs at the ankle. For the trunk there is a 3 dofs waist, while each arm has currently 4 dofs: 3 dofs at the shoulder and 1 dof at the elbow level. Finally a 2 dofs neck provides the head pitch and roll motions. In addition to the previous generic specifications, and in order to permit the experimental scenarios of the AMARSI project, there was a need to incorporate compliance properties through a synergistic combination of both active and passive elasticity principles. Passive compliance based on series elastic actuation (SEA) was added to 14 of the 25 dofs, including all flexion/extension dofs of the legs, the flexion/extension of the shoulder and

elbow, and the shoulder abduction/adduction. Finally, the range of motion for the joints of COMAN were defined using human ergonomic data, and data from other successful humanoid platforms. Table 2.1 shows the range of motion of the joints of COMAN.

Table 2.1: Range of motion of the joints

Joint	Range of motion (°)
Hip Flexion/Extension	$+45, -110$
Hip Abduction/adduction	$+60, -25$
Thigh Rotation	$+50, -50$
Knee Flexion/Extension	$+110, -10$
Ankle Flexion/Extension	$+70, -50$
Ankle Inversion/Eversion	$+35, -35$
Ankle Twist	Not Implemented
Waist Pitch	$+50, -20$
Waist Roll	$+30, -30$
Waist Yaw	$+80, -80$
Shoulder Flexion/Extension	$+95, -195$
Shoulder Abduction/adduction	$+120, -18$
Upper Arm Rotation	$+90, -90$
Elbow Flexion/Extension	$+135, 0$

In the mechanical construction of COMAN particular attention was paid to optimize the integration, weight and modularity of the mechanical assembly. The high density of the integration is due to the mechanical implementation of a modular series elastic actuation unit. To achieve modularity, minimize dimensions, while achieving high rotary stiffness the SEA module developed in Tsagarakis et al [2009], and described in Section 2.3.3, was employed to actuate the joints of COMAN. The following subsections provide details on the realization of the COMAN body subsystems.

Leg Mechanics

COMAN leg has an anthropomorphic kinematic structure which is composed of the hip, the thigh with the knee joint, the calf with the ankle joint and the foot (Figure 2.3). The hip joint is constructed as a cantilever base structure with a pitch-roll-yaw configuration. The hip pitch (flexion/extension) motion is implemented using the SEA unit (peak torque of 55Nm) while the roll and yaw motion actuators are conventional stiff modules (Kollmorgen Brushless DC motor combined with a 100:1 Harmonic reduction drive giving a peak torque of 55Nm). The hip roll motor is placed below the hip center transmitting its torque to the hip roll using a four bar mechanism. The hip yaw motion is powered by an actuator enclosed inside the thigh structure. The knee joint is directly driven by a compliant actuation group (peak torque of 55Nm) at the center of the knee joint (Figure 2.3). The ankle roll motion is driven by a stiff actuation unit (peak torque of 55Nm)

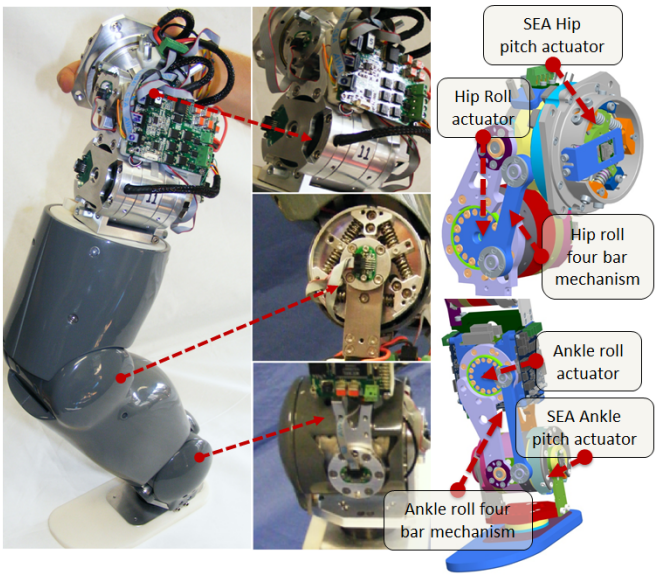

Figure 2.3: Mechanical assembly of a leg of COMAN

placed at the calf. Torque to the ankle roll motion is transferred through a four bar link transmission. The last dof which produces ankle flexion/extension uses a SEA actuator (peak torque of $55Nm$) located at the ankle center and directly coupled to the ankle pitch joint. Torque sensors developed specifically for the robot have been integrated in all joints of the leg to also permit regulation of the joint compliance through active control. In addition, custom-made 6 dofs force/torque sensors have been integrated below the ankle joint to measure the interaction forces between each foot and the ground.

Torso and Arm Mechanics

The torso of COMAN, in Figure 2.4, serves as a housing for the on-board processing and power units. The on-board processing unit is composed of an embedded dual core Pentium PC104 unit running at $2.5GHz$. The power unit includes the battery cells and the battery management system. The battery is a custom Lithium polymer battery with a gravimetric energy density of $180Wh/Kg$. The core of the torso is made in titanium alloy to give stiffness strength and low weight to this critical central structure. This structure also serves as the mounting support of the shoulder flexion dof of each arm and the neck module.

The current version of the arms of COMAN has 4 dofs consisting of a typical pitch-roll-yaw shoulder kinematic arrangement, and an elbow flexion/extension joint. The shoulder flexion/extension unit is housed inside the torso and is actuated by SEA unit (peak torque of $55Nm$). The shoulder abduction/adduction (roll) is also powered by a SEA unit with the same torque capacity and is placed at the center of the shoulder joint. The last shoulder dof (upper arm rotation) is actuated by a stiff actuator located inside the upper arm. Finally, the elbow joint is directly driven by a SEA unit (peak torque of

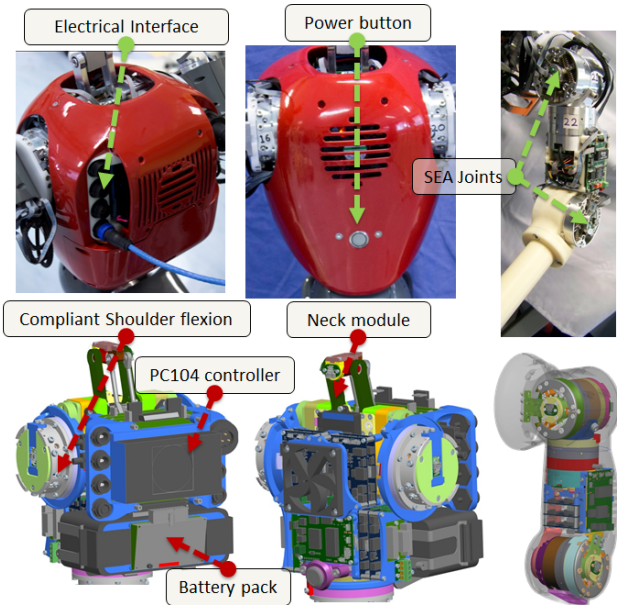

Figure 2.4: Mechanical assembly of torso and arm of COMAN

$55Nm$).

With regards to the actual fabrication of COMAN body, most of medium/highly stressed components (motor and bearing housing and link structures) were machined from Aluminum alloy 7075 (Ergal). Joint shafts and torque sensors were fabricated from Stainless steel 17-4PH, which delivers an excellent combination of good oxidation and corrosion resistance together with high strength. Body covers were made of ABS plastic using rapid prototyping fabrication.

2.3.3 Passive Compliant Actuation Unit

The mechanical realization of a soft actuation unit is based on the serial elastic actuator concept, but particular attention has been paid to satisfying the dimension and weight requirements of the robot.

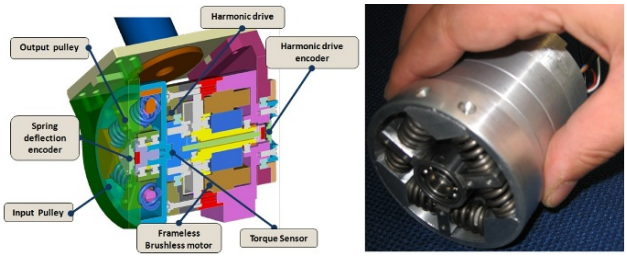

Figure 2.5: The compliant actuation unit of COMAN

The high integration density is due to the novel mechanical compliant module. To minimize dimensions while achieving high rotary stiffness a mechanical structure with a three spoke output component, a circular input pulley and six linear springs has been designed and fabricated. The circular component forms the input of the compliant module and is fixed to the output of the reduction drive. The three spoke element rotates on bearings with respect to the circular base and is coupled with it by means of six springs (Figure 2.5). The three spoke component forms the output of the compliant module and the mounting base of the output link. The six linear springs, when inserted in the arrangement shown in Figure 2.5, experience a pre-contraction equal to half of the maximum acceptable deflection. Deflections larger than the maximum allowable are prevented by mechanical pin based locks. Two 12 bit absolute position sensors are integrated within the actuation group measuring respectively the mechanical angle of the motor after the reduction drive, and the deflection angle of the compliant module. These sensors not only allow the monitoring of the link position but also allow the evaluation of the joint torque. Because of the compliance introduced it is possible to use the sensor measuring the compliant module deflection to estimate the torque.

Stiffness Model of the Compliance Module

In this subsection the stiffness model of the three spoke spring structure is presented. The deflection of the compliant module results in torques through compression of the spring elements along their main axis (Figure 2.6).

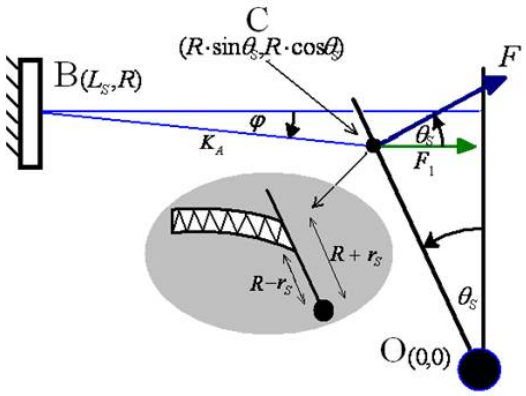

Figure 2.6: Compression of the spring as a result of the module deflection

Considering one of the antagonist linear spring pairs in Figure 2.7, the axial forces generated by each of the springs when the compliant three spoke module is deflected from the equilibrium position by an angle of θ_S is given by:

$$F_1 = K_A(x_p + x(\theta_S)), F_2 = K_A(x_p - x(\theta_S)) \tag{2.1}$$

where x_p is the spring pre-contraction and $x(\theta_S) = R \cdot sin(\theta_S)$ is the resulted deflection of the two springs along their main axis, K_A is the spring axial stiffness, and R the length of the spoke arm. The combined axial force applied in any spoke is therefore:

$$F = F_1 - F_2 = 2K_A \cdot sin(\theta_S) \tag{2.2}$$

The corresponding torque generated at the joint because of the axial forces of one antagonistic pair of springs is equal to:

$$T = FR \cdot cos(\theta_S) = 2K_A R^2 \cdot sin(\theta_S) \cdot cos(\theta_S) \tag{2.3}$$

So far we consider that the axial spring force is concentrated at one point. Considering that the spring has an external radius of r_S, Figure 2.6 shows that the axial spring compression is not equal for the whole surface area in contact with the spoke. The areas farthest from the center of rotation are subject to larger deflections creating higher forces.

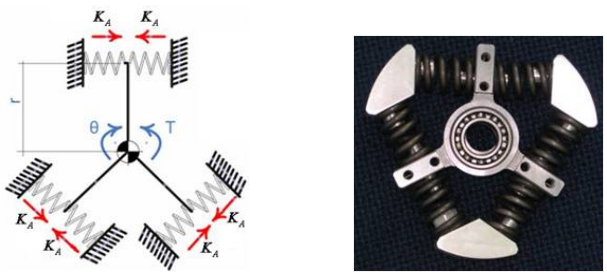

(a) (b)

Figure 2.7: The three spoke spring coupling arrangement

As a result, the torque generated by the axial deflection of the antagonistic pair of springs can be computed by:

$$\begin{aligned} T &= \frac{1}{2r_S} \int_{R-r_S}^{R+r_S} 2K_A R^2 \cdot sin(\theta_S) \cdot cos(\theta_S) dR = \\ &= 2K_A \left(R^2 + \frac{r_S^2}{3} \right) \cdot sin(\theta_S) \cdot cos(\theta_S) \end{aligned} \tag{2.4}$$

Thus, the combined torque at the joint considering the axial forces from all three

pairs is:

$$T_{Total} = 3T = 6K_A \left(R^2 + \frac{r_S^2}{3} \right) \cdot sin(\theta_S) \cdot cos(\theta_S) \tag{2.5}$$

By differentiating (6), the rotary stiffness of the three spoke module due to the axial deflection of the springs is:

$$K_S = \frac{dT_{Total}}{d\theta_S} = 6K_A \left(R^2 + \frac{r_S^2}{3} \right) cos(2\theta_S) \tag{2.6}$$

Figure 2.8(a) shows the theoretical stiffness of the module within the range of the deflection angle, for the first prototype module with the following parameters: $K_A = 62kN/m$, $R = 20.5mm$, $r_S = 6.3mm$.

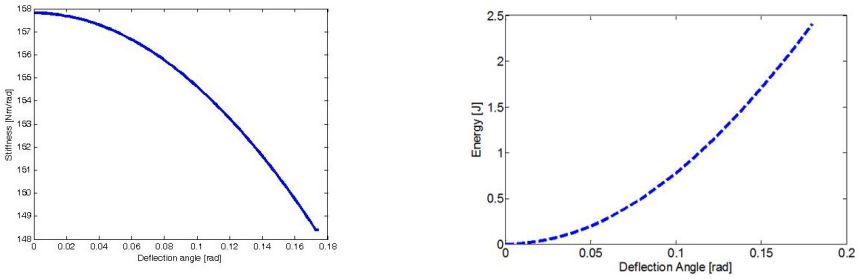

(a) (b)

Figure 2.8: (a) The stiffness profile of the compliant actuation unit, and (b) The energy stored by the springs at different deflection angles

It can be seen that the stiffness is slightly reduced as the deflection angle increases (notice that y axis does not start from zero).

Figure 2.8(b) shows the amount of energy stored by the springs at different deflections. A maximum of $2.5J$ can be stored by this prototype of the actuation unit. A more detailed description of the compliant joints of COMAN can be found in Tsagarakis et al [2009].

3

The kinematic Motion Primitives (kMPs)

This Chapter reports on the analysis performed on the data recorded from human motion, that led to the identification of the so-called *kinematic Motion Primitives*. These are defined as invariant waveforms, and it will be shown that a small set of kMPs is sufficient to explain a wide variety of complex coordinated motions, both periodic (e.g., walking and running), and discrete (e.g., reaching for a target with one hand). This work demonstrates that kMPs are independent of the subject and robust to disturbances. For locomotion five kMPs are identified. They describe different gaits of walking at different velocities and running, and gaits with constrained arm motion. The work is further developed to consider reaching, and two kMPs are identified for this class of motions. The kMPs extracted from both discrete and periodic motions can be combined to produce a new set of kMPs that describes the complex motion that is the simultaneous execution of the source basic motions (e.g., reaching for a target with one hand while walking). It

is interesting to notice that, from the kinematic point of view, the combined motion is neither the sequencing nor the simple superposition of the source motions.

The kMPs of locomotion were also used to generate by reconstruction a human-like walking gait that was successfully validated with the COMAN robot. The kMPs-based gait was the basis for a study with aim to verify that compliance can be exploited to improve energy efficiency. It will be shown that walking in the resonance allows to reduce energy consumption of about 15 %.

The work on human kMPs was then extended to quadrupedal locomotion. Horse kMPs were identified and used to generate horse-like gaits that were tested with the compliant EPFL Cheetah-Cub robot. The effects of frequency scaling were investigated, and a gait transition strategy was proposed and tested on the robot.

3.1 Experimental Setup

Five healthy male subjects, aged 25 - 28 years old, participated in the experiments. They differ in nationality, fitness level, and physical features (height: 170 - 185, weight: 60 - 90).

Movement data were collected using a Vicon MX series T motion capture system with 6 T10 infrared cameras of 1 million pixels resolution, operating at 250 Hz. 39 passive markers were attached to the subjects and used to fit a full body model. The Plug-in Gait, provided with the Vicon software, was used to derive the kinematics (i.e., 34 joint trajectories).

The supplemental equipment used for the experiments includes an electrical treadmill (Christopeit Runner Pro I, velocity range: 1 - 12 km/h), a foam ball (6.5 cm of diameter), that was used as a target for the reaching experiments, and a standard gym 5 kg load.

Figure 3.1 shows the set-up with one subject performing some of the gaits analyzed, wearing a black suit with the passive markers.

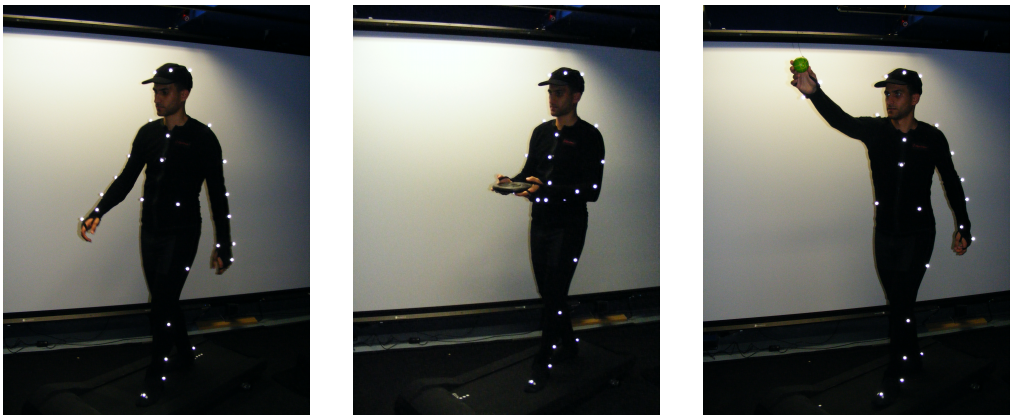

(a) (b) (c)

Figure 3.1: One of the subjects (a) walking on a treadmill with no constraints, (b) walking on a treadmill holding a 5 kg load, and (c) reaching for a ball with his right hand while walking on a treadmill

The set of motions recorded includes locomotion (periodic motion), reaching for a target object (discrete motion), and a combination of these two motions/tasks.

For what concerns the periodic motions, three different velocities were considered, two for walking, and one for running:

WLS Walking at Low-Speed - 2 km/h

WHS Walking at High-Speed - 4 km/h

RUN Running - 6 km/h

In addition to the unconstrained walking (hands free), the subjects were asked to walk/run while carrying an object which affected the movements of the arms. Again, three arm parameters were considered: unconstrained arms, holding an empty box, and holding a 5 kg load. These three conditions are designated as:

– Normal

–B Holding an empty box with two hands

–5 Holding a 5 kg load with two hands

In the notation adopted, for instance, WHSB means ”walking at high-speed while holding an empty box”. The combination of different speeds and constraints resulted in nine gait scenarios. For each of these gaits five trials per subject were recorded, where a trial consists of several steps taken by the subject at steady-state speed.

The above set-up allowed testing of the locomotion cycle which was considered as a period activity. Similar tests were carried out for the discrete motion of the arm. In these tests the subjects were asked to reach for a target (foam ball) with their hand. The position of the ball was fixed at the same height as the eyes of the subject, 20 cm to the left side with respect to the sagittal plane, at a reaching distance of approximately 50 cm. This made not symmetric the reaching of the ball with the left or the right hand.

BallUp_Left Reaching for the ball position with the left hand

BallUp_Right Reaching for the ball position with the right hand

Finally, the subjects were asked to perform a set of task motions that is a combination of the described periodic and discrete activities, i.e., reaching for the ball with either hand while walking on the treadmill (e.g., WLSBallUp_Left is ”reaching for the ball with the left hand while walking at a low-speed”).

From the trajectories recorded with the motion capture system for each of these scenarios, the kinematic Motion Primitives (kMPs) were extracted. In the next section the method adopted will be described.

3.2 Methodology

The output of the motion capture system is a set of 34 joint trajectories for each trial (7 for each arm: 3 for the shoulder, 1 for the elbow, 3 for the wrist; 7 for each leg: 3 for the hip, 1 for the knee, 3 for the ankle; 3 for the spine; 3 for the neck). Although efforts were taken to ensure that all the markers could be seen from the cameras, there were occasions when occlusions did occur. As expected this was more common in some test scenarios than others. There was some degradation of the quality of the data for fast motions (i.e., running), motions involving supporting objects that could occlude some of the markers (i.e., holding the box), or motions with self-occlusion (i.e., reaching for the ball). Data sets where there was a significant loss of tracking points were neglected and not considered in the analysis.

Among the many dimensionality reduction techniques available in the literature, the widely used Principal Component Analysis (PCA) was chosen and applied to the sets of trajectories to extract the kMPs. PCA is a linear transformation [Pearson, 1901], and is significantly simpler than most of the other dimensionality reduction methods. Even if in certain situations PCA was proven to be not powerful enough (e.g., EMG signals), it fits well in the case of kinematic data, which are less susceptible to noise. All 34 joint trajectories describing the motion of the subjects were used as the input to PCA to maximise the information available for analysis. It was decided to apply not any normalization among the joint trajectories: this guarantees that a higher importance is given to the joint with a wider displacement.

In the case of locomotion, as shown in Figure 3.2, the first five components explained about 99% of the cumulative variance. For the reaching tasks, and the combination of discrete and periodic motions (reaching while walking), two and four components were

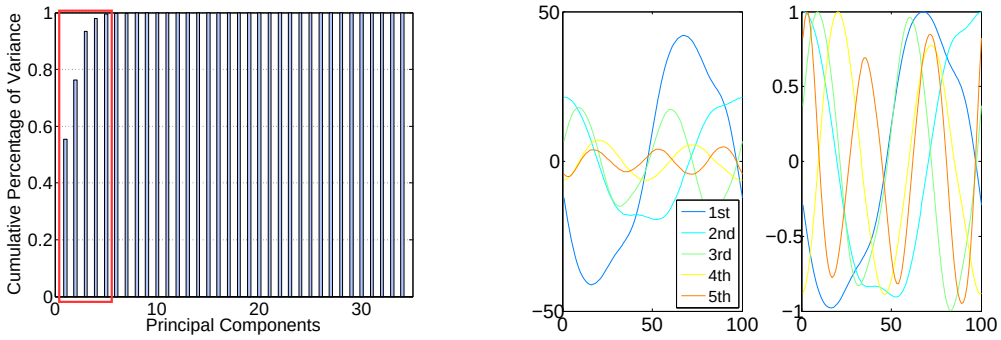

(a) (b)

Figure 3.2: (a) Cumulative percentage of variance accounted for by principal components, and (b) the first five components extracted from the gait of one of the subjects before and after normalization in amplitude

considered, respectively, for a cumulative variance explained of approximately 95%. The components considered were called *kinematic Motion Primitives (kMP)*, since it will be shown that they are invariant between the different subjects and for different gaits, and that they can describe in a lower dimensionality the complex motions of the subjects.

3.3 kMPs Analysis

The analysis performed aimed to investigate the effects on the extracted kMPs when the subject, the velocity and the constraints on the arms (in the case of locomotion), or the hand used (in the case of reaching) change. The combination of periodic and discrete motions was also studied.

To compare the kMPs extracted a visual representation of the kMPs is provided for each experiment, together with related statistical information. To quantify the similarity between two sets of kMPs the maximum cross-covariance between each corresponding

Table 3.1: Generic table schema for the report of statistics

	1^{st}	2^{nd}	...	i^{th}	Average	Sum	Weight
Var Gait1	VG_{1_1}	VG_{1_2}	...	VG_{1_i}	/	VG_{1_Sum}	/
Var Gait2	VG_{2_1}	VG_{2_2}	...	VG_{2_i}	/	VG_{2_Sum}	/
...	...	...	...	...	/	...	/
Var Gaitj	VG_{j_1}	VG_{j_2}	...	VG_{j_i}	/	VG_{j_Sum}	/
Var Aver	V_{Av_1}	V_{Av_2}	...	V_{Av_i}	/	V_{Av_Sum}	/
Xcov G1_G2	XG_{12_1}	XG_{12_2}	...	XG_{12_i}	XG_{12_Av}	/	XG_{12_W}
...	...	...	...	...	...	/	...
Xcov Gj_Gk	XG_{jk_1}	XG_{jk_2}	...	XG_{jk_i}	XG_{jk_Av}	/	XG_{jk_W}
Xcov Aver	X_{Av_1}	X_{Av_2}	...	X_{Av_i}	X_{Av_Av}	/	$\mathbf{X_{Av\_W}}$
Del G1_G2	DG_{12_1}	DG_{12_2}	...	DG_{12_i}	DG_{12_Av}	/	DG_{12_W}
...	...	...	...	...	...	/	...
Del Gj_Gk	DG_{jk_1}	DG_{jk_2}	...	DG_{jk_i}	DG_{jk_Av}	/	DG_{jk_W}
Del Aver	D_{Av_1}	D_{Av_2}	...	D_{Av_i}	D_{Av_Av}	/	$\mathbf{D_{Av\_W}}$

kMP (sliding in time) was calculated, and normalized so that the auto-covariance is 1. The delay between any two compared kMPs is also returned. This value indicates how much time-slip is needed in a signal to maximize the cross-covariance. Again this is normalized so that a slip of an entire cycle has a value of 1. An indication of the similarity (and delay) between the two entire sets is provided as the weighted average of the cross-covariance of the different kMPs. The weight used is the average of the corresponding variance explained by the kMPs compared.

Table 3.1 shows the statistical analysis performed, where VG_{j_i} is the variance of the joint trajectories of Gait j explained by the i^{th} kMP, XG_{jk_i} is the cross-covariance between the i^{th} kMP extracted from Gait j and the i^{th} kMP extracted from the Gait k.

Similarly, DG_{jk_i} is the delay between the i^{th} kMP extracted from the Gait j and the i^{th} kMP extracted from the Gait k.

Other cells in the table represent the sum or the average of the corresponding row/column, apart from those in the last column. Equations (3.1) and (3.2) indicate how XG_{jk_W} and X_{Av_W} are defined, respectively.

$$\begin{gathered}\forall j \in \{1 \dots m\}, \forall k \in \{j+1 \dots m\}, \\ XG_{jk\_W} = \left(\sum_{i=1}^{n} XG_{jk\_i} \cdot \frac{VG_{j\_i}+VG_{k\_i}}{2}\right) \cdot \frac{2}{VG_{j\_Sum}+VG_{k\_Sum}}\end{gathered} \tag{3.1}$$

$$X_{Av\_W} = \frac{\sum_{j=1}^{m}\sum_{j=j+1}^{m} XG_{jk\_W}}{\binom{m}{2}} = \frac{\sum_{i=1}^{n} X_{Av\_i} \cdot V_{Av\_i}}{V_{Av\_Sum}} \tag{3.2}$$

In the same way, Equations (3.3) and (3.4) define DG_{jk_W} and D_{Av_W}, respectively.

$$\begin{gathered}\forall j \in \{1 \dots m\}, \forall k \in \{j+1 \dots m\}, \\ DG_{jk\_W} = \left(\sum_{i=1}^{n} |DG_{jk\_i}| \cdot \frac{VG_{j\_i}+VG_{k\_i}}{2}\right) \cdot \frac{2}{VG_{j\_Sum}+VG_{k\_Sum}}\end{gathered} \tag{3.3}$$

$$D_{Av\_W} = \frac{\sum_{j=1}^{m}\sum_{j=j+1}^{m} DG_{jk\_W}}{\binom{m}{2}} = \frac{\sum_{i=1}^{n} D_{Av\_i} \cdot D_{Av\_i}}{D_{Av\_Sum}} \tag{3.4}$$

Intermediate results are omitted in tables from 3.2 to 3.10 for the sake of clarity. Also notice that the statistics reported are not intended to provide a statistical proof, rather they are a quantification of what is already evident from the visual representation.

3.3.1 Periodic Motions

In this subsection the kMPs extracted from different subjects, walking at different velocities or running, with different constraining conditions on the arms, are compared.

In particular, in the Experiment 1.1 the kMPs of five subjects performing a low-speed walking (WLS) are compared. Next, in the Experiment 1.2, the kMPs of WLS will be compared to those of WHS. This will be extended in the Experiment 1.3 to the kMPs of running. Finally, in the Experiment 1.4 different conditions of the arms motion are considered, and the kMPs extracted from a locomotion when the arms are constrained to hold a box or a 5 kg load are compared to those of free walking. For each of the gaits in each experiment, 34 joint trajectories are recorded over a sequence of four gait cycles. These data were normalized in time (from 0% to 100% of the gait cycle) and averaged, to reduce noise (Figure 3.3 shows the typical results of this procedure for the left knee trajectory).

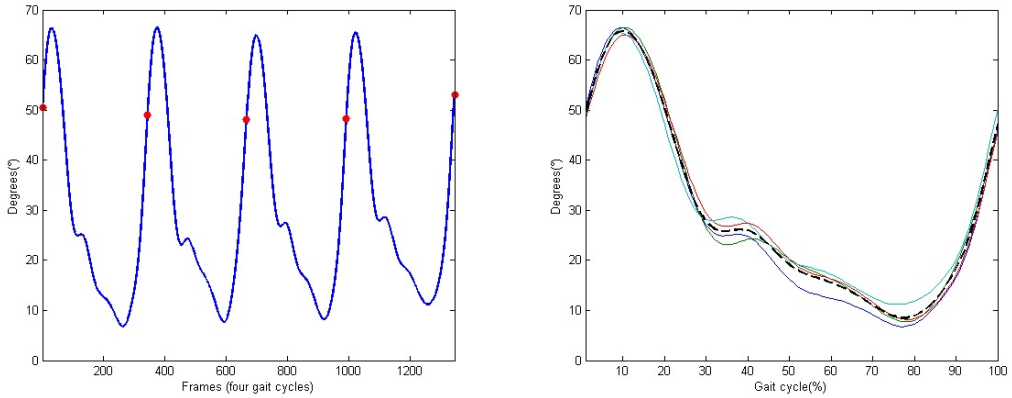

Figure 3.3: On the left is the original left knee angle trajectory (four complete gait cycles), while on the right an averaged and normalized in time left knee trajectory is derived (dotted line) from the trajectories of the four consecutive gait cycles.

Experiment 1.1: Comparison between different subjects

In this experiment the five subjects are performing a slow walk (WLS), and all the markers are always clearly observable by the cameras. This resulted in very low noise in the

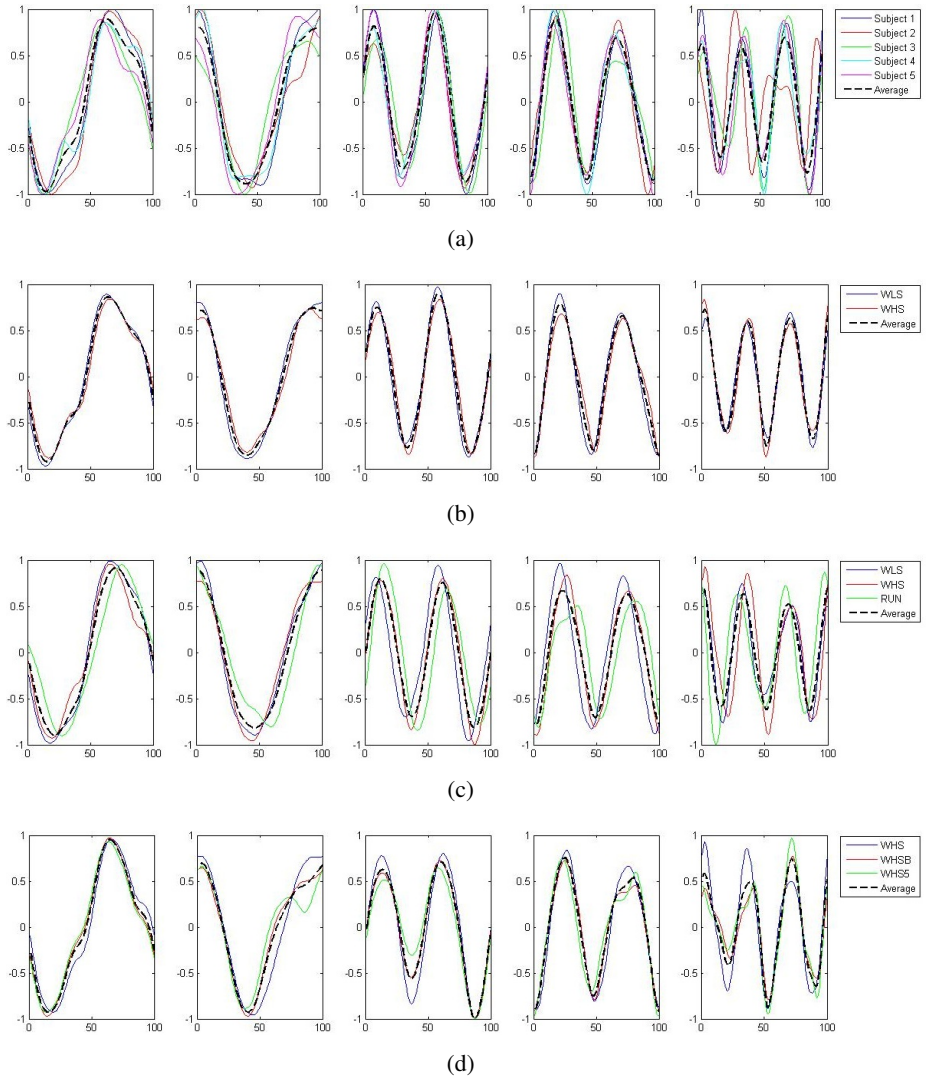

Figure 3.4: (a) The five kMPs extracted from five subjects walking at low velocity (2 km/h), (b) Comparison between the average kMPs of walking at low velocity (2 km/h) and walking at high velocity (4 km/h), (c) Comparison between the average kMPs of walking at low velocity (2 km/h), at high velocity (4 km/h), and running (6 km/h), (d) Comparison between the average kMPs of unconstrained walking at high velocity (4 km/h), and constrained (holding an empty box, and holding a 5 kg load) walking at high velocity (4 km/h)

joint trajectories recorded, and for this reason only one trial per subject was randomly selected and used in the analysis. Five kMPs for subject were extracted from these data, as described in Section 3.2. In Figure 3.4(a) the five kMPs are represented. The dotted line in each plot shows the average kMPs (among subjects). On the x-axis is the percentage of the period of the gait, from 0 to 100, while the values on the y-axis are between -1 and 1, indicating normalized kMPs. From these results it is clear that the first two kMPs have the same frequency as the gait, while the third and the fourth are coupled with the step (i.e., twice the gait frequency). The frequency of the fifth kMP, instead, is approximately three times the gait frequency.

Considering the general profile of the kMPs of the different subjects, it is already evident visually that the shape of the signals compared is almost identical, and the delay also is very close to zero. The statistical analysis performed, the results of which are reported in Table 3.2, gave a quantitative indication of the similarity between the different signals, confirming what was observed.

Table 3.2: Walking at low velocity kMPs (5 subjects)

	1st	2nd	3rd	4th	5th	Average	Sum	Weight
Var Av	0.5764	0.2368	0.1346	0.0308	0.0112	/	0.9899	/
Xcov	0.9648	0.9215	0.9706	0.9292	0.8506	0.9273	/	**0.9527**
Delay	0.0320	0.0150	0.0170	0.0080	0.0300	0.0204	/	**0.0249**

The first five kMPs, on average, explain the 58%, the 24%, the 13%, the 3%, and the 1% of variance, respectively, for a cumulative variance explained of about the 99%. The kMPs of each subject were compared to those of all the other subjects, to obtain the cross-covariances, and the delays. The averages of these values were calculated, and it was observed that the third kMP has the least variation, with a 97% similarity.

The overall similarity between the kMPs of different subjects walking at low speed was calculated as the weighted average of the values found for the single kMPs, using the average percentage of variance explained by that kMP as a weighting coefficient. This demonstrated a similarity between the kMPs of the different subjects of approximately 95%. The same method was used to evaluate the average delay, and it resulted to be about 2% of the gait cycle.

Experiment 1.2: Comparison between different walking velocities

What reported in the previous experiment was also verified for the five subjects walking at a high speed.

In this experiment the average kMPs of WLS are compared to the average kMPs of WHS (with data from five subjects). From Figure 3.4(b) it can be seen that the kMPs from gaits at different velocities are almost identical, with respect to both shape and phase. This means that the kMPs of walking, for the different subjects, are not affected by the walking speed. The results of the statistical analysis of this experiment are reported in Table 3.3.

Table 3.3: Walking at low and high velocity kMPs (5 subjects)

	1st	2nd	3rd	4th	5th	Average	Sum	Weight
Var Av	0.5397	0.2590	0.1486	0.0310	0.0119	/	0.9900	/
Xcov	0.9955	0.9826	0.9884	0.9520	0.9551	0.9747	/	**0.9894**
Delay	-0.0200	0	-0.0200	0	0	0.0080	/	**0.0139**

It can be noticed that the first kMP of WLS and WHS have a cross-covariance of more than the 99%, and that for the second and the third kMPs this value is between 98% and 99%. These three components together explain about the 95% of variance, and

this results in an overall weighted average of about the 99%.

Experiment 1.3: Comparison between walking and running

The third experiment is an extension of the previous: the kMPs of running (RUN) are compared to those of walking at a low speed (WLS) and at a high speed (WHS) (Figure 3.4(c)). The data from some of the subjects were more noisy than in the previous tests due to occlusions or slight movement of the markers caused by the stretching of the elastic suit worn by the subjects. To avoid having results corrupted by noise, the data from only three of the subjects, those whose data had the best quality, were used. The kMPs of the subjects performing the three gaits were averaged, and the resulting kMPs of WLS, WHS, and RUN were compared.

Table 3.4: Walking at low and high velocity and running kMPs (3 subjects)

	1st	2nd	3rd	4th	5th	Average	Sum	Weighted
Var Av	0.5294	0.2697	0.1535	0.0279	0.0104	/	0.9908	/
Xcov	0.9872	0.9305	0.9673	0.8545	0.8419	0.9163	/	**0.9635**
Delay	0.0433	0.0066	0.0533	0.0400	0.0367	0.0360	/	**0.0347**

A first observation is that the similarity between WLS and WHS, that in the previous experiment with five subjects was reported to be 99%, is now about 98% (Table 3.4). The 1% difference is believed to be caused by the reduction in the number of subjects itself. The noise in the data of every subject, and in the resulting kMPs, is reduced in the average kMPs as the number of subjects increases.

The comparison between the RUN kMPs and the WLS and WHS kMPs, considered one per time, is instead of the 95% and 96%, respectively. The average between these two values, and the one between WLS and WHS, represents the similarity between the

different locomotion gaits, and is more than 96%.

Experiment 1.4: Comparison between unconstrained and constrained walking

The final experiment into periodic motions considered a comparison between unconstrained walking, as explored in each of the previous experiments, and walking while holding an object with the two hands, which introduced a constraint on the ability to swing the arms (Figure 3.4(d)). Two cases were analyzed. In the first the subjects were asked to hold an empty box, which introduced a constraint on the motion, but negligible physical loading. In the second scenario the object was a 5 kg load, which not only constrained the motion of the arms, but also introduced a constant force due to gravity pushing the hands down. The goal of this test was to determine if the kinematics of the motion, analyzed by means of kMPs, was affected by constraints imposed with this holding of objects.

Table 3.5: Walking at high velocity unconstrained, holding a box, and holding a load (3 subjects)

	1st	2nd	3rd	4th	5th	Average	Sum	Weight
Var Av	0.5129	0.2697	0.1633	0.0336	0.0097	/	0.9893	/
Xcov	0.9925	0.9369	0.9545	0.9590	0.9022	0.9490	/	**0.9566**
Delay	0.0200	0	0.0067	0	0.0067	0.0067	/	**0.0116**

From the results reported in Table 3.5 it can be seen that the similarity between the gaits is high, and this means that the respective kMPs are not much affected by the constraints imposed. The first kMP in the three cases is almost identical: in the three comparisons the cross-covariance is always of about 99%. The average cross-correlation of the other kMPs slightly reduces, but it remains between the 90% of the fifth kMP and

the 96% of the fourth kMP.

The resulting overall similarity among the different gaits is more than 96%, indicating that the kMPs of locomotion remain invariant even if a constraint on the swing motion of the arms is imposed.

3.3.2 Discrete Motions

The second set of experiments was focused on the discrete motion of reaching for a target with the hand. The target was a foam ball with a diameter of 6.5 cm, suspended in front of the subject at the same height as the eyes of the subject. The ball was 20 cm to the left of the centerline, at a distance from the subject of about 50 cm. The subjects were asked to assume an initial pose (standing, arms by their sides), to reach for the target with one hand, and finally to move back to the initial position. The data collected in these experiments were affected by self-occlusion: when the subjects were asked to reach for the target with the hand, some of the markers placed on their trunk were occluded to the cameras by their own arm. For this reason the data coming from only two subjects, which were considered clean enough, were used in the analysis.

Both reaching with the left hand and reaching with the right hand were recorded (since the ball was not located in the sagittal plane of the subjects, their motion of reaching with the left and the right hand was not symmetric).

In the Experiment 2.1 the kMPs of the different subjects performing the reaching motion with the left hand will be compared. Next, similarly to what done for the periodic motions, in the Experiment 2.2 the kMPs of reaching with the left hand will be compared to those of reaching with the right hand.

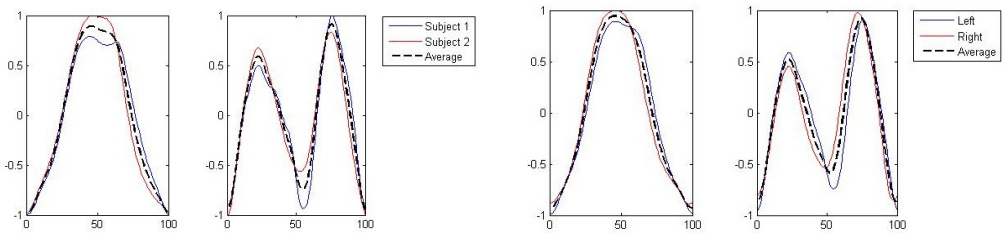

(a) (b)

Figure 3.5: (a) The two kMPs extracted from two subjects reaching for a target with the left hand, (b) Comparison between the average kMPs of reaching for a target with the left and the right hand

Experiment 2.1: Comparison between different subjects

In this experiment the subjects were asked to stand in a neutral initial position in front of the target as previously described, to reach for it with the left hand, and to move back to the initial position. No constraint on the timing to complete the motion was imposed.
In Figure 3.5(a) the two kMPs, that together explain on average the 97% of variance, are shown. The first of these kMP has a single peak, while in the second kMP two peaks are present: each peak takes approximately 50% of the total reaching time, and the first peak has an amplitude that is about 25% smaller than the amplitude of the second peak.

Table 3.6: Reaching a target with the left hand (2 subjects)

	1st	2nd	Average	Sum	Weight
Var Av	0.8201	0.1510	/	0.9711	/
Xcov	0.9662	0.9253	0.9457	/	**0.9598**
Delay	0	0	0	/	**0**

As reported in Table 3.6, the weighted average cross-covariance between the kMPs is about 96%, showing that the similarity between the reaching motion of the two subjects,

in terms of kMPs, is significant. It is also interesting to notice that in all cases there is no delay between the kMPs of the different subjects. This indicates that what stated on the periodic motions (described by five invariant kMPs) can also be extended to the discrete motions (described by two invariant kMPs).

Experiment 2.2: Comparison between reaching with the left and the right hand

Having demonstrated that the kMPs of different subjects performing the same discrete motion are closely related, two reaching motions that are slightly different were compared. The first set of kMPs came from the previous experiments, and describes the reaching motion with the left hand. The second is the set of kMPs that describe reaching with the right hand, and was extracted from the data of the same subjects. The kMPs extracted are reported in Figure 3.5(b).

Table 3.7: Reaching a target with the left and the right hand (2 subjects)

	1st	2nd	Average	Sum	Weight
Var Av	0.8326	0.1332	/	0.9658	/
Xcov	0.9693	0.8745	0.9219	/	**0.9562**
Delay	0	0.0100	0.0050	/	**0.0014**

Table 3.7 shows that the first kMP has a cross-covariance of about 97%, while in the second instance this value is about 87%. This results in a weighted average of almost 96%, with no noticeable delays between the kMPs. It is now reasonable to state that also the discrete motions can be described by means of a set of two invariant kMPs. It is interesting to notice that, although reaching with the left or the right hand is not symmetrical (the location of the target ball was not in the sagittal plane of the subject), this difference is not reflected in the extracted kMPs, which are once again the same.

3.3.3 Combination of Periodic and Discrete Movements

After having shown that both periodic and discrete motions can be described by a small set of invariant kMPs, in this last set of experiments the focus is on more complex motions that combine a periodic and a discrete basic task. The subjects were asked to perform the reaching motion described above (Experiment 2), while walking on a treadmill at a low speed (Experiment 1). The two subtasks were synchronous: the subjects were asked to complete the reaching task (both the motion to reach for the ball, and the motion back from the ball to the initial position) in a time that was approximately the same as the period of two steps, that is a full gait cycle. The subjects reported that this requirement was easy to satisfy: a motivation for this observation can be found in

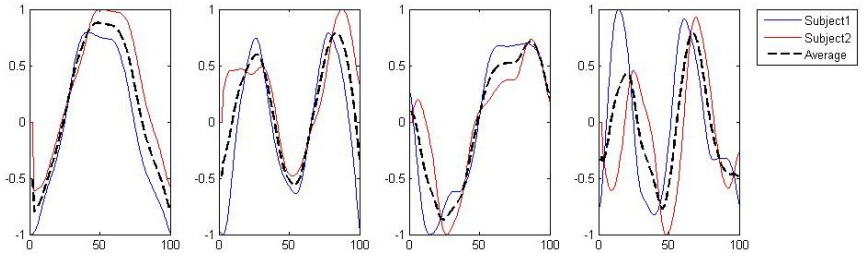

(a)

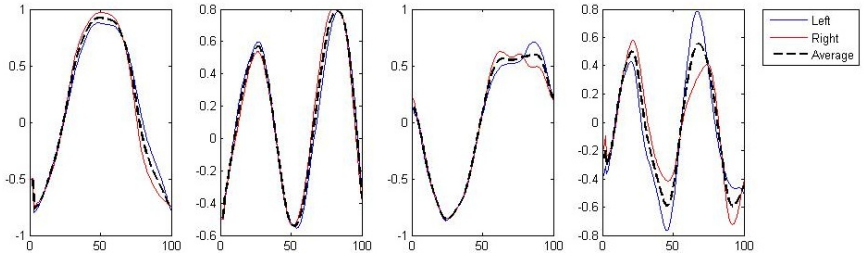

(b)

Figure 3.6: (a) The four kMPs extracted from the two subjects reaching for a target with the left hand while walking, (b) Comparison between the average kMPs of reaching for a target with the left and the right hand

Michaels and Bongers [1994], Sternad et al [2000], and De Rugy and Sternad [2003]. It is important to notice that the combination of tasks analyzed in this experiment is different from the analysis available in the literature: it is not a sequencing of tasks, and not even a simple superposition, since the swinging motion (coming from the walking) of the arm used for reaching is suppressed in the period of time when the subject is actually performing the reaching task.

Experiment 3.1: Comparison between different subjects

In the same way as it was in the Experiment 2.1 the subjects were asked to reach for the target ball with the left hand. Differently from the previous case, for these experiments the reaching task had to be accomplished while walking at low speed on the treadmill. The complex reaching while walking task was then a combination of the periodic motion WLS presented in the first set of experiments, and the discrete motion BallUpLeft from the second set of experiments. The kMPs extracted from the joint trajectories of the two subjects performing this composite task are reported in Figure 3.6(a).

Table 3.8: Reaching fora target with the left hand while walking (2 subjects)

	1st	2nd	3rd	4th	Average	Sum	Weight
Var Av	0.7770	0.0946	0.0720	0.0277	/	0.9689	/
Xcov	0.9347	0.6070	0.8971	0.8697	0.8271	/	**0.9004**
Delay	-0.0200	-0.0500	-0.0700	-0.0100	0.0375	/	**0.0264**

The first four kMPs together explain on average the 97% of variance. The overall weighted average cross-covariance is 90%, as reported in Table 3.8, and this proves that the motion of the two subjects, analyzed by means of the kMPs, has a good level of similarity.

Experiment 3.2: Comparison between reaching with the left and with the right hand while walking

In this experiment the average kMPs of reaching for the target with the left hand while walking on the treadmill at low speed (WLSBallUp_Left) are compared to the corresponding kMPs of reaching for the target with the right hand while walking on the treadmill at low speed (WLSBallUp_Right), as reported in Figure 3.6(b).

Table 3.9: Reaching for a target with the left and the right hand while walking (2 subjects)

	1st	2nd	3rd	4th	Average	Sum	Weight
Var Av	0.7837	0.0895	0.0677	0.0276	/	0.9672	/
Xcov	0.9827	0.9759	0.9862	0.8654	0.9526	/	**0.9803**
Delay	0	0	0	-0.0200	0.0050	/	**0.0006**

The first three kMPs are almost identical, with a cross-covariance of 98%, 98%, and 99%, respectively (Table 3.9). The overall weighted average is thus approximately 98%, while the delay approaches 0%. Also in this case, the motion for reaching with the left hand, and the motion for reaching with the right hand were not symmetrical, but this difference does not reflect on the corresponding kMPs extracted, that once again resulted to be the same.

Experiment 3.3: Comparison between reaching while walking and reaching and walking separately

This experiment was the most challenging among those in this analysis. What was compared, in fact, was not a set of kMPs from the same motion, but the kMPs of reaching while walking, with the kMPs of reaching and the kMPs of walking, separately. A cor-

respondence between the kMPs extracted from the reaching while walking motion, and some of the kMPs extracted from the two simpler motions was noticed. More specifically, the first and the second kMPs of WLSBallUp (blue line in the first and second graph, Figure 3.7) were very similar to the first and the second kMPs of BallUp (red line in the first and second graph, Figure 3.7), respectively. The third and the fourth kMPs of WLSBallUp (blue line in the third and fourth graph, Figure 3.7), instead, were very similar to the first and the fourth kMPs of WLS (red line in the third and fourth graph, Figure 3.7), respectively.

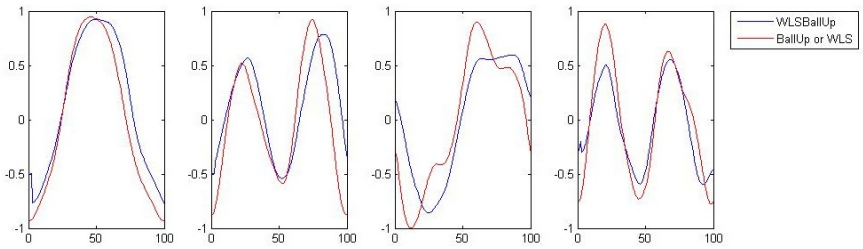

Figure 3.7: Comparison between the average kMPs of reaching for a target with the hand while walking (blue line) and the average kMPs of reaching (red line, first and second graph), and walking (red line, third and fourth graph)

From Table 3.10 it can be noticed that the cross-correlation between the kMPs is high: the maximum value observed is the one corresponding to the comparison between the first kMP of WLSBallUp and the first kMP of BallUp, which is 98%, while the minimum, which is for the comparison between the second kMP of WLSBallUp and the second kMP of BallUp, is 81%. The other two comparisons resulted in a cross-correlation of 95% and 93%, respectively, for an overall weighted average of about 96%. The weights used for the definition of this synthetic indicator of similarity, in this case, are the amount of variance explained by the single kMPs of the WLSBallUp only, since the second set of kMPs is a combination of the sets of kMPs of two different motions.

It can also be observed that the weighted average delay between the two sets of kMPs under comparison is less than 1% of the cycle period.

Table 3.10: Combination of the kMPs of walking and the kMPs of reaching (2 subjects)

	1st	2nd	3rd	4th	Average	Sum	Weight
WLS	/	/	1st kMP	4rd kMP	/	/	/
BallUp	1st kMP	2nd kMP	/	/	/	/	/
Var	0.7837	0.0895	0.0677	0.0276	/	0.9672	/
Xcov	0.9762	0.8085	0.9480	0.9339	0.9167	/	**0.9588**
Delay	0	0.0300	0.0700	0	0.0250	/	**0.0077**

The results achieved in this experiment show how the kMPs extracted from the periodic and the discrete motions can be combined to produce more complex motions that are a combination of the simpler source movements. The resultant complex motions guarantee the execution of the two tasks, one periodic and the other discrete, and can be described neither by the simple superposition, nor by the sequencing of the motions to perform the two tasks separately. The kMPs of this complex motion, instead, are a proper combination of the kMPs extracted from the two basic tasks.

These results allow certain conclusions to be drawn on how human motion control and coordination is performed: according to this study five kMPs can effectively describe the different periodic motions, while two kMPs can be responsible for synthesizing different discrete motions. A combination of kMPs of the periodic and discrete motions may be used to generate different complex motions, that simultaneously accomplish the periodic and discrete tasks.

3.4 Trajectories Reconstruction from kMPs

This section focuses on the synthesis of joint trajectories starting from the kMPs. This reconstruction is represented by:

$$\begin{bmatrix} q_1 \\ \vdots \\ q_i \end{bmatrix} = \begin{bmatrix} s_{1,1} & \dots & s_{1,j} \\ \vdots & \ddots & \vdots \\ s_{i,1} & \dots & s_{i,j} \end{bmatrix} \times \begin{bmatrix} P_1 \\ \vdots \\ P_j \end{bmatrix} + \begin{bmatrix} \overline{Z_1} \\ \vdots \\ \overline{Z_i} \end{bmatrix} \tag{3.5}$$

where $[q_1 \dots q_i] \in \mathbb{R}^i$, with $i = 34$, representing the joint trajectories vector, $[P_1 \dots P_j] \in \mathbb{R}^j$, with j equal to the number of kMPs, being the kMPs vector, and $[\overline{Z_1} \dots \overline{Z_i}] \in \mathbb{R}^i$, with $i = 34$, being a zero offset mean vector. $\overline{Z_i}$ is added back to the i^{th} joint trajectory (PCA was applied on the zero-mean normalized trajectories). The matrix $S = [s_{1,1} \dots s_{i,j}] \in \mathbb{R}^{i,j}$ represents the kMPs synergy map. If only a subset of the joint trajectories is required, it is possible to consider a submatrix, composed only of the rows corresponding to the joints of interest. The reference vector for the joint variables is therefore a linear combination of the kMPs through the synergetic coefficients of the matrix S. The columns of this matrix map the contribution of each primitive to the joint space. Using the extracted kMPs, the joint trajectories can be reconstructed according to the above formula.

A simple model of the legs was also developed, and the hip, knee, and ankle trajectories were reconstructed from the single kMPs, and tested on the simulation model. This analysis revealed that the first two kMPs are mainly responsible of the alternate swinging of the legs, while the third and the fourth kMPs are related to the vertical motion of the pelvis (generated with bending the knees). The combination of the effects of the single kMPs results in the complex human motion.

3.4.1 Partial Reconstruction of Joint Trajectory from kMPs

In this subsection the contribution of the kMPs to the joint trajectories is analyzed, showing the left knee trajectory generated by reconstruction from single kMPs and from subsets of the five kMPs. Figure 3.8 shows that no single kMP is sufficient to guarantee a

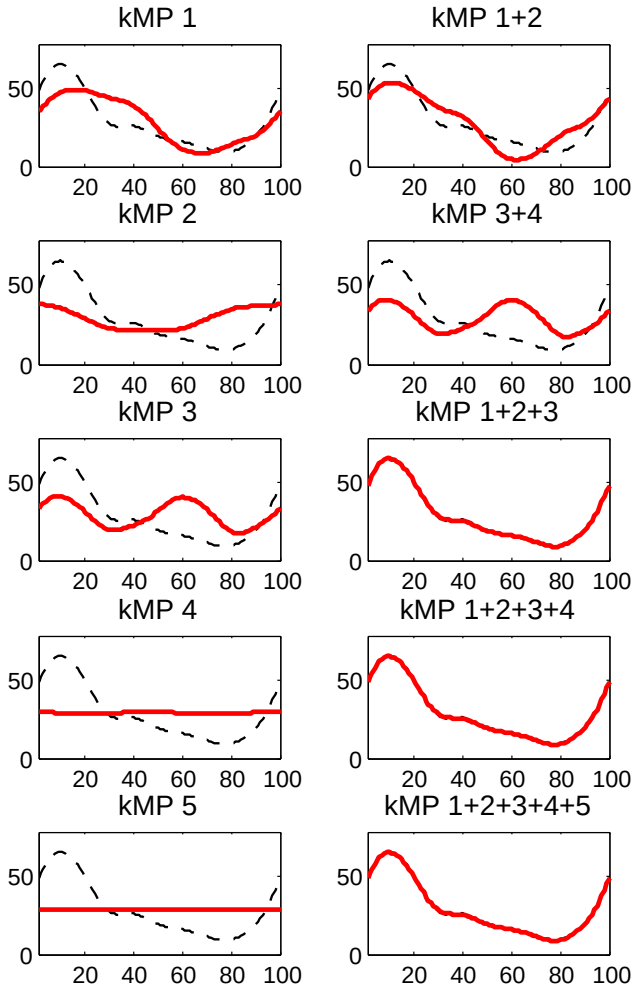

Figure 3.8: Left knee trajectory generated by reconstruction from kMPs (solid line) compared to the original left knee trajectory (dotted line). On the x-axis the percentage of a gait cycle (from 0% to 100%), and on the y-axis the knee angle in degrees.

good accuracy in the reconstruction. In this specific example, the first three kMPs describe most of the original motion, and when they are considered together the trajectory reconstructed is very close to the original one, while the introduction of the fourth and the fifth kMPs only brings an improvement that is negligible.

3.4.2 Partial Reconstruction of Foot Trajectory from kMPs

This subsection considers the contribution of the single kMPs to the foot trajectory. In Figure 3.9 the blue line is the right foot trajectory (relative to the pelvis) of a subject walking at low speed, projected on the sagittal plane (Figure 3.9(a)) and on the coronal plane (Figure 3.9(b)), respectively. In both figures the first row of graphs compare the foot trajectory reconstructed from an individual kMP (labelled on top), in red, to the original trajectory, dotted. The second row compares foot trajectories reconstructed from a combinations of kMPs, in red, again to the original trajectory, dotted.

The displacement of the foot trajectory on the longitudinal axis is about 20 cm, while on the medial axis it is about 60 cm, and on the transverse axis it is about 10 cm. The first two kMPs together are sufficient to give a hint on what the range of motion of the foot is. When the third kMP is also included, the reconstructed trajectory already has a shape that is similar to the one of the original trajectory. It can also be noticed that if all five kMPs are used, the resulting foot trajectory obtained by reconstruction is almost identical to the original trajectory.

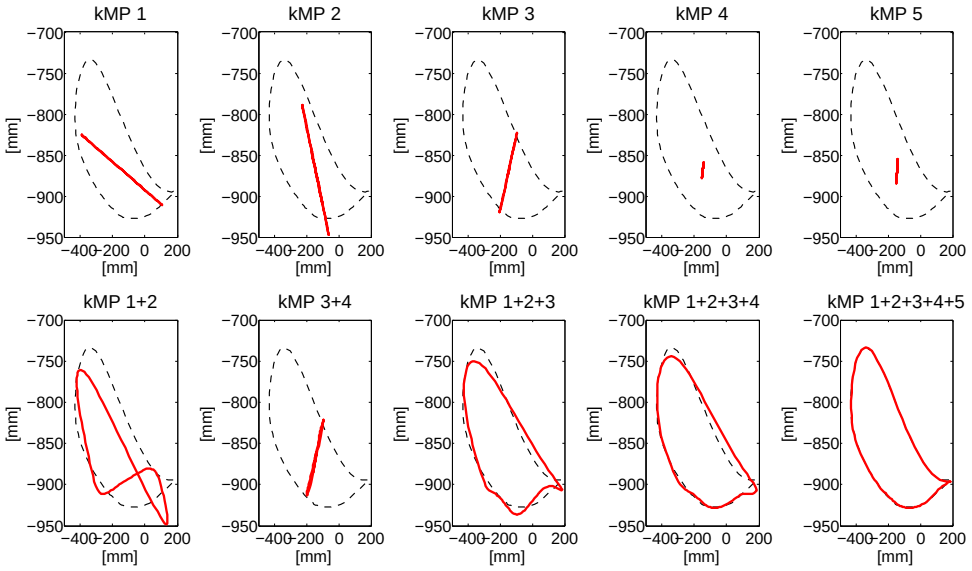

(a)

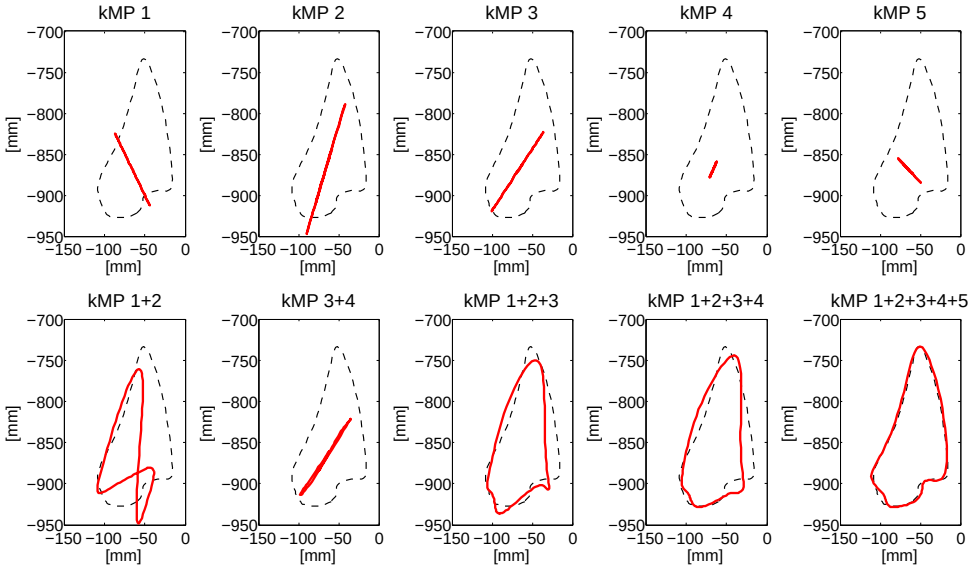

(b)

Figure 3.9: Partial reconstruction from kMPs of the right foot trajectory (a) projected on the sagittal plane, and (b) projected on the coronal plane

3.5 Application: Human-like Walking from kMPs with COMAN

A first application of our research was to generate human-like trajectories for the humanoid robot COMAN. The analysis performed on human data led us to the kinematic Motion Primitives (kMPs). Unfortunately the procedure to generate joint trajectories from kMPs, described in Section 3.4.1, could not be applied directly to generate reference trajectories for the robot. PCA, in fact, returns values for the matrix S to reconstruct trajectories that fit the kinematics of the human subject. The dimensions of the robot and, in smaller part, its kinematics are different from those of humans. The solution adopted to overcome this issue was to add the Center of Mass (CoM) x,y,z trajectories of the subjects to the set of their 34 joint trajectories, and then apply PCA again.

The CoM trajectories are coupled to the joint trajectories, and this resulted in the same kMPs extracted. The matrix S returned by PCA was composed of the rows relative to the joint trajectories, and by the rows that allowed to generate the x,y,z CoM trajectory

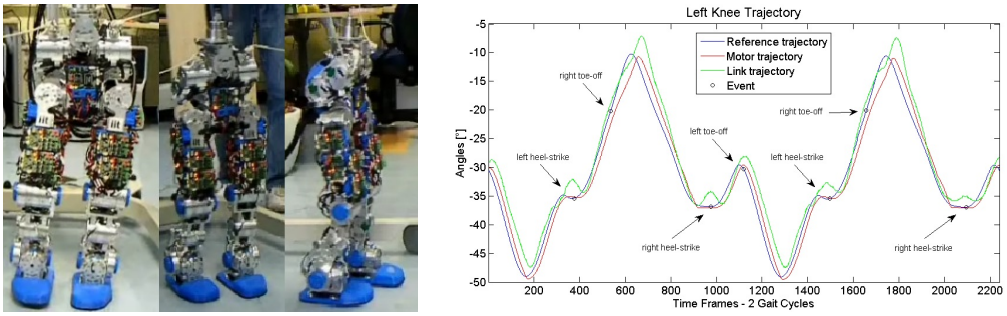

(a) (b)

Figure 3.10: a) Snapshots from the video of the COMAN robot walking human-like (the full video can be found at the link: http://www.youtube.com/watch?v=bnlCAZLhHz0), and b) left knee trajectory

by reconstruction. These Cartesian trajectories were finally scaled down to the dimensions of the robot (approx. 1.7:1). Originally the idea was to use this CoM reconstructed trajectory together with foot trajectories generated by reconstruction from kMPs as well, to derive the reference joint trajectories for the COMAN robot with inverse kinematics. This turned out to be not possible, because of the constraints on the step length of the robot: the version of the feet used at the time of the experiments was rigid, and did not allow to use heel-strike/toe-off gaits. Because of these limitations engineered foot trajectories were generated, that satisfy these constraints.

The joint trajectories were then derived with inverse kinematics from the kMPs-based CoM trajectory and the engineered foot trajectories. A low level PD control was used to track the reference kMPs-based joint trajectories.

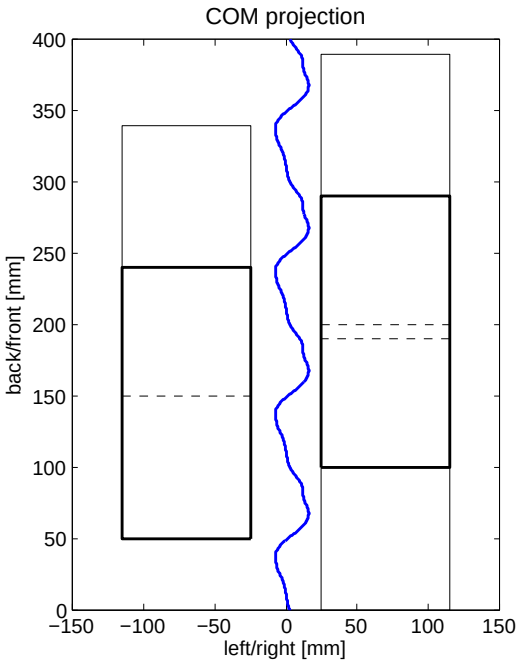

Figure 3.11: Center of mass trajectory projected on the ground plane with foot stamps

The robot could perform a valid, stable walk (in Figure 3.10(a) three snapshots of the robot walking are shown), with a gait frequency of 0.89 Hz that is the same as in the original gait of the human subject. The features of the human gait could be clearly recognized in the gait of the robot: the significant vertical displacement of the CoM, the knee straightening (that was not imposed in any way) are not common in robot gaits based on fully engineered trajectories. Notice also that no stability constraint was imposed: the open-loop gait generated by reconstruction from kMPs, though, was verified to be intrinsically stable. Moreover, Figure 3.11 shows the kMPs-based CoM trajectory of the robot projected on the ground plane (also notice it is not symmetric): in the single support phases the CoM projection is out of the support polygon. The gait generated,

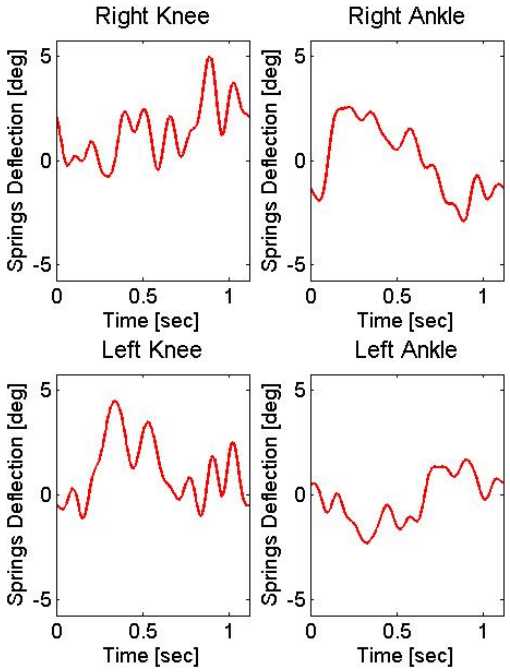

Figure 3.12: The four spring deflections during a gait cycle

hence, was dynamic, and this resulted in spring deflections that are wider than they usually are in the case of engineered gaits (Figure 3.12). The left knee trajectory is reported in Figure 3.10(b). The difference between the motor trajectory and the link trajectory represents the spring deflection. Notice that the knee straightens up to about -5° (knee angles are negative in the COMAN robot).

3.6 Extension 1: Resonance Exploitation for Energy Efficiency

A key prerequisite for an effective everyday use of humanoid robots is autonomy. From this point of view, the energy consumption of state-of-the-art robots is still a serious limitation. This constraint is being addressed on the one hand through hardware (design of elastic units to store energy and new longer lasting batteries), and on the other hand by developments in software and control aimed at improving the energy efficiency of robots [Silva and Machado, 1999]; [Kuo, 2002]; [Yamasaki et al, 2002]; [Fujimoto, 2004]; [Kurazame et al, 2005]; [Collins et al, 2005]; [Moro et al, 2012b]; [Kormushev et al, 2011].

Compliance has been originally introduced in the actuation units of robots to guarantee a safer interaction. Recent studies, though, show that compliance can also be exploited to improve the energy efficiency of robots performing rhytmic motions, e.g., locomotion. Recent works [Vanderborght et al, 2006]; [Jafari et al, 2011] demonstrated on simple systems that energy efficiency can be obtained by tuning the motion frequency to match one of the main resonance frequencies of the system.

The kMPs-based gait described in the previous section showed a wide spring deflection. For this reason it was used as the basis for a study on the effects of walking at different frequencies in terms of energy efficiency. Subsection 3.6.1 presents the anal-

ysis performed to identify the main resonant modes of the COMAN robot. Following, in Subsection 3.6.2, it will be shown that resonance can be exploited to improve the performance of walking in terms of energy efficiency.

3.6.1 The Spring-Mass Model and the Resonance Frequencies of COMAN

In order to understand the behavior of the robot, as far as its natural frequencies are concerned, a theoretical analysis was performed to determine the band of the natural frequencies of the system for the different configurations of the legs (single and double support). The purpose of this analysis was to finely tune the frequency of the gait reconstructed from kMPs within the band of the natural frequencies, and to prove that, in the case of compliant robots, walking in the resonance is beneficial in terms of energy efficiency. Previous works have only managed to show this energy gain in simple systems with a small number of degrees of freedom [Vanderborght et al, 2006]; [Jafari et al, 2011]. COMAN, instead, has multiple resonance frequencies which vary depending on its configuration, and the reference joint trajectories for walking are not simple sinusoidal trajectories. The intrinsic physical elasticity in some of the joints of the COMAN robot results in a multi-dof nonlinear mass-spring system, the dynamics of which can be described by the following equation:

$$M(q)\ddot{q} + C(q,\dot{q}) + h(q) = \tau \tag{3.6}$$

where τ is the joint torque vector, $M(q)$ is the inertia matrix, $C(q,\dot{q})$ is the Coriolis/centripetal matrix, and $h(q)$ is the gravity matrix of the robot. For the purpose of the natural analysis, and taking into account the fact that in the prototype of COMAN that was used for the experiments described in this Chapter the physical elasticity is present

only at the knee and the ankle joints, we consider the robot (for both single and double support state) as a simplified double pendulum with a spring at each joint (Figure 3.13). In this way for a particular configuration of the rest of the joints (excluding the compliant ones) the model in (3.6) can be represented by the simplified double pendulum model.

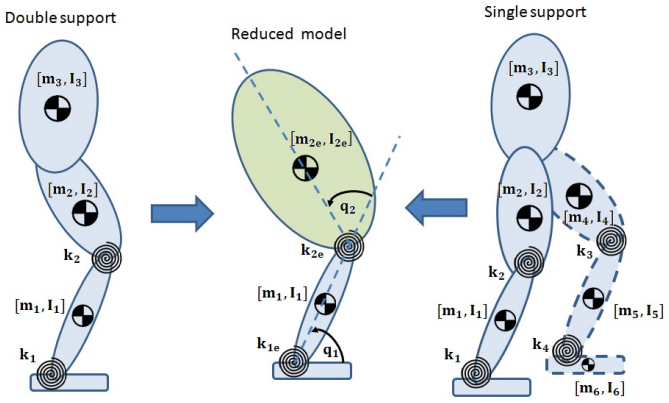

Figure 3.13: Single, double support, and the reduced double pendulum model

In particular, in double support, the two legs are considered equivalent, with all the body parts above the two knees considered as a single rigid body. The stiffness of the joints of the equivalent double pendulum representing the double support case is twice the stiffness of the knee and ankle joints of the robot.

In single support, all the upper parts above the support knee and the swing leg are also considered as an entire rigid body. A further simplification here is that the compliant joints of the swing leg are considered stiff in order to maintain the double pendulum equivalent also in this case. Considering that the mass of the calf/foot of the swing leg represents only 14% of the mass of the entire combined rigid body above the knee of the support leg, it is expected that this further reduction of DOFs in the case of the single support will not significantly affect the results of the analysis.

Based on the above simplifications, the overall system for both the double and single support cases can be described by the following reduced model:

$$M_r(q)\ddot{q} + C_r(q,\dot{q}) + h_r(q) = \tau \tag{3.7}$$

Where τ is the 2x1 joint torque vector, and $M_r(q)$ $C_r(q,\dot{q})$ and $h_r(q)$ represent the inertia, Coriolis/centripetal, and gravity matrices, respectively, of the reduced model. In order to derive the natural frequencies of the system the above nonlinear model needs to be linearized. Assuming that the generalized coordinates slightly change around an equilibrium configuration, and that their time derivatives are all small, the Coriolis/centripetal forces can be neglected. At the equilibrium configuration $q = \theta = q_e$ (θ is the joint motor equilibrium position before the compliant element) we can write:

$$M_r(q_e)\ddot{q} + h_r(q) = \tau \tag{3.8}$$

At the equilibrium the vector of the generalized torques τ is given: $\tau = -K(q-\theta) = -K(q-q_e)$, where K is the diagonal stiffness matrix. By substituting in (3.8) it can be written as:

$$M_r(q_e)\ddot{q} + K(q-q_e) + h_r(q) = 0 \tag{3.9}$$

By linearizing the gravity matrix around the equilibrium configuration and rearranging (3.9) it can be obtained:

$$M_r(q_e)\ddot{q} + [K + J_{h_r}(q_e)]q = [K + J_{h_r}(q_e)]q_e - h_r(q_e) \tag{3.10}$$

where $h_r(q_e)$ is the the gravity vector at the equilibrium position. The above equation is now in the general form of the equation of motion $\overline{M}\ddot{x}+\overline{K}x=\overline{F}$ for a vibrating system where q represents the time dependent vector that describes the motion, and M_r and $[K+J_{h_r}(q_e)]$ are mass and stiffness matrices. At its equilibrium, the resonance frequencies can be obtained by determining the eigenvalues of the system dynamics.

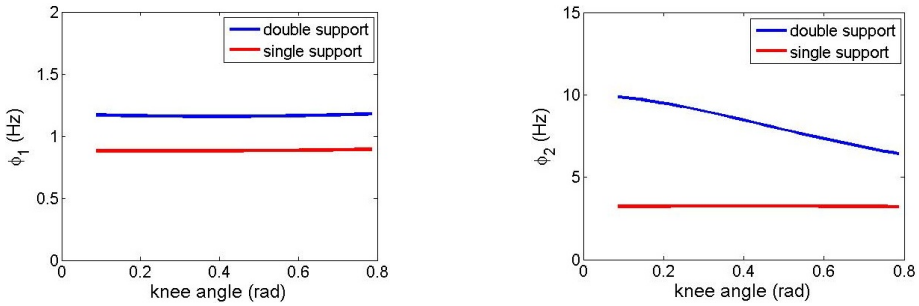

(a) (b)

Figure 3.14: The resonance modes of the COMAN robot in single and double support for different knee angles

Assuming $A=M_r(q_e)^{-1}[K+J_{h_r}(q_e)]$, the natural frequencies around the equilibrium are given by $\omega_n^2=\lambda_n$, $n=1,2$ where λ_n represent the eigenvalues of A. The resonance frequencies are therefore obtained as $\phi_n=\frac{1}{2\pi}\sqrt{\lambda_n}$, $n=1,2$.

Figure 3.14 introduces the two resonance frequencies of the equivalent double pendulum model. As it can be observed, the lowest of the two resonance frequencies, ϕ_1, is in the band of 0.8 Hz to 1.2 Hz, and is the most relevant, while the second resonance for both single (4 Hz) and double support (7-10 Hz) is out of the band of normal walking gaits, that have frequencies in the region of 1 Hz. The resonances are mostly affected by the gait phase (single or double support), though a small variation can be also noticed as a function of the configuration of the legs (knee angle). In the followings the efficiency of the robot will be evaluated for different gait frequencies within the region of ϕ_1, the

lowest of the resonances observed (Figure 3.14(a)).

3.6.2 Walking in the Resonance

The benefits of compliance in terms of safety (for the robot, to reduce damages, and for the people around the robot) are known and have been studied exhaustively. But a compliant actuation system can also be exploited to improve energy efficiency. This also is theoretically known, and has been shown on simple robotic systems. Aim of the analysis presented in this section is to prove that this is valid also with a complex compliant system as the COMAN robot is.

Analysis of the Overall Energy Consumption

The features observed on the kMPs-based walk of the COMAN robot, described in Section 3.5, introduce a wide deflection of the springs in the actuators. For this reason this gait fits well for studying the relation between gait frequency and energy consumption.

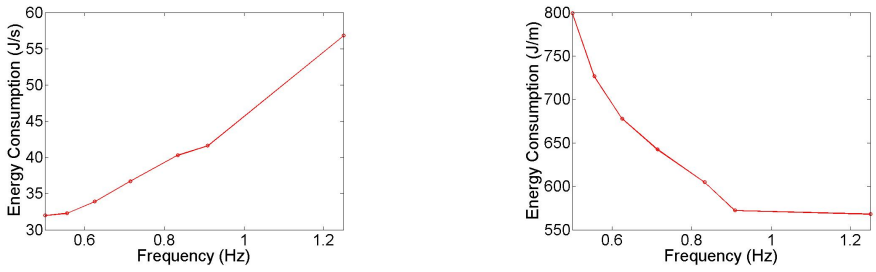

(a) (b)

Figure 3.15: Energy consumption at different gait frequencies a) to walk for 1 s, and b) to walk 1 m distance

The joint trajectories of the kMPs-based walking were scaled to obtain gait periods (frequencies) in a range from 0.8 s (1.25 Hz) to 2.0 s (0.5 Hz). The robot was able to

walk at all the frequencies tested, and the overall energy consumption was recorded. Figure 3.15(a) shows the results collected in terms of energy per second.

The energy consumption per second grows as the motion becomes faster, and this was expected. But the distance covered by the robot walking at a lower frequency (and consequently more slowly) is minor as well. For this reason a more interesting information extracted is how much energy the robot requires to cover the same distance at different gait frequencies. Figure 3.15(b) shows that when the robot is walking at higher frequencies the energy consumption reduces significantly. According to the data reported, when the robot walks at a frequency that is in the neighborhood of one of the main resonance frequencies of the mechanism (0.8 Hz to 1.2 Hz) the energy required is about the 70% of the energy necessary to cover the same distance at lower frequencies. To verify whether this achievement was actually obtained by exploitation of the resonance, the contribution of the springs to the motion was analyzed in detail.

The Contribution of the Springs to the Motion

It has been proven that the energetic performance of the robot varies substantially as the gait frequency changes. This subsection aims to show that the intrinsic compliance of the actuators is in fact exploited when the robot walks in the resonance. The analysis performed shows that the springs are responsible of these performance variation: initially the overall contribution of the springs to the motion will be reported, down to the detail of the work done by the single springs. Figure 3.16(a) shows the total work done by the springs in a gait cycle.

The mechanical work done by the springs is considered as positive when it is contributing positively to track the joint reference trajectories, and as negative when the

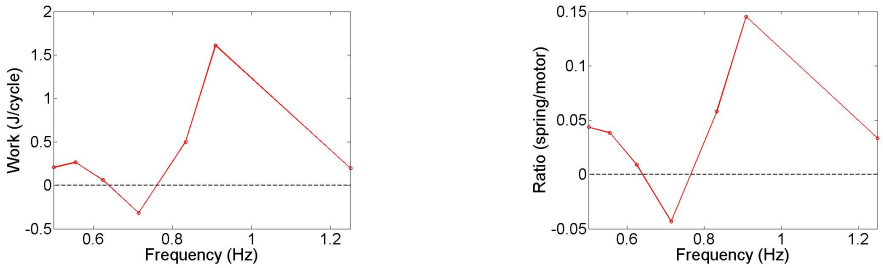

(a) (b)

Figure 3.16: a) Total work done by the springs at different frequencies, and b) ratio between spring contribution and motor energy consumption

force generated by the springs goes in the opposite direction with respect to the desired trajectories. The contribution of each spring was integrated over one cycle, and the overall contribution of the springs is the sum of the contributions of the single springs. The total work of the springs is the difference in terms of energy consumption between the work done by the motors of the compliant robot, and the work that the motors of an equivalent stiff robot would have had to do to follow the same trajectories. This experiment verifies on a multi-dof compliant robot what often hypothesized in the literature: energy efficiency can be improved by exploiting the compliance of a robot. The total work of the springs can both be positive or negative: when the gait period is 1.4, for instance, the overall contribution of the springs is negative. In this case the energy consumption of the compliant robot is higher than it would have been if the robot was stiff. The best performance, instead, was measured when the robot was walking in the resonance.

Figure 3.16(b) shows the ratio between the work done by the springs, and the mechanical work done by the motors in the four compliant joints at different frequencies. Only the mechanical work used to track the trajectories was considered, excluding the

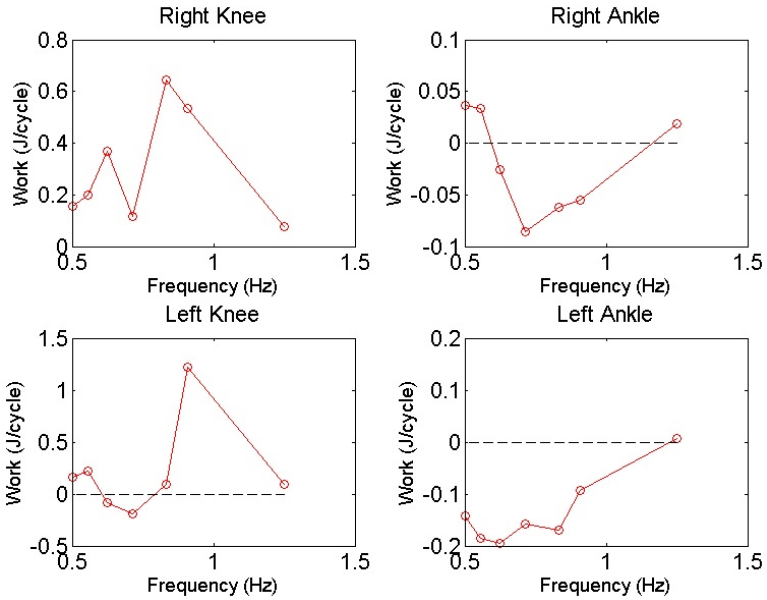

Figure 3.17: Work done by the single springs at different frequencies

losses due to friction and any other electrical energy loss. Notice that, when the robot walks in the resonance, the springs contribute with about 15% of the mechanical work necessary to perform the motion.

Figure 3.17 extends the analysis on energy efficiency with a focus on the contribution of the single springs. A first observation is that there is no symmetry between left and right leg: this is because the reference joint trajectories are derived from the kMPs of a human subject, and the original human gait was not symmetric. These graphs also reveal that the work of the springs, whether positive or negative, is major in the knees than in the ankles.

To understand better the behavior of the springs, in Figure 3.18 both the positive (blue line) and the negative (red line) contribution of the springs at the different frequencies are explicitly shown. The total mechanical work done by the springs corresponds

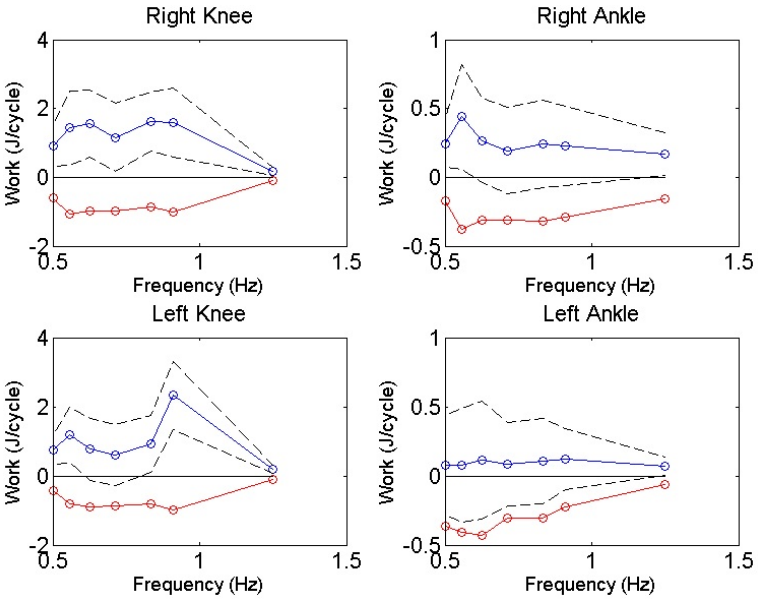

Figure 3.18: Detail on the positive and negative work done by the single springs at different frequencies

to the dotted line above all the others, and is the sum of positive and negative work, without caring if it is helping the motion or not. When the robot walks in the resonance the springs are excited more, and both the positive and the negative work (in the knees) increase. The difference between the two, though, shows that the amount of positive work is major than the negative work around the resonance frequency (0.8 Hz to 1.2 Hz). This information is represented by the dotted line between the blue and the red lines, and correspond to what already reported in Figure 3.17.

3.7 Extension 2: Horse-like Walking, Trotting, and Galloping from kMPs with a Compliant Quadruped Robot

Anthropomorphism allows humanoids to share the same environments of humans. There are circumstances, though, such that multi-legged robots can perform better. Quadrupeds, in particular, are more stable and typically more powerful than bipeds, and these characteristics can make them well suited for outdoor tasks, such as assisting humans transporting heavy loads for them, or even operating autonomously in a hostile environment. To try to exploit the potential of legged locomotion a number of solutions have been developed for robots of varying size, powered by diverse energy sources. Among these, notable examples include Fujita and Kitano [1998]; Berns et al [1998]; Canderle and Caldwell [2000]; Nichol et al [2004]; Poulakakis et al [2005]; Buehler et al [2005]; Zhang et al [2005]; Kimura et al [2007]; Raibert et al [2008]; Hirose et al [2009]; Semini et al [2011]; Hutter et al [2011]; Spröwitz et al [2013].

Quadrupedal locomotion presents good intrinsic stability features, but the coordination of the motion of four legs is non-trivial to control. Different trajectory generation techniques have been adopted [Kimura et al, 1989]; [Raibert, 1990]; [Sakakibara et al, 1990]; [Kramy and Orin, 2003]; [Golubovic and Hu, 2003a,b]; [Tsujita et al, 2005]; [Hu and Gu, 2005]; [Iida et al, 2005]; [Kim et al, 2006]; [Rebula et al, 2007]; [Pongas et al, 2007]; [Hebbel et al, 2007]; [Chae and Park, 2008]; [Kim et al, 2008], and the efforts in this field of research led to proficient results in the development of different gaits, from the slow walk to gallop. Raibert [1986] provides a good overview of legged locomotion, with particular attention given to quadrupeds.

The results achieved, however, are still far from the proficient, efficient, and fluid motion of animal locomotion. For this reason many researchers have sought to analyze

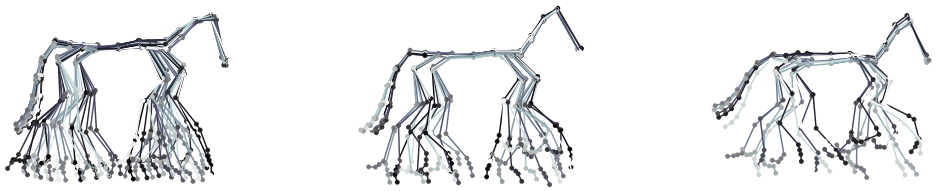

(a) (b) (c)

Figure 3.19: The source data (visualization at $12Hz$) of the horse a) walking, b) trotting, and c) galloping on a treadmill.

animal gait [Hoyt and Taylor, 1981], with the aim of reproducing this on robots. Different methods for biological inspirations have been proposed, with the well known theory of Central Pattern Generators (CPG) forming a common theme.

Motivated by the good results of the application of human kMPs to generate a human-like walking, an extension to achieve a biologically-inspired quadrupedal locomotion was investigated. The research described in this Section aimed to identify the kMPs of horse locomotion, and to use them to directly transfer the biological features of horse gaits to a quadruped robot. The compliant quadruped robot Cheetah-Cub [Spröwitz et al, 2013] was used to test the horse-like trajectories synthesized. Subsequently, the trajectories were scaled in frequency to evaluate the performance of locomotion at different gait frequencies. This analysis was triggered by the research presented in Heglund and Taylor [1988]. Finally, a gait transition strategy is proposed. Developing an effective gait transition is fundamental for achieving a good performance in quadrupedal locomotion. Vilensky et al [1991]; Inagaki and Kobayashi [1993]; Lin and Song [2002]; Griffin et al [2004] proposed interesting researches on this topic. Walk to trot and trot to walk transitions generated according to the proposed strategy were successfully tested on the Cheetah-Cub robot.

The source data used in these experiments were purchased from the U.K. based commercial company Kinetic Impulse. These data consist of the joint trajectories of a horse (Figure 3.19) performing a walking gait, a trotting gait, and a galloping gait on a treadmill (horse dimensions: hips to the ground at rest position: $1.472m$; hips to shoulders distance: $1.197m$; right hip to left hip distance: $0.269m$; right shoulder to left shoulder distance: $0.205m$. These last two data refer to the distance between joints that are internal to the horse body, and are the first joints of the limbs from the spine). For each of the three gaits, three sequential gait cycles were arbitrarily selected, and the respective full-body joint angle trajectories (only those with a range of motion of at least 10^o were considered) were averaged to reduce the peculiarity of the single cycle.

On these trajectories a Principal Component Analysis (PCA) was subsequently applied. For each of the three gaits the first four components were selected. In the case of the walk gait these components together accounted for 97% of the variance. Similar values were observed also in the case of the trot gait, and in the case of the gallop gait, with a cumulative percentage of variance accounted for of 96% and of 97%, respectively. These four components, normalized in time (from 0% to 100% of gait cycle) and amplitude (such that the maximum absolute value was 1) form the four kinematic Motion Primitives (kMPs) of walking, trotting, and galloping.

As it was in the case of human kMPs, a similarity among the kMPs extracted from the three gaits was noticed by observation. If in the walk and the trot gaits the order of the kMPs remains the same, the first and the second kMPs of gallop have an inverted order with respect to the other two gaits. The third and the fourth kMPs, instead, maintain the same order in all the gaits analyzed. In Figure 3.20 the corresponding four kMPs from the walk, trot, and gallop gaits are superimposed to facilitate a comparison.

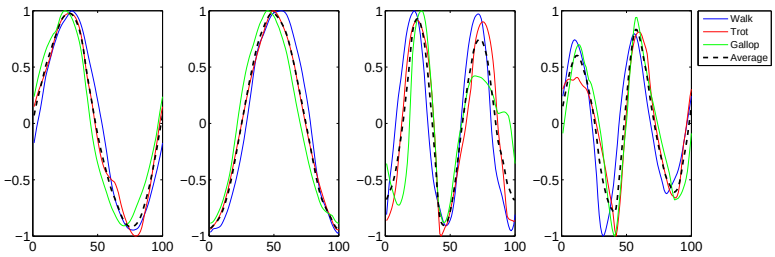

Figure 3.20: Comparison among the corresponding kMPs extracted from the walk, trot, and gallop gaits

The similarity in terms of shape and phase observed by visualization in Figure 3.20 was confirmed by means of a statistical analysis, which was described in Section 3.3, that provided a quantification of the degree of similarity between gaits. The following tables summarize the results of this analysis:

Table 3.11: Statistical analysis of similarity among kMPs extracted from walk (W), trot (T), and gallop (G) - Cross-covariance

	1st	2nd	3rd	4th	Average	Weight
W_T	0.9844	0.9783	0.9207	0.9141	0.9494	0.9722
T_G	0.9934	0.9170	0.7282	0.9674	0.9015	0.9277
W_G	0.9876	0.9713	0.8120	0.9418	0.9282	0.9560

Table 3.12: Statistical analysis of similarity among kMPs extracted from walk (W), trot (T), and gallop (G) - Delay

	1st	2nd	3rd	4th	Average	Weight
W_T	0.03	0	0.03	-0.04	0.005	0.0227
T_G	0.03	0	-0.01	-0.01	0.0025	0.0144
W_G	0.06	-0.02	-0.06	-0.06	-0.02	0.0482

The kMPs of the three gaits have a similarity that is in all cases significant (Table 1). This led to an overall similarity between walk and trot gait of 97%. This value reduced to 93% in the case of trot and gallop. The last comparison, between walk and gallop,

have a degree of similarity of 96%. In Table 2 the delay between kMPs is reported: it can be noticed that the weighted average delay is smaller than 5% in all three comparisons between gaits. This result indicates an evident correlation between the kMPs of the different gaits. A possible interpretation is that the kMPs extracted from walk, trot, and gallop are in fact the same set of kMPs, that together are sufficient to describe the three different gaits.

Cheetah-Cub, the compliant quadruped robot used for experimentation (Figure 3.21), was designed at the Biorobotics laboratory at EPFL, Switzerland. The system specifications are show in Table 3.13. More details on the Cheetah-Cub robot can be found in Spröwitz et al [2013].

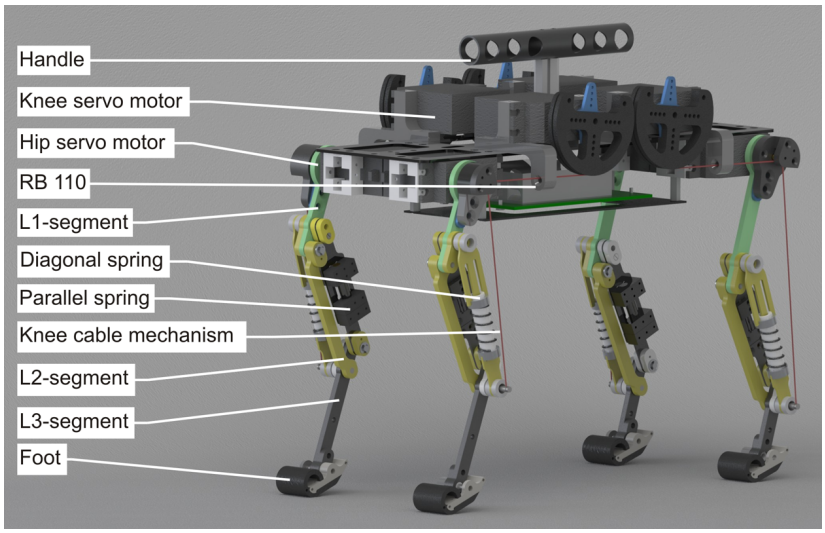

Figure 3.21: Cheetah-Cub, the compliant quadruped robot used for experimentation (rendered image), developed at Biorobotics laboratory, EPFL, Switzerland. Snapshots of the real robot during walking and trotting are provided in Figure.3.22. This robot configuration weights $m \approx 1.1kg$, and has the size of a small house cat. Power to the robot was provided through a tether. During experiments, the tether was carefully kept slack.

Table 3.13: Robot characteristics and comparison with the horse dimensions. Distances for the horse refer to functional joints that are internal to the horse body

Characteristic	Value	Horse
Mass m_{robot}	1.1kg	
Standing hip height h_{hip}	0.158m	1.472m
Distance d_{sh-sh}	0.1m	0.205m
Distance $d_{hip-hip}$	0.1m	0.269m
Distance d_{hip-sh}	0.205m	1.197m
RC servo motors (8x)	Kondo Krs2350 ics	
Control board	Roboard RB110	
Operation system	Linux Xenomai	
Communication	Wifi Via VT6655	
Power supply (tethered)	10.5V	
Stall torque RC servo	2Nm (6V)	
Speed max RC servo	$0.16^{\circ}/60^{\circ}$ (6V)	
Spr. stiffness $k_{diagonal}$	2300N/m	
Spr. stiffness $k_{paral,front}$	4800N/m	

The similarity between kMPs of different horse gaits suggests that a unique set of four kMPs is at the basis of walk, trot, and gallop gaits. Hence, these kMPs can ideally be used to reconstruct any of the three gaits considered, just by varying the values of matrix S (Equation 3.5).

Since the values required to reconstruct a specific gait are not known, however, it was not possible to follow this procedure. The kMPs extracted from each gait, instead, were used to reconstruct the corresponding gait for the quadruped robot. PCA was applied on an enriched set of trajectories, that includes not only the joint trajectories, but also the four Cartesian foot trajectories with respect to a frame located in the middle of the spine. These trajectories are coupled with the joint trajectories, and it was verified that

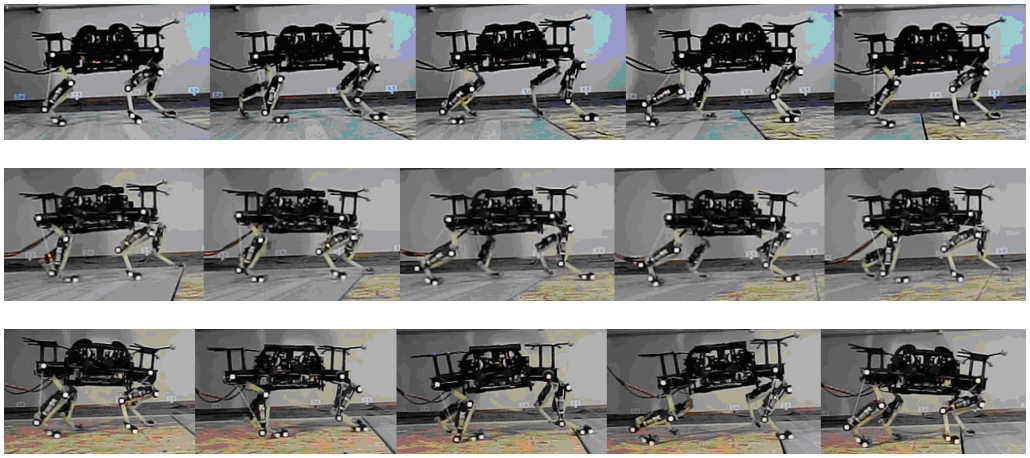

Figure 3.22: Snapshots of walk (top), trot (center), and gallop (bottom) gaits with the compliant quadruped robot Cheetah-Cub (the full video can be found at the link: http://www.youtube.com/watch?v=zJF_-2Rbaxo)

the kMPs extracted do not change when this information is added. In this way, though, the coefficients to reconstruct the Cartesian foot trajectories of the horse are known. The reconstructed foot trajectories are then proportionally scaled down according to the dimensions of the robot.

These trajectories had to be slightly modified to satisfy the mechanical constraints of the robot. They are first projected on the sagittal plane, since there is no adduction/abduction degree of freedom in the legs of the robot. Then their range of motion is further scaled down to ensure they do not exceed the joint limits. The range of motion of the legs of the robot, in fact, is smaller than it is for a horse, and this is mainly because the robot does not have a flexible spine. The reference positions for the motors of the robot are then derived from the foot trajectories with inverse kinematics. In the proposed approach the differences between the kinematics of the horse and the kinematics of the robot are not a limitation. What is maintained is the end-effector (foot) trajectory shape.

This method does not require the robot to have the same kinematics as the horse. The robot could successfully perform a valid, stable locomotion in all three cases (Figure 3.22).

Figure 3.23 shows the foot trajectories for a walk gait reconstructed from kMPs. It is possible to notice the symmetry between left and right foot trajectories. The hindleg foot trajectories, in both cases, have the shape of a triangle with two rounded angles on the left and a spike on the right. The foreleg trajectories, instead, have a shape that reminds of a bean. The range of motion is also very similar. The gait frequency is maintained the same as the original one of the horse walking at 0.97 Hz.

The foot trajectories for the trot gait reconstructed from kMPs are shown in Figure 3.24. The vertical displacement in the forelegs is wider than in the case of walking. The gait frequency is also higher at 1.59 Hz, and it is the same as that of the horse trotting.

Figure 3.25 shows the foot trajectories of a gallop gait reconstructed from kMPs. The trajectories are less regular than it was in the other cases, and the displacement is

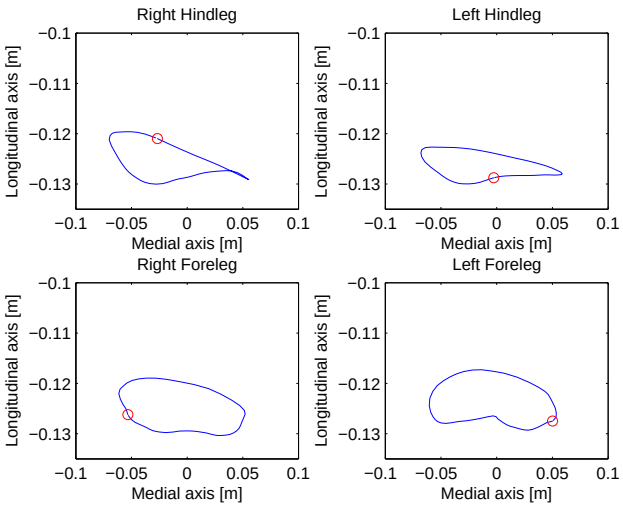

Figure 3.23: The foot trajectories of the walk gait reconstructed from kMPs

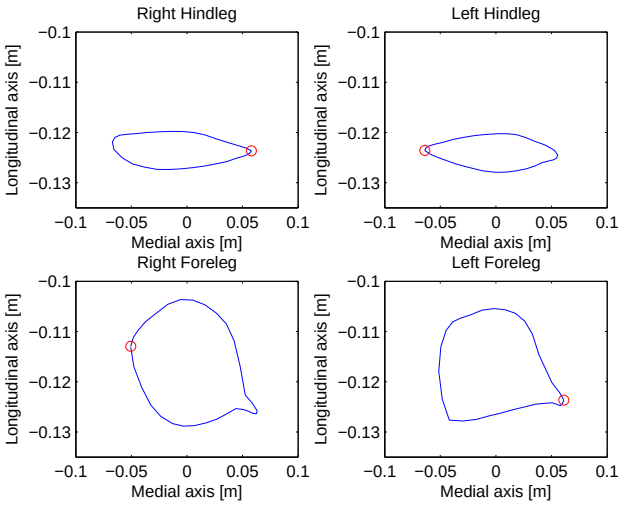

Figure 3.24: The foot trajectories of the trot gait reconstructed from kMPs

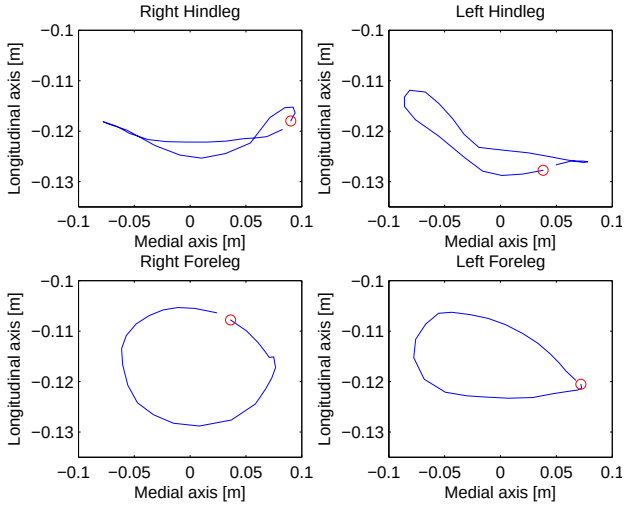

Figure 3.25: The foot trajectories of the gallop gait reconstructed from kMPs

wider in both directions. The gait frequency has increased further up to 2.01 Hz, the same frequency of the horse galloping.

3.7.1 Analysis on the Effects of Gait Frequency Scaling

The quadruped robot could successfully perform stable walk, trot, and gallop gaits at their original frequency. The performance of gallop though was not satisfactory. High speed video footage indicates that this was caused by the missing spine movement: while horses and other mammalian quadrupeds extensively use their spine at high speed gaits, the robot has a stiff trunk. The method proposed matches the kinematic features of both legs and spine motion of the horse with the legs motion of the robot. The resulting trajectories required high torques to be tracked, and this led to massive inter-limb and contact forces that, consequently, caused major foot slippage. For this reason the experiments described from here on focused on the walk and trot gaits.

In the gaits reconstructed from kMPs, the decision had been taken to maintain the same gait frequency as the original one: $f_{\mathbf{walk}} = 0.97Hz$ and $f_{\mathbf{trot}} = 1.59Hz$, respectively (Table 3.14). The dimensions of the robot, though, are different from those of the horse whose gaits were used as source data. In the literature Heglund and Taylor [1988] reportes on animal locomotion and body size scaling. It is shown that gait frequency is inversely proportional to the dimensions of the animal itself. For this reason

Table 3.14: Cartesian speed of the robot walking, and trotting

m	f_{walk}	f_{trot}	v_{walk}	v_{trot}
1.0	0.97	1.59	0.13	0.28
1.5	1.45	2.39	0.24	0.39
2.0	1.94	3.18	0.29	0.53
2.5	2.42	3.98	0.36	0.59
3.0	2.90	4.77	0.40	0.56
3.5	3.39	5.57	0.41	0.42

in the following experiments the gait frequencies of walk and trot gaits were increased systematically by a multiplication factor $m = [1 : 0.5 : 3.5]$. In the case of the trot gait, this resulted in locomotion frequencies between $f = 1.6Hz - 5.6Hz$. Heglund and Taylor [1988] reports that an animal of approximately equal size (dog, $m = 0.96kg$) as the quadruped robot reached its maximum trot-gait speed at a gait frequency of $f = 4.5Hz$. We expected a speed maximum roughly in the same frequency domain.

Walk gait speed Results in Figure 3.26 indicate that the speed of the robot scaled almost linearly, with the base frequency being scaled up to a locomotion frequency of $f = 2.42Hz$. The average robot speed at $f = 2.42Hz$ was $v = 0.35mps$. For two higher frequencies ($2.9Hz$ and $3.39Hz$), robot speed still increased. Plots in Figure 3.26 indicate that the maximum walking speed was reached close to the highest applied locomotion frequency of $f = 3.39Hz$, with $v = 0.43mps$, or roughly 2BL/s (body lengths per second).

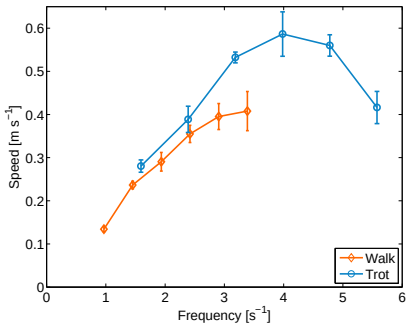

Figure 3.26: Speed versus frequency of three different gaits, run on the compliant quadruped robot platform. Walking speed ranged from 0.14mps to 0.42mps, with a speed-maximum at $f = 2.9Hz$. Trotting speed ranged from 0.29mps to 0.62mps, with its speed maximum at $f = 3.8Hz$. For gallop, only the base-frequency of $f \approx 2Hz$ lead to a stable gait, with a speed of $v = 0.2mps$.

Trot gait speed The base trot frequency applied ($f = 1.59Hz$) resulted in an average robot speed of $v = 0.26mps$, or 1.2BL/s. The fastest trot gait frequency was found at $3.98Hz$, with $v = 0.59mps$, or 2.8BL/s. Speed of the robot increased mostly steadily until the maximum speed. The robot speed decreased for any higher control frequency, down to $v = 0.42mps$ at $f = 5.57Hz$.

Pitch and roll angle phase plots Walk and trot gaits could be identified by their corresponding phase plots (e.g. Figure 3.31(b), orange and blue), which changed with the applied locomotion frequency. Typically, walking patterns presented themselves with a higher roll than pitch angle range, compared to those of the corresponding trot gait patterns. This was likely due to the higher symmetry in trot footfall patterns, compared to walk footfall patterns. With increasing robot speed, roll and pitch angles range decreased (Figure 3.27). As only the system's frequency was increased, and no other parameter was altered, it is assumed that this stabilizing effect is mechanical.

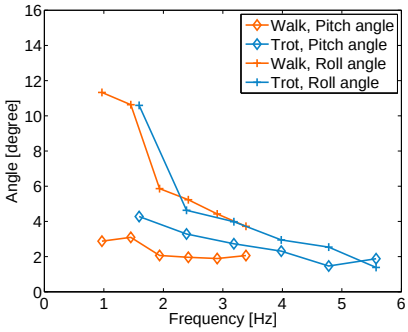

Figure 3.27: Decreasing roll and pitch angle ranges, for increasing robot speed. All combinations for walk and trot, and roll and pitch are shown. Decreasing roll and pitch angles with increasing gait frequency indicate self-stabilizing properties of the applied gait.

3.7.2 Gait Transition in Quadrupedal Locomotion

The walk and trot gaits reconstructed from horse kMPs were the base gaits for the gait transition experiments conducted on the robot and reported in this section.

Methodology

The foot trajectories of the four legs (Right Forelimb - RF, Left Forelimb - LF, Right Hindlimb - RH, Left Hindlimb - LH) for the walk and the trot gaits, derived as described in Section 3.7, are resampled to obtain 100 points per gait cycle. For each of the two gaits a "pivot" for the transition is identified using Equation (3.11):

$$\begin{aligned}\left[\widehat{i},\widehat{j}\right] = \min_{i,j} \big(&d\left(RF_{Walk}(i), RF_{Trot}(j)\right) + \\ &+ d\left(LF_{Walk}(i), LF_{Trot}(j)\right) + \\ &+ d\left(RH_{Walk}(i), RH_{Trot}(j)\right) + \\ &+ d\left(LH_{Walk}(i), LH_{Trot}(j)\right)\big)\end{aligned} \tag{3.11}$$

Pivots indicate those points in the walk and the trot gaits, respectively, such that the cumulative distance (among the four legs) between walk trajectory and trot trajectory is minimal.

In Figure 3.28, foot trajectories for walking and trotting are plotted together, and the pivot points of each gait are indicated with a dot. The transition period was set to take $3/4$ of a gait cycle to be completed: $3/8$ of trajectory before the pivot point, and $3/8$ of trajectory after the pivot point of each gait are considered. The walk to trot transition trajectory is a weighted average of the walk trajectory and the trot trajectory, with the

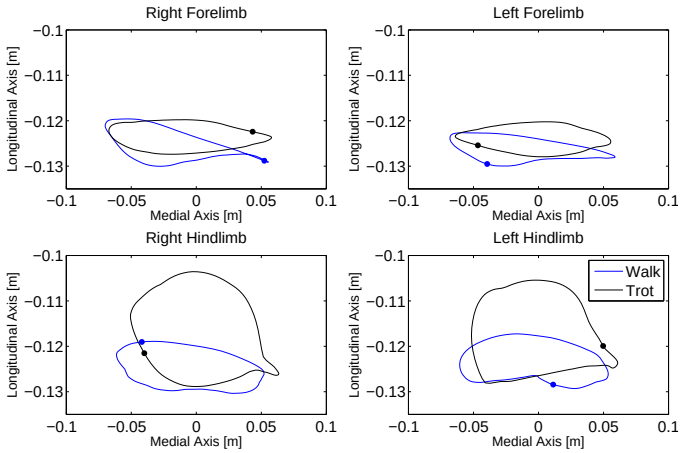

Figure 3.28: The foot trajectories of walking and trotting. The dot indicates the pivot for the walk/trot transition.

weight of trot growing linearly from 0 to 1, and the weight of walk decreasing linearly from 1 to 0.

Walk and trot also have different gait frequencies that result in a different sampling rate for the respective trajectories. The transition trajectory, hence, has a variable sampling rate: in the case of the walk to trot transition this rate changes linearly from the sampling rate of walk to the one of trot. Figure 3.29 shows the four foot trajectories during three different locomotion phases: a complete walk gait cycle, the transition from walk to trot, and a complete trot cycle. The samples are also shown. The reference motor positions derived from these data through inverse kinematics are sent to the robot at $f = 50Hz$.

The foot trajectories for the trot to walk transition are defined in a similar manner, just with the weight of the walk increasing linearly from 0 to 1 and the one of trot decreasing linearly from 1 to 0, and the sampling rate going linearly from the sampling rate of trot to the sampling rate of walk, i.e., inverting the roles of walk and trot (Figure 3.30).

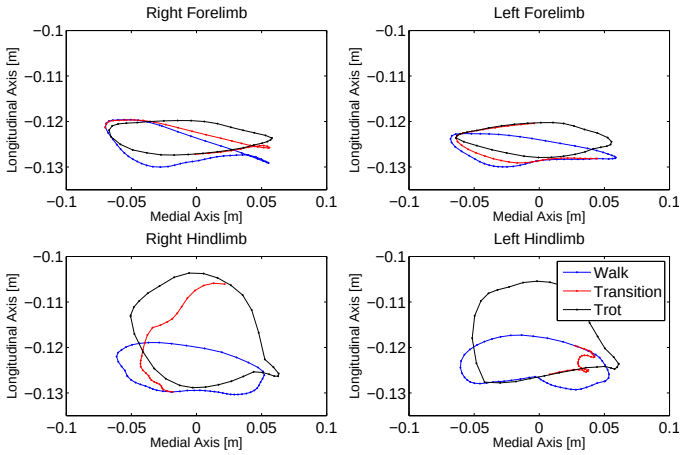

Figure 3.29: The foot trajectories of walk, transition from walking to trotting, and trot

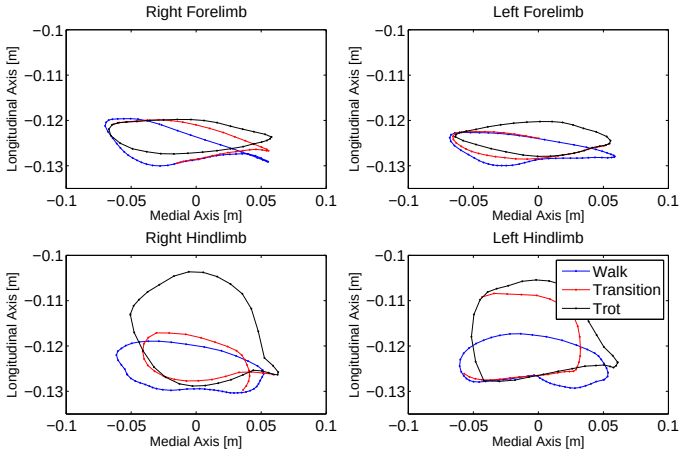

Figure 3.30: The foot trajectories of trot, transition from trotting to walking, and walk

Both types, walk/trot and trot/walk transitions were tested on the compliant quadruped robot. Experiments on scaling the gait in frequency were held as well (scaling factor $m = [1 : 0.5 : 3.5]$). The results of these experiments are reported in the next section.

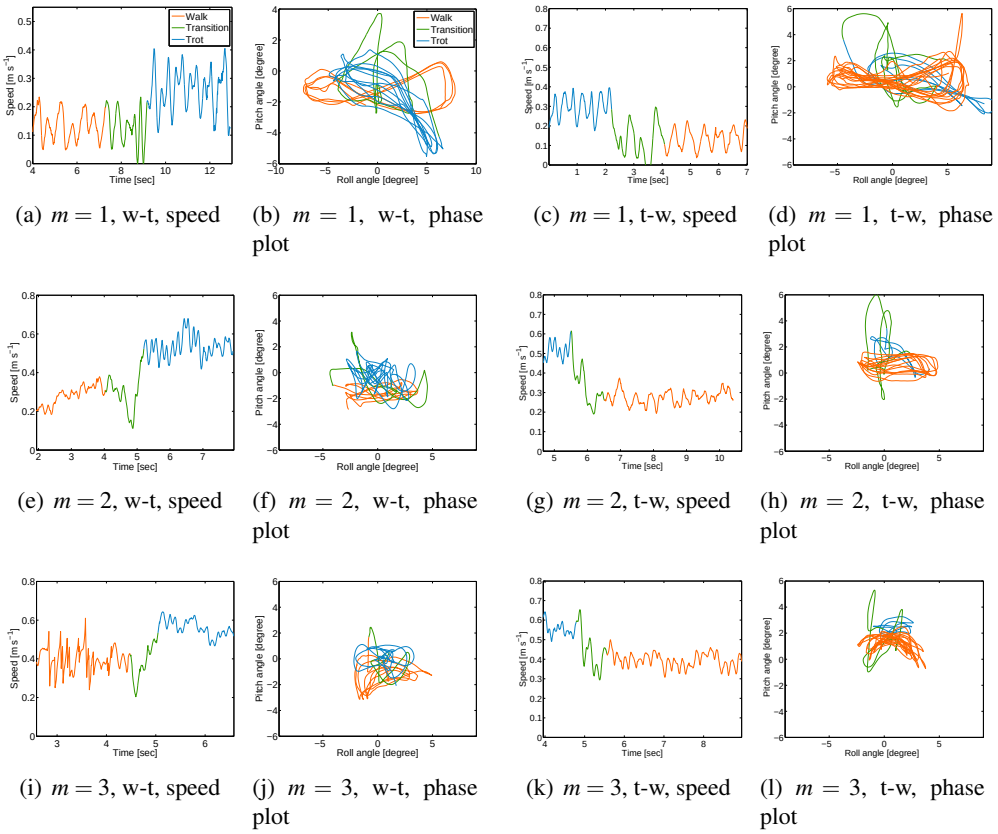

(a) $m = 1$, w-t, speed (b) $m = 1$, w-t, phase plot (c) $m = 1$, t-w, speed (d) $m = 1$, t-w, phase plot

(e) $m = 2$, w-t, speed (f) $m = 2$, w-t, phase plot (g) $m = 2$, t-w, speed (h) $m = 2$, t-w, phase plot

(i) $m = 3$, w-t, speed (j) $m = 3$, w-t, phase plot (k) $m = 3$, t-w, speed (l) $m = 3$, t-w, phase plot

Figure 3.31: Robot gait transition experiments with the *three-quarter* strategy (Table 3.15, plots of forward speed versus time and phase plots of roll and pitch angles. Rows from top to down: frequency multiplier $m = [1 : 1 : 3]$. Left two columns: walk-trot transition (w-t), right two columns: trot-walk transition (t-w). For each run, instantaneous robot speed and roll-pitch data are plotted. Data was recored with the help of a motion capture system, which tracked three markers at the robot's trunk at $f = 240Hz$. Orange trajectories refer to walking gait patterns, green trajectories to gait transition, and blue trajectories to trot-gait patterns. Visible is a general decrease of pitching and rolling angles at increased robot speed. For low speed gait transition, instantaneous robot speed briefly drops to zero, less than 200ms, before it recovers. At higher speed, gait transition caused less prominent speed drops. In ideal cases (e.g. Fig. 3.31(g) and Fig. 3.31(k)) no speed drop is visible, gaits were switched with no speed perturbation to the system.

Experimental Results

The gait transition characteristics of the robot are analyzed by measuring the range of pitch and roll movements for each gait after reaching steady state, and during the transition phase. In addition, instantaneous speed was recorded before, during, and after each transition. Roll and pitch angle phase plots are shown in Figure 3.31. Phase plots in Figure 3.31 are colored according to the commanded gait patterns, blue for trot gaits, orange for walking gait patterns, whilst green lines indicate transition times. The identical color coding was chosen for speed plots. Gait transitions were identified and marked manually by placing start and end with the help of the speed plots, as a first rough approximation. Phase plots and characteristic shapes of walk and trot phase patterns were then used to separate more precisely transition times from steady gait locomotion. Qualitative plots are shown in Figure 3.31.

Frequency multiplication resulted typically in an increase in robot speed from walk to trot. All walk-trot and trot-walk gait transitions on flat ground were run successfully: the robot never stumbled nor fell. However, not all gait transitions worked equally well. One can see this by observing transition times and instantaneous transition robot speed (Figure 3.31). Typically, transitions went more smoothly with higher robot speed. In those cases transition happened more swiftly, and with less speed drop. Independently from the "direction" of the gait transition, stable patterns typically emerged after a transition time of roughly $t = 1.2/1.3s$.

A supplemental analysis was then performed to verify the effectiveness of the proposed method. The performance of the transition method proposed (for both walk to trot and trot to walk, with frequency scaling factor from 1 to 3.5) was compared in terms of transition time to i) the "no transition" case, with a sudden switch from one gait to

Table 3.15: Average transition times (in sec) for three transition strategies: *Proposed method*, *No transition*, and *Not optimal pivot points*. Average was taken over transition times of all multipliers. In average, the proposed method showed shortest transition times. Trot-walk transitions of the *no-transition* strategy had a tendency to produce non-stable walking gait patterns, with increasing pitch and roll angles (transition times only shown for stable runs).

Strategy	Walk-Trot	Trot-Walk
Proposed method	1.2	1.3
No transition	1.7	1.5
Not optimal pivot points	1.4	1.3

the other, and to ii) the case of a transition that happens around pivot points that are not optimal. For the latter we set as transition pivots those points in the walk and trot gaits such that the cumulative distance among the four legs between walk trajectory and trot trajectory is maximal, i.e., in this case Equation (3.11) is modified substituting *min* with *max*.

The gait transition took 26% longer for the "no transition" strategy, compared to the transition method proposed. In the second case (non-optimal pivot points), the transition time was 9% longer. This indicates that the choice of good pivot points improves the quality of gait transition (Table 3.15).

4

An Attractor-Based Whole-Body Motion Control (WBMC) System

The class of Whole-Body Control Systems aims to exploit the full capabilities of redundant robots to achieve a task, and to allow the simultaneous execution of several tasks. With an experience of millennia of evolution, humans are extremely proficient in this. The first two/three years of life represent a fundamental stage for children, since it is in this phase that most of their motor capabilities are developed and refined through a fine and continuous learning process.

If robots can even occasionally outperform humans on the single task (e.g., running, climbing stairs), there is still no example of a robot that can show the same flexibility and adaptability to different scenarios that instead characterize humans.

This Chapter reports on the work done to develop a novel Whole-Body Motion Control (WBMC) System. Nature was a great source of inspiration, and the results of the analysis of human motion described in the previous Chapter were the foundations on

which the proposed WBMC System laid its basis.

4.1 Biological Inspiration

There is a clear evidence that many different human movements, both discrete and periodic, can be reduced to small sets of *primitives*. These modules can also be combined to produce composite movements. The work presented in Chapter 3 on the kinematic Motion Primitives (kMPs) showed this at a kinematic level. Other previous works led to similar results starting from an analysis of the EMGs, e.g., Ivanenko et al [2004, 2005]. These works, and those on CPG [Ijspeert, 2008], seem to indicate that humans are able to control a vast variety of motion through a simple set of modular rules.

From this perspective, Giszter et al [1993] proposed an interesting interpretation: the primitives can be seen not as signals, but as force fields. The authors experimentally validated their thesis on frogs. The idea is fascinating, and allows a more straightforward implementation for the control of robots.

Next Section will present the WBMC System as it was designed. It will be possible to notice that many are the points of contact with what observed in nature and described in Giszter et al [1993].

4.2 The Modular WBMC System Based on Attractors

The WBMC system is a model-based, torque-control framework. It allows simultaneous execution of several tasks, which can be either permanent or temporary. Permanent tasks are such as maintaining balance, while an example of temporary task would be to reach for an object with one hand. Each task is handled by an attractor that generates a torque

command to modify the robot's state toward a preferred one. In a more precise definition, an attractor f is a function having a vector of joint torques as output, which controls a certain quantity that is itself a function of $(q, \dot{q})$, i.e., the state of the system. This concept can be expressed as $\tau = f(g(q, \dot{q}))$. Particularly, the attractor f is a convergent force field, typically the gradient of g with respect to either q or $\dot{q}$, hence $f = \nabla g$, where $\nabla g = \left[\frac{\partial g}{q_1} \cdots \frac{\partial g}{q_n}\right]$, or $\nabla g = \left[\frac{\partial g}{\dot{q}_1} \cdots \frac{\partial g}{\dot{q}_n}\right]$. An attractor converges to a preferred state, locally minimizing g. A specific non-zero desired value $\overline{g}$ can also be imposed. In this case the attractor f is the gradient of the error between g and $\overline{g}$, i.e., $f = \nabla(|g - \overline{g}|)$. This formulation describes the typical nature of an attractor. Small variations were applied in order to adapt this concept to best fit to the specific task, e.g., *MinEff* (Section 4.4.1), *JLim* (Section 4.5).

The overall torque applied to the joints is the linear combination (Figure 4.1) of the torques generated by each attractor, plus a model-based gravity compensation that is described in Section 4.2:

$$\tau = \tau_{GC} + \tau_{ME} + \tau_{MJ} + \tau_{LMC} + \tau_{AMC} + \tau_{JL} + \tau_{EE} + \cdots \tag{4.1}$$

The equilibrium is guaranteed by a set of four attractors that will be presented in Section 4.4. A repulsion from the joint limits has also been developed, and will be described in Section 4.5. Finally, position/force end-effector attractors will be presented in Section 4.6. The modularity of the WBMC system ensures that other attractors can be easily implemented and added to the current ones (e.g., self collision avoidance).

It is also important to notice that each quantity associated to the attractors presented has a stand-alone value, that is independent from the entire WBMC system, and can be easily adapted to be included in other kinds of control systems.

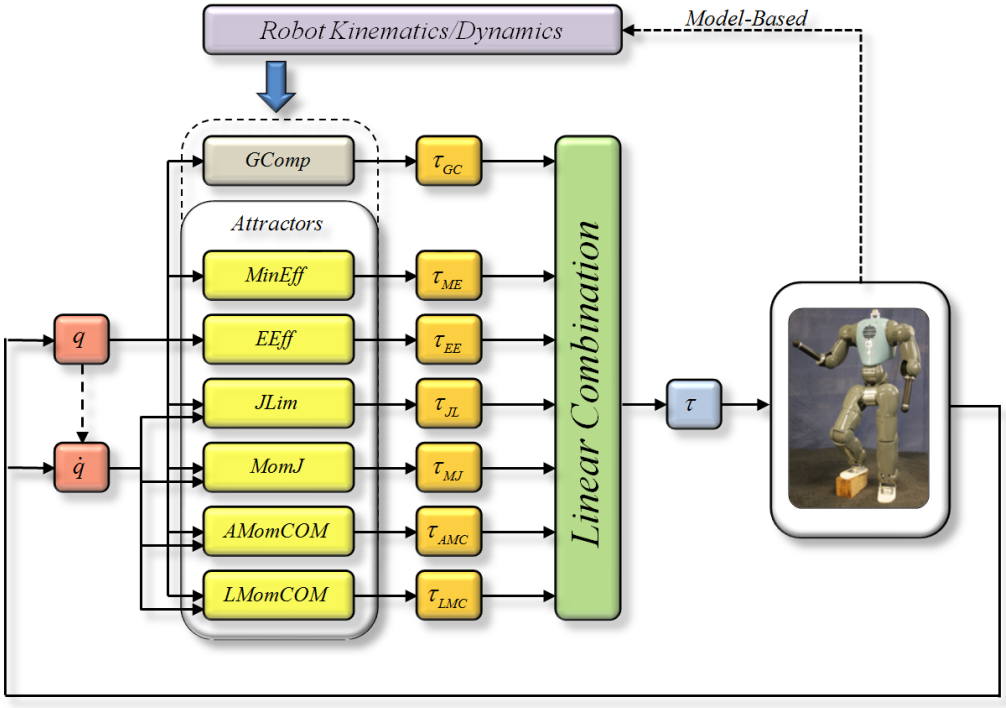

Figure 4.1: The WBMC system is based on a set of *attractors* (yellow blocks), each of which corresponds to a given task. A linear combination of the torques generated by each attractors is applied to perform a whole-body motion. The modular structure of the proposed control system easily allows extensions.

4.3 Gravity Compensation for Free-Floating Base Robots

The WBMC system is based on a set of attractors that affect the robot state to minimize the error with respect to the tasks they are undertaking. They are all closed-loop controls, and for this reason their accuracy at steady-state is affected by constant disturbances, such as the gravitational effects. Therefore, a model-based gravity compensation is applied. This also allows to reduce the weight of the attractors.

It has turned out that the orthogonal decomposition method for gravity compensation of floating-base system [Mistry et al, 2010]; [Righetti et al, 2011] is advantageous due

to its computational efficiency, and its open-loop character. In this approach contacts are considered as rigid, ideal constraints. Other works [Abe et al, 2007]; [Wensing and Orin, 2013] propose more accurate models that also account for unilateral contacts with friction, however they are computationally still too expensive for hard real-time demands.

The full-body COmpliant huMANoid (COMAN) robot was modeled as a 29-dofs system, 6 of which are unactuated and represent the floating base, while the other 23 are the actual joints of the robot. From the fundamental equation of the dynamics of a floating-base robot $M(q)\ddot{q}+C(q,\dot{q})\dot{q}+h(q)-J(q)^T F = S^T\tau$, neglecting the Coriolis term, and considering a static case, the following expression for gravity compensation can be derived [Mistry et al, 2010]; [Righetti et al, 2011]:

$$\tau_{GC}(q) = (N_c(q)S^T)^+ N_c(q)h(q) \tag{4.2}$$

where $N_c(q) = I - J_c(q)^+ J_c(q)$ is the null-space of the contacts with the environment, $J_c(q) = [J_{c1}(q)^T J_{c2}(q)^T \cdots J_{cm}(q)^T]^T$ is the concatenation of the Jacobians of the m contacts, $S = [0_{n\times 6} I_{n\times n}]$ is a selection matrix, with n being the number of active dofs, I is the identity matrix, and $^+$ is the pseudo-inverse operator. $P(q) = (N_c(q)S^T)^+ N_c(q)$ hence projects the $6+n$ torques given by $h(q)$ into n torques to be applied by the active joints to compensate for gravity. Whenever the system is subject to other external forces (e.g., the robot is holding an object, or is being pushed), these can be compensated at the same time adding $J_{ext}(q)^T F_{ext}$ up to $h(q)$, and applying the same projection P.

In order to improve the computational efficiency, P can be reduced to a simpler form.

Expanding the above pseudo-inverse, we get:

$$P = ((N_c S^T)^T (N_c S^T))^{-1} (N_c S^T)^T N_c$$

$$= (S N_c^T N_c S^T)^{-1} S N_c^T N_c$$

Matrix N_c is idempotent: $N_c^T N_c = N_c$, and we get:

$$P = (S N_c S^T)^{-1} S N_c$$

If V_c is the orthonormal basis of the contact null-space, this expression can be further reduced by substituting N_c with $V_c V_c^T$, becoming:

$$P = (S V_c V_c^T S^T)^+ S V_c V_c^T$$

$$= ((S V_c)^+)^T V_c^T \tag{4.3}$$

In the case of $n = 23$ joints, as it is for the COMAN robot, with both feet on the ground, $N_c S^T$ in (4.2) is a (29×23) matrix, while $S V_c$ in (4.3) is a (17×23) matrix. Since the pseudo-inverse is the most expensive operation among those used, Equation (4.3) is used to derive P, to reduce the computational time.

4.4 Equilibrium of a Multibody System

Balance plays a fundamental role in whole-body control. A system that aims to coordinate the simultaneous execution of many tasks is always subject to the necessary

condition that the robot must not fall while performing the desired actions. As already mentioned, ZMP [Vukobratovic and Borovac, 2004] has been the most widely adopted method to guarantee balance over the last decades. This, and other methods [Popovic et al, 2005]; [Goswami and Kallem, 2004] that were proposed more recently, have successfully accomplished this goal, but still represent only a sufficient condition for balancing, and do not capture the full complexity of human balance.

The system proposed in this dissertation aims to be as general as possible, and to not be constrained by any assumption, such as the number of contacts or the conditions of the terrain. For this reason a very basic definition of equilibrium coming from *Classical Mechanics* by Corben and Stehle [1960], page 113, was considered: *"A system of particles is in static equilibrium when all the particles of the system are at rest and the total force on each particle is permanently zero."* This is a very strict definition, but describes clearly what a preferred condition for a system is (i.e., an *attractive* situation).

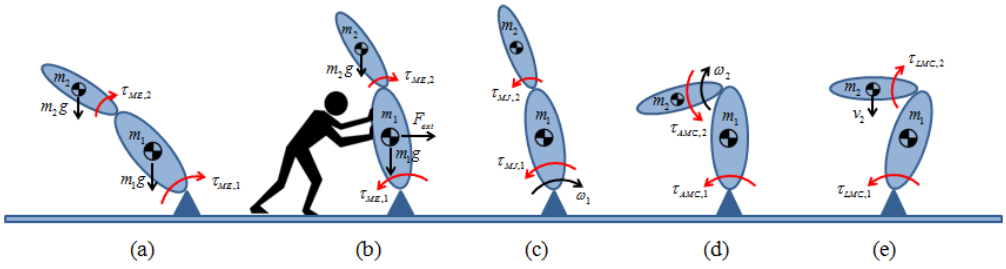

Figure 4.2: The behavior of the WBMC system is not always easy to predict. The torques generated by the *MinEff* attractor in the case of a 2-link fixed-base robot, for instance, aim to bring the robot to a vertical position when gravity is the only external force acting on the robot (a). If another external force is applied (b), instead, the *MinEff* locally searches for a configuration that minimizes all external disturbances. In (c) the effect of the *MomJ* is shown. A positive torque in both joints is generated to compensate for the effects of a negative angular velocity w_1 in joint 1. Similarly, the *AMomCOM* and *LMomCOM* generate a torque in all joints to reduce the velocity of the CoM caused, in this case, by w_2 and v_2, respectively.

In the case of floating-base multi-body systems the equilibrium refers both to the "inter-bodies" condition, and to the state of the system with respect to the inertial frame. The latter is well described by the CoM of the entire system. The safest and most "under control" situation for a robot can be defined by the following terms:

1. the resultant force/torque acting on the system is zero, i.e., $F_{COM} = 0_{6\times1}$, where F_{COM} is the vector of the spacial resultant force projected onto the CoM;

2. the "internal" torques generated by the external forces applied to the system are all zero, i.e., $\tau_j = 0_{n\times1}$, where τ_j is the vector of the joint torques;

3. the system is at rest with respect to the world, i.e., $v_{COM} = 0_{6\times1}$, where v_{COM} is the vector of the spacial velocities of the CoM;

4. the system is "internally" at rest, i.e., $v_j = 0_{n\times1}$, where v_j is the vector of the n joint velocities.

If these conditions were continuously satisfied the robot would be practically unable to act. The execution of a task requires these rules to be compliant: the robot is allowed to leave this preferred state, but never to get too far away from it. Loss of equilibrium means losing control of the robot: intuitively, if the controlled variables (velocities and forces) grow too large, the motors may not be powerful enough to generate the torques required to bring the system back to the equilibrium.

Based on these considerations, a set of attractors has been developed to guarantee that the robot always stays in the neighborhood of the equilibrium.

4.4.1 The Minimum Effort (MinEff) Attractor

Conditions 1 and 2 from the list in Section 4.4 are closely related to gravity (plus external forces) compensation. Whenever they are satisfied, $h(q) + J_{ext}(q)^T F_{ext}$ (contact reaction forces here are considered as external forces) will be equal to zero. This means that, if the system is also at rest (conditions 3 and 4), no torque needs to be applied by the motors to prevent it from starting to move (both internally and with respect to the world frame). This also means that, as the external disturbances grow, a larger torque will be required to compensate for their effect. We define the robot effort as:

$$E = \tau_{GC}^T W \tau_{GC} \tag{4.4}$$

with τ_{GC} compensating for both gravity and any other external force, and where W is a weighting diagonal matrix that can be used to favor specific joints over others. A minimization of the effort E is therefore beneficial not only, as is obvious, to reduce the energy consumption, but also to constrain the robot to a configuration that is closer to the equilibrium. To achieve this task, an attractor to the minimum effort (*MinEff*) was developed. Its expected behavior is the one of a gradient descent, where the gradient of the effort can be derived as:

$$\nabla E = \left[\frac{\partial E}{\partial q_1} \cdots \frac{\partial E}{\partial q_n} \right]^T \tag{4.5}$$

It can be verified that the behavior of an attractor of the kind $\tau_{ME} = -k_{ME} \nabla E$ can be further improved.

Applying it to a 1-link system attached to a fixed base by a rotational joint (Figure 4.3), with only gravity acting upon it, the link will be forced to move to a vertical posi-

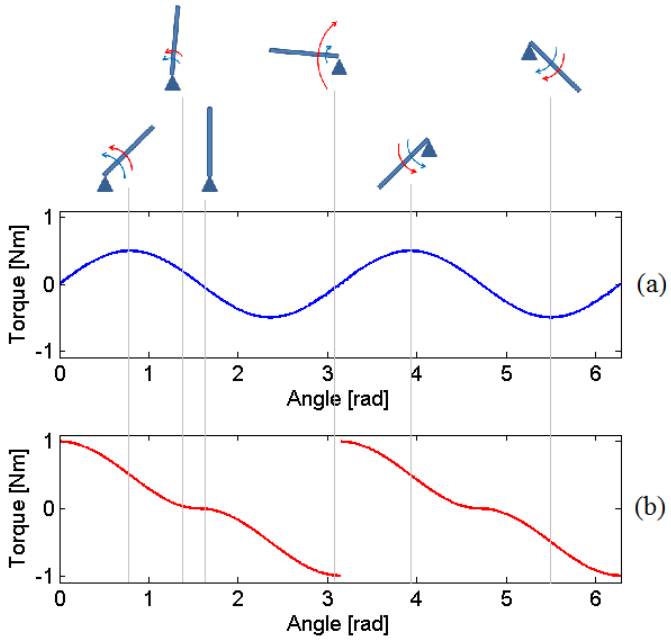

Figure 4.3: The blue line in (a) represents the torque generated by the *MinEff* if $\tau_{ME} = -k_{ME}\nabla E$ in the case of a 1-link fixed-base system. The torque generated always has a correct direction, but when the link is almost horizontal (close to π in the example) the absolute value of the torque is small. A preferred behavior is depicted in graph (b) (red line), where $\tau_{ME} = -k_{ME} sign(\nabla E) \circ (\tau_{GC} \circ \tau_{GC})$. The direction is still coming from the gradient of effort E, but the absolute value monotonically increases as the angle diverges from the optimal configuration.

tion, either up or down ($\pm\pi/2$ if the zero is set at the link being horizontal). These two configurations are both minima in terms of effort, since link and gravity are parallel. As the angle changes from $\pm\pi/2$ to 0 (or $\pm\pi$), the effort E will increase proportionally to the squared cosine of the angle. The gradient descent, hence, indicates the correct direction of movement. The absolute value of ∇E, though, is not monotonically increasing between $\pm\pi/2$ and 0 (or $\pm\pi$). If we consider the upper right quadrant, for instance, ∇E grows from zero, when the angle is $\pi/2$, to a maximum, when the angle is $\pi/4$, and then decreases again to zero, when the angle is 0 (the same applies to the other quadrants).

If we set $\tau_{ME} \propto \nabla E$, then a small torque will be generated when the link is almost horizontal, while a bigger corrective torque is expected as the robot moves away from the equilibrium.

A better formulation of the MinEff attractor is thus:

$$\tau_{ME} = -k_{ME} sign(\nabla E) \circ (\tau_{GC} \circ \tau_{GC}) \tag{4.6}$$

where the operator $\circ$ is the element-wise Hadamard product. Two discontinuities are at 0° and 180°. Between these two angles (that represent the maximum effort configurations) the behavior is similar to that of a quadratic spring with equilibrium at $\pm\pi/2$. Tuning the weight k_{ME} produces more conservative or more relaxed behaviors. It is important to notice that in more complex cases (many dofs, external forces, etc) the minimum effort configuration is not known as it is in the trivial example of the 1 link system (Figures 4.2(a) and 4.2(b)). The *MinEff* attractor performs a local search, and keeps modifying the configuration until a minimum is reached.

4.4.2 The Joint Momentum (MomJ) Attractor

One of the conditions for system equilibrium is that all joint velocities are zero (condition 4 from the list in Section 4.4). Intuitively, this attractor is expected to behave as a damper. There are disadvantages, however, in simply setting this attractor as $\tau_{MJ} = -k_{MJ}\dot{q}$. The first is that each joint connects two subsystems that have an inertia that is typically different from the inertia seen by other joints. A unique k_{MJ} would not fit all cases. A specific k would have to be associated to each joint, and consequently this leads to a difficult tuning problem. The second problem to be considered is that in a multi-dofs system each joint is affected by the motion of the other joints to which it is connected: it

would not be accurate to treat each joint as if it was independent from the others.

These considerations triggered the introduction of the concept of *joint momentum*, defined as:

$$h_j = M\dot{q} \tag{4.7}$$

where M is the inertia matrix of the robot. The quantity h_j has been rarely exploited to control humanoid robots, although recently Orin et al [2013] have described its relation with other momenta.

The *MomJ* attractor is therefore defined as:

$$\tau_{MJ} = -k_{MJ}(M\dot{q}) \tag{4.8}$$

It depends on the joint velocities (Figure 4.2(c)), and attracts the system to a zero joint momentum state.

4.4.3 The Linear and Angular Momenta about the Center of Mass (MomCOM) Attractors

The *MinEff* and *MomJ* attractors control the quantities described at points 1,2, and 4 from the conditions list in Section 4.4. Whenever the system is in rigid, ideal contact with the environment, if the joint velocities are zero, the CoM velocities are also zero (condition 3). Even not considering the case of no contacts (though not so unusual, e.g., flight phase in running or jumping) having a direct control on the CoM velocities is fundamental for balance. There are situations where increasing the momentum at a certain specific joint can even be desirable, for instance to compensate for a large momentum in another joint, and reduce the overall momentum of the system. In the

formulation proposed in Orin and Goswami [2008]; Orin et al [2013], the linear and angular momenta about the CoM are treated as a unique quantity (i.e., the *centroidal momentum*, a fundamental physical quantity for the control of a humanoid robot [Kajita et al, 2003b]; [Ugurlu and Kawamura, 2010]; [Wensing et al, 2013]). In the WBMC system, instead, it was decided to keep them separated with a dedicated attractor: this allows a priority to be imposed between the two (as in Lee and Goswami [2012]). It can for instance be preferable to have a rigid control over the linear momentum, and be willing to be more relaxed on the angular momentum, or vice versa. The desired behavior can be accomplished by properly tuning the weight of the attractors.

The linear and the angular momenta about the CoM are calculated, respectively, as follows:

$$h_{g,lin} = \left(\sum_i m_i J_{T,COM,i} \right) \cdot \dot{q} \tag{4.9}$$

$$h_{g,ang} = \left(\sum_i m_i \tilde{r}_{COM,i} J_{T,COM,i} + I_i J_{R,i} \right) \cdot \dot{q} \tag{4.10}$$

where m_i is the mass of the i-th link, $J_{T,COM,i}$ is the translational part of the Jacobian to the CoM of the i-th link, $\tilde{r}_{COM,i}$ is the skew-symmetric form of $r_{COM,i}$, the relative position of the CoM of the i-th link, I_i is the inertia of the i-th link, and $J_{R,i}$ is the rotational part of the Jacobian to the end-effector of the i-th link.

In the case where the robot is standing in place the linear momentum is expected to be close to zero (Figure 4.2(e)), while a non-zero reference can be set when the robot is, for instance, walking. If $\bar{v}$ is the vector of the desired instantaneous CoM velocity, the desired linear momentum can be indicated as $\bar{h}_{g,lin} = \bar{v} \sum_i m_i$. The *LMomCOM* attractor

can therefore be defined as:

$$\tau_{LMC,i} = -k_{LMC} \frac{\partial(|h_{g,lin} - \overline{h}_{g,lin}|)}{\partial \dot{q}_i} \tag{4.11}$$

The preferred angular momentum, instead, is typically always zero (Figure 4.2(d)). The *AMomCOM* attractor, hence, can be expressed as:

$$\tau_{AMC,i} = -k_{AMC} \frac{\partial(|h_{g,ang}|)}{\partial \dot{q}_i} \tag{4.12}$$

Whenever a non-zero angular momentum reference is desired, this can be easily set by modifying Equation (4.12) accordingly.

4.5 Repulsion from the Joint Limits (JLim)

Maintaining equilibrium is not the only permanent task for a robot. It is vital to have accurate control on the motion of the robot near the joint limits to prevent the robot from damaging itself. A special attractor was designed to achieve this purpose: unlike the other attractors, this is more the case of a *"repeller"* from undesired configurations (i.e., joint limits). In order to not affect the behavior of the other attractors unnecessarily, a piecewise function was used, such that $\tau_{JL} = 0$ as long as the measured joint angle is not close to one of the limits. For each joint i, a positive (θ_i^+) and a negative (θ_i^-) threshold value are set. This functions both a safety margin $0.0 \leq \Delta \leq 0.5$, and the joint range $(q_i^+ - q_i^-)$. In detail, $\theta_i^+ = q_i^+ - \Delta(q_i^+ - q_i^-)$, and, similarly, $\theta_i^- = q_i^- + \Delta(q_i^+ - q_i^-)$. The joint range is hence divided into three parts by θ_i^- and θ_i^+: it works like a repulsive quadratic spring, linear damper, when q_i exceeds the thresholds, and has no effect otherwise.

If $q_i < \theta_i^-$, then:

$$\tau_{JL,i} = k_{JL,S}\left(\frac{q_i - \theta_i^-}{q_i^- - \theta_i^-}\right)^2 - k_{JL,D}(\dot{q}_i) \tag{4.13}$$

When, instead, $\theta_i^- \leq q_i \leq \theta_i^+$:

$$\tau_{JL,i} = 0 \tag{4.14}$$

Last, if $q_i > \theta_i^+$, then:

$$\tau_{JL,i} = -k_{JL,S}\left(\frac{q_i - \theta_i^+}{q_i^+ - \theta_i^+}\right)^2 - k_{JL,D}(\dot{q}_i) \tag{4.15}$$

To avoid a "sticky" effect, $\tau_{JL,i}$ in Equation (4.13) always has to be greater than or equal to zero, while in Equation (4.15) it has to be less than or equal to zero.

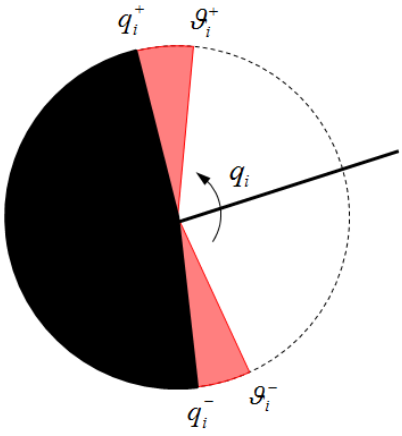

Figure 4.4: The JLim repeller works like a repulsive quadratic spring, linear damper, when q_i approaches one limit, and has no effect otherwise.

4.6 The Position/Force End-Effector (EEff) Attractors

The end-effector attractors work similar to the operational space formulation [Khatib, 1987] for underactuated systems [Sentis, 2007, 2010], to the impedance control [Hogan, 1985], and to the virtual model [Pratt et al, 2001]. An end-effector force is generated from the error in the end-effector position and velocity (linear spring and damper): $F_{EE} = k_{EE,S}(\bar{x}_{EE} - x_{EE}) + k_{EE,D}(\dot{\bar{x}}_{EE} - \dot{x}_{EE})$. The joint torques are derived from F_{EE} through the end-effector Jacobian J_{EE}, and the projection P from Section 4.3:

$$\tau_{EE} = P(J_{EE}^T F_{EE}) \tag{4.16}$$

This formulation can be easily modified to directly track a reference force instead of a position, for instance when a well determined force has to be applied in a contact.

4.7 Experimental Results

The effectiveness of the proposed method was initially tested in simulation, and the results are reported in Section 4.7.1. Once the reliability of the system was verified, the WBMC was used to torque-control the real COMAN humanoid robot (Figure 4.5) [Moro et al, 2011]; [Tsagarakis et al, 2013]. Results are reported as proof of concept in Section 4.7.2.

4.7.1 Tests in Simulation

The validity of the proposed approach was first tested in simulation. The 29-dofs model of COMAN was developed in Robotran [Dallali et al, 2013], including the information on the full dynamics of the robot obtained from the CAD of the real prototype (Figure

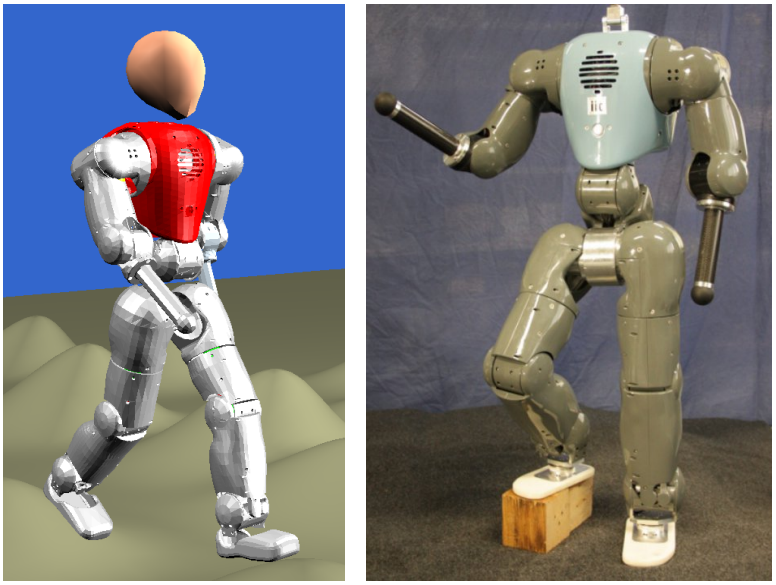

(a) (b)

Figure 4.5: (a) The Robotran model of the COMAN robot (the head was added for a visualization purpose only), and (b) the 'light blue version' of the real COMAN

4.5(a)). The focus of the tests was on the interaction between the attractors responsible for the equilibrium, i.e., *MinEff*, *MomJ*, *MomCOM*. The following example shows the behavior of the robot when subject to the effect of these attractors, together with the gravity compensation term, and the repulsion from the *JLim*.

The weights of the attractors were adjusted to match the expected behavior of the system. The simulation starts with COMAN standing in place with bent knees, i.e., in a non-minimum effort configuration. All initial joint velocities are set to zero. The WBMC starts controlling all joints of the robot at $2sec$. The combined effect of the attractors results in a stable straightening of the legs toward a balanced, minimum effort configuration in about 1 second. Figure 4.6 shows the results for the right knee. Particularly, in Figure 4.6(a) the torques generated by the different attractors are reported. It can

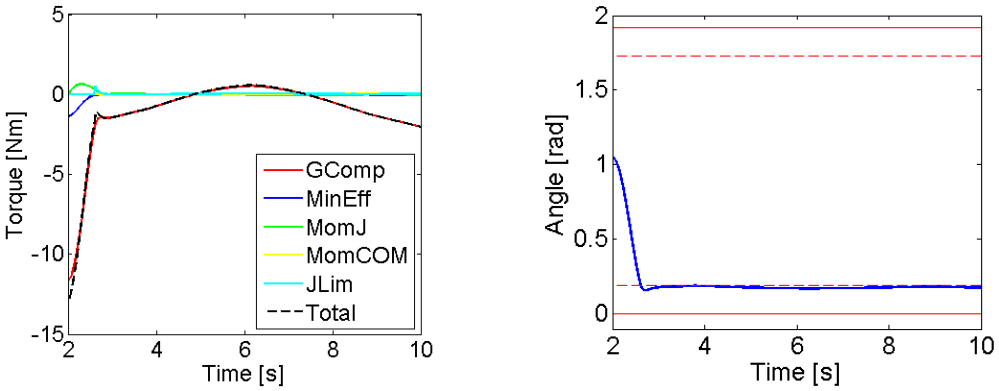

(a) (b)

Figure 4.6: (a) Right knee torques generated by the attractors. The *MinEff* contributes to straighten the knee to a configuration that requires a torque that is significantly smaller to compensate the effects of gravity. The *MomJ* behaves like a damping on the joint velocity, while the effects of the *MomCOM* are negligible in this case. The *JLim*, instead, produces a torque that prevents the joint limit to be reached. This is clearer in (b), where the knee angle is shown. It can be noticed that the knee straightening happens in less than 1 second, and that the joint limit is never reached. This reduces the risk to damage the robot itself.

be noticed that the torque required for compensating gravity reduces from about $12Nm$ (in absolute value) to less than $2Nm$. This occurs as the torque generated by the *MinEff* (blue line) contributes to the straightening of the legs. The *MomJ* (green line) generates a torque with sign opposite to the velocity, acting as a damping. The *MomCOM* (yellow line) have a negligible effect in this case. It can also be noted that a small peak of torque is generated by the *JLim* (light blue) as the knee approached its limit. This is clearer in Figure 4.6(b), that shows the trajectory of the knee joint angle: from about $1rad$ the knees reaches fast the threshold of approximatively $0.19rad$. The knee is not allowed to stretch much more to avoid the reaching of the joint limit, i.e., $0rad$. The knee angle stabilizes around $0.18rad$ with negligible oscillations.

The behavior of the overall system can be appreciated from Figure 4.7, that shows how the controlled measures change as the WBMC affects the state of the robot. The effort of the robot significantly reduces to a value that is 10 times smaller than the initial. The momenta, instead, initially grow as the robot starts moving, and then reduce again to very small values. The small peak in the *MomJ* graph around 3*sec* is caused by the *JLim* repulsion.

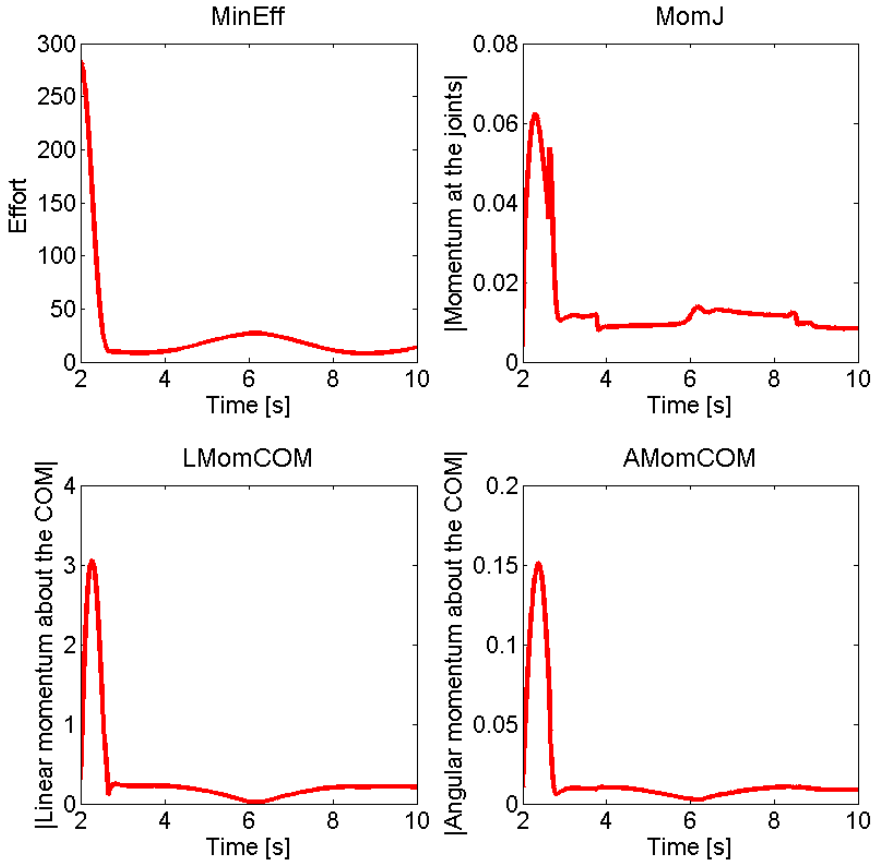

Figure 4.7: The four graphs above show how the values of the measures that are controlled in the simulation change over time. Particularly, the effort reduces to a value that is ten times smaller than the initial. The momenta, instead, initially grow as the robot starts moving, and then reduce again to small values with negligible oscillations.

4.7.2 Tests with the COMAN Robot

As the reliability of the WBMC system was verified in simulation, some preliminary tests were performed with the real full-body COMAN robot (Figure 4.5(b)) [Moro et al, 2011]; [Tsagarakis et al, 2013]. The reference torques generated by the WBMC were tracked in each joint by a PI torque control loop at $1kHz$. Few are the examples of torque controlled humanoid robots in the state-of-the-art. Among these, successful instances are Stephens and Atkeson [2010]; Ott et al [2012]; Herzog et al [2013]. In this first test, the waist pitch and roll joints are controlled by the WBMC, the shoulder pitch and roll of the right arm are zero-torque controlled, and all other joints are controlled in position (Figure 4.8 shows some snapshots from the video of the experiments with COMAN). In this simplified scenario the effect of the *MomCOM* is not significant: for this reason only the gravity compensation term, the *MinEff* attractor, and the *MomJ* attractor are activated. The weights of the attractors are set basing on the experience in simulation.

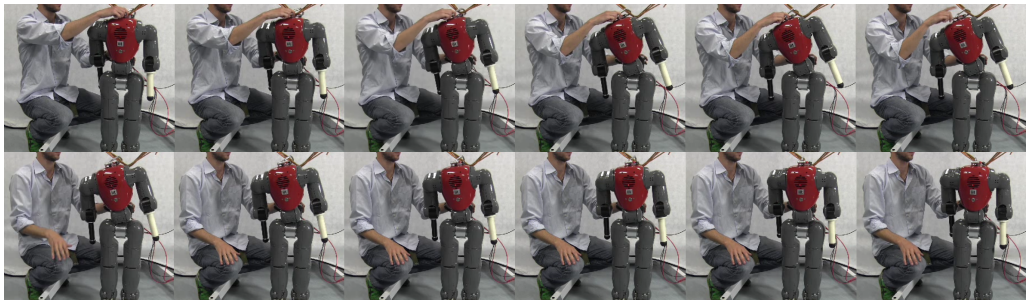

Figure 4.8: Snapshots from the video of the experimental validation of the WBMC with the COMAN robot (taken at $2Hz$). The full video can be found at the link: `http://www.youtube.com/watch?v=MxFuXWzi6lg`. In this instance the robot configuration is perturbed by forcing the waist roll joint to change its angle. As the robot is released the *MinEff* brings the robot back to a vertical, minimum effort configuration. The resulting motion is damped by the *MomJ* attractor, that prevents the velocity to grow uncontrolled.

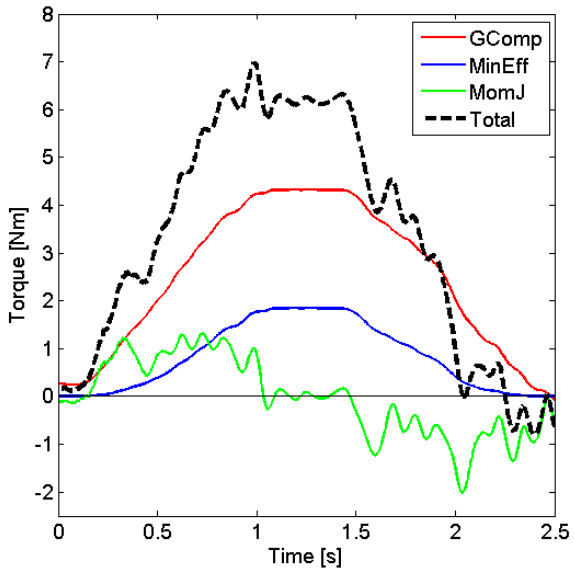

Figure 4.9: As the configuration of the waist pitch joint is perturbed, the torque required to compensate gravity grows to about $4Nm$. Also the torque generated by the *MinEff* increases, as it attempts to bring back to robot to its preferred configuration. The velocity of the motion also produced a damping torque by means of the *MomJ*. This drops down to zero when the robot is maintained in the position. As the robot is released, instead, the *MinEff* brings it back to the minimum effort configuration. To verify this, it can be noticed that the torque generated by the gravity compensation term reduces as well. The torque generated by the *MomJ* has a negative sign in this phase, since the joint velocity is now positive.

This experiment starts with COMAN in the minimum effort configuration, with zero joint velocities. An external disturbance perturbs the equilibrium, with the WBMC opposing to this imposed displacement. At release, COMAN moves back to its preferred state. Figure 4.9 shows the results obtained for the pitch waist joint. Between $0s$ and $1s$ the robot is pushed forward. As a consequence, the torque required to compensate the effects of gravity grow to about $4Nm$. The *MinEff* grows as well, as it tries to bring the robot back. Also the *MomJ* is pushing back, in a direction that is the opposite of the joint

velocity. The robot is kept in a bent configuration for $0.5s$ (between $1s$ and $1.5s$): both gravity compensation and *MinEff* remain constant, while the torque generated by *MomJ* drops down to zero, since there is no joint velocity. The robot is then released, and the *MinEff* brings it back to the preferred configuration in $1s$ (between $1.5s$ and $2.5s$). As an effect, also the gravity compensation decreases. In this last phase, instead, the *MomJ* is pushing forward, behaving as a damping on the joint velocity.

It can be noticed that the torques generated to compensate gravity, and by the *MinEff* are very smooth. The *MomJ*, instead, is more noisy: this is because this measure depends on the joint velocity, that is derived numerically from the joint angle.

5

Discussion

Developing a good, reliable Whole-Body Control is fundamental for taking the next big step in robotics, that is to bring robots in the real world. The solutions in the state-of-the-art are still far from what we can see in nature. Humans and animals represent an example roboticists have to take inspiration from to develop robots that are able to operate in dynamic environments, in interaction with other robots and humans.

The study described in Chapter 3 aimed to understand better the way humans are able to perform multiple, complex tasks. The kinematic Motion Primitives (kMPs) represent an evidence of an underlying CPG, observed at a kinematic level. The results presented confirm the findings of researchers in Motor Control, e.g., Ivanenko et al [2004, 2005], that performed a similar analysis starting from recorded EMG signals.

A first interpretation of *biological-inspiration* is to try to directly transfer the features observed in nature to the artificial system that is being controlled. An example of this solution was described in Section 3.5. The results were satisfactory: COMAN could perform a stable kMPs-based walking that was more human-like than it typically is when

engineered trajectories are used, and this is because the main features of human walking were directly transfered to the robot walking (e.g., knee straightening, wide CoM vertical displacement). It was nevertheless shown that this methodology is not always straightforward, and it is not easy to generalize and extend the results obtained on the single gait to valid gaits with different characteristics (e.g., step length, foot clearance, stepping frequency).

An alternative solution for biological-inspiration is to take advantage of what observed in nature, trying to understand how human control really works, and to reproduce the same behavior on robots. This is the case of the proposed Whole-Body Motion Control (WBMC) System that was presented in Chapter 4. The theory proposed by Giszter et al [1993] with primitives defined as force fields was a source of inspiration for developing the attractors that are at the basis of the WMBC.

The work on the kMPs was important for designing the WBMC. Two are the main characteristics that were observed in humans and reproduced in the proposed control system for robots. The first is *simplicity*: the goal was to identify a few, simple rules that were sufficient to handle a majority of possible different situations. The second feature is *modularity*: inspired by what was observed in humans, the WBMC was developed based on modules, i.e., the attractors. These can be combined to scale up and obtain the desired behavior.

5.1 Comparative Analysis between WBMC and Other Methods

The attractor-based Whole-Body Motion Control (WBMC) System presented in this dissertation aimed to represent a further step toward having robots operating in the real world. Other Whole-Body Control solutions were available in the state-of-the-art, and alternative solutions could have been adopted.

In this Section the WBMC System is compared to these other methods in order to point out the main strengths and weaknesses of the solution proposed, and to motivate the decisions taken.

Nullspace-based Systems

A vast majority of the whole-body control systems in the state-of-the-art is based on the nullspace formulation. This solution is very solid, but seems to be too conservative in certain scenarios. The WBMC system aims to provide a more flexible solution, particularly in the following situations:

- **Task feasibility**

  The nullspace-based systems are by definition constrained by the redundancy availability. Whenever it is not possible to execute a task in the nullspace of the higher priority tasks, this is declared unfeasible and discarded, as explained in Sentis [2010], Section 3.2.4. In most of the cases, though, a relaxation of the higher priority tasks (e.g., balance) would not affect the correct execution of the same tasks, allowing at the same time to complete all lower priority tasks.

- **Dynamic stack of tasks**

  It is likely that the prioritization of the tasks does not remain unvaried at all times. A new task may need to be added, a completed tasks should be removed, and the order of the tasks in terms of priority could possibly change. This introduces the need for a transition strategy, to avoid undesired discontinuities. There is no straightforward solution to this in the nullspace formulation. A recent work by Jarquín et al [2013] analyzed all possible solutions and concluded that the most practical one is to put all intermittent tasks in the same priority level, and to switch from one to the other using weights. If you want to be able to modify the priority of any task, then you will have to put all tasks in the same priority level with different weights, i.e., WBMC system.

Potential Fields

There is only a slight, technical difference between WBMC and the classical potential fields:

- **Velocity-based domain** Typically a potential field is generated as a function of the configuration of the robot (i.e., position only). In the WBMC system each attractor generates a convergent force field that depends on the state of the robot (i.e., positions and velocities).

The concept, though, is the same, and for this reason it makes sense to say that the attractors generate a sort of potential fields. It was anyway decided not to use this term, simply to be as general as possible. The only required feature for the attractors is that the torque/forces they generate are convergent.

Optimization with Unique Objective Function

A typical approach in optimization is to define a unique objective function to be minimized, possibly comprising many tasks. In the case, for instance, in which a gradient descent is used, this solution directly generates an overall torque vector. Conceptually the WBMC follows an opposite philosophy: all the attractors are independent one from the other, and each of them outputs a torque vector. The overall torque is computed at a later stage, combining the output of the individual attractors. From a practical point of view few are the differences between these two approaches:

- **Unique descent technique** The *unique objective function* solution constrains the choice of a unique technique to descend the function. In the WBMC system you can choose how to locally minimize the error on the single task depending on the desired behavior of the overall system.
- **Velocity-based domain** Some of the attractors (e.g., momenta about the CoM) are designed to descend the gradient defined as the partial derivatives with respect to the joint velocities (not positions). It would probably be not trivial to combine position-based attractors, and velocity-based attractors in the same unique objective function to be minimized.

Final Notes

It is nevertheless possible to reduce the WBMC system to behave like the other foremen-tioned methods:

- If the ratio between the weights of two attractors is very high, the resulting behavior can be approximated to what happens in the nullspace-based systems with the

two tasks being in different priority levels.

- If all attractors are defined as a function of position only, then the system behaves as a classical potential field.
- If the previous condition lasts, and all attractors use the same local search criterion (e.g., gradient descent), then it is possible to write the equivalent *unique objective function* solution.

6

Conclusions

The work presented in this dissertation aims to contribute to the evolution of the state-of-the-art in Whole-Body Control, with a long term goal of providing humanoids those skills that are necessary to operate in dynamic real world environments.

Particularly, a robotic control system can be included in the class of Whole-Body Controls whenever i) it exploits the full capabilities of the entire body of a redundant robot to achieve a task, and ii) allows the simultaneous execution of multiple tasks.

A common trend in this research field is to define a task prioritization in a hierarchical manner. This approach was first proposed by Khatib [1987], and extended to floating-base robots by Sentis [2007, 2010]. Several related works, a description of which is provided in Section 2.2, contributed to improve this methodology, while maintaining unvaried the underlying nullspace structure.

This solution proved effective in most of the scenarios tested. There are cases, though, when the system is pushed to the limit, that show how the rigid constraints imposed in this approach represent a serious limitation. For this reason an alternative

and more flexible solution based on the so-called *attractors* is proposed.

The Whole-Body Motion Control (WBMC) System was inspired by what observed in nature. A first part of this dissertation (Chapter 3) is dedicated to the analysis of human motion, and the work described resulted in the identification of the *kinematic Motion Primitives (kMPs)*. These kMPs are invariant waveforms at the basis of both periodic and discrete motions. The same kMPs can be combined to produce more complex motions that are a combination of discrete and periodic movements. These findings confirm what hypothesized in the well known theory of CPG.

As a first, direct application, the kMPs of periodic motion were used to generate by reconstruction a human-like walking that was successfully tested with the COmpliant huMANoid COMAN. It was observed that the dynamic gait obtained, with knees straightening up to less than 5°, produced a significant deflection of the springs in the actuation units.

This simple observation triggered a research aimed to verify that compliance can be beneficial in terms of energy efficiency. The kMPs-based gait was scaled in frequency in a range from 0.5 Hz to 1.25 Hz. It was shown that when the robot "walks in the resonance frequency" (i.e., the gait frequency is close to one of the main resonance frequencies of the mechanism) the springs contribute with about 15% of the work required to track the reference trajectories, by storing and releasing elastic energy at the right time.

The results obtained with the work on human kMPs were then extended to quadrupedal locomotion. A set of kMPs was extracted from recorded data of a horse walking, trotting, and galloping on a treadmill. The kMPs identified were then used to generate horse-like gaits that were tested with the compliant quadruped Cheetah-Cub. Walk and trot were subsequently scaled in frequency, and a optimal gait frequency was identified for each

of these two gaits.

A gait transition strategy was also proposed: walk-trot transition, and trot-walk transition were successfully tested with the Cheetah-Cub robot.

As discussed in Chapter 5, the analysis related to kMPs was a precious source of inspiration, and helped defining which were the features that it was important to reproduce in the Whole-Body Motion Control (WBMC) System that was proposed and described in Chapter 4. This novel WMBC System is based on attractors, that are defined as "atomic control modules that affect the state of the robot driving it towards a more preferred one". Each controlled task is associated to an attractor.

A computationally efficient gravity compensation for floating-base systems was derived starting from the work by Mistry et al [2010]; Righetti et al [2011]. This open-loop term sums up to the torques generated by the attractors, helping improving the accuracy of the motion that is generated.

Balance, of course, plays a fundamental role in Whole-Body Control. The proposed approach is to take a step back to a basic definition of equilibrium coming from classical mechanics. A set of attractors was then designated to maintain the system in the neighborhood of this equilibrium condition. More in detail, one attractor is responsible for the minimization of the effort of the robot's joints. A second attractor controls the joint momentum, a measure that was rarely used in the control of robots, and that was recently defined by Orin et al [2013]. Last, attractors on the linear and angular momenta about the CoM were developed.

These attractors, together with the joint limit repulsion and the attractors on the end-effectors, represent the current implementation of the WBMC System. The modular structure of the system proposed allows easy extensions.

The WBMC was first tested in simulation, and then applied to control the torque-controlled COMAN robot.

6.1 Future Work

There are several possible extensions that will be investigated in the near future to extend the research presented in this dissertation.

For what concerns the work on the kMPs it was shown that the main limitation to their direct application to generate robot motion is the difficulty faced to generalize the results obtained on the single gait to different gaits. A possible solution to this issue is provided by the learning methods, and their effectiveness in this scope will be verified soon.

The research on WBMC, instead, is open to several possible improvements. A first instance is the gravity compensation adopted, that considers all contacts as rigid and ideal. This, of course, is not the best possible solution, and alternatives will be investigated.

Other attractors will also be developed, an example of which is the one responsible for self collision avoidance.

Further testing with the COMAN robot has also already been scheduled, to validate the system in more complex scenarios involving multiple tasks. As the test scenarios become more complex, though, it will also be more complicated to properly tune the weight of the attractors. For this reason it will be necessary to define more systematic criteria for automatic tuning, and solutions in this direction will be verified.

Another important extension is to include stepping/walking capabilities in the WBMC System. This necessarily requires a prediction on the state of the robot in a short horizon,

and needs to be handled accordingly.

Related to this is a possible research to define where and when to set and release a contact with the environment in order to better control the forces acting on the entire system.

Last, the WBMC System is thought to control a robot and maintain it in a state that is close enough to a equilibrium condition. There are cases, though, such that external disturbances may unavoidably compromise balance. In these situations the WBMC should be disabled, and a safe fall module should take its place. This extension would represent a further step that still needs to be taken to have robots that are sufficiently independent to safely operate in the real world.

Appendix A

Curriculum Vitae et Studiorum

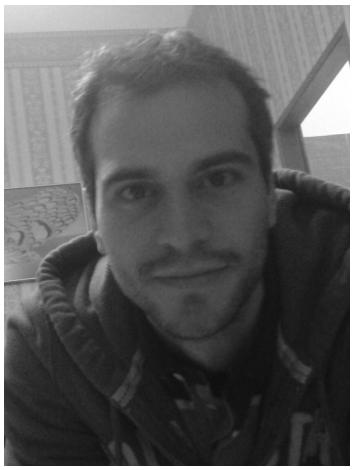

Last Name, First Name	Moro, Federico Lorenzo
Affiliation	Humanoids & Human Centered Mechatronics Lab
	Department of Advanced Robotics
	Istituto Italiano di Tecnologia (IIT)
Date and place of birth	May 10th, 1985 in Milano, Italy
Nationality	Italian
Email	federico.moro@iit.it

A.1 Short Bio

Federico L. Moro received his Bachelor's degree (2007) and Master's degree (2010) in Computer Engineering from Politecnico di Milano, and his Master's degree (2010) in Computer Science from University of Illinois at Chicago, with theses on the control and energy optimization of locomotion of the humanoid robot LARP. In these years he also collaborated with the Institute Mihailo Pupin of Belgrade.

In 2011 he joined the Department of Advanced Robotics, Istituto Italiano di Tecnologia (IIT) as a PhD Student, where he has been working on the motion control of COMAN. His current research includes the work on the kinematic Motion Primitives (kMPs), aimed at transferring human skills to the COMAN robot. This work has also been extended to quadrupedal locomotion in collaboration with EPFL. He has also been working on the development of a Whole-Body Motion Control (WBMC) system for humanoid robots, jointly with the Honda Research Institute.

A.2 Detailed Bio

May 1985	Federico Lorenzo Moro was born in Milano, Italy
Sep 2007	He received his **Bachelor's degree** in **Computer Engineering** from **Politecnico di Milano (PoliMi)**, Italy. Thesis Title: *"Analisi e Sviluppo di un Modello per la Camminata Dinamica di un Robot Bipede"* (Analysis and Development of a Model for the Dynamic Walking of a Biped Robot) Advisor: *Dr. Ing. Michele Folgheraiter*
Jul 2009	He was hosted for a period of **joint research and collaboration** at the **Robotics Laboratory, Institute Mihailo Pupin (IMP)**, Belgrade, Serbia, by invitation from *Prof. Aleksandar Rodić* and *Prof. Duško Katic*

Aug 2010	He received his **Master's degree** in **Computer Science** from **University of Illinois at Chicago (UIC)**, USA. Thesis Title: *"A Systematic Analysis of Energy Consumption of Bipedal Walking with the Aim of Designing a Humanoid Robot"* Advisors: *Prof. Miloš Žefran* and *Prof. Giuseppina Gini*
Aug 2010	He was selected to participate to the **JAIST International Summer School** *"Locomotive and Cooperative Robotic Systems"*, in Kanazawa, Japan
Dec 2010	He received his **Master's degree** in **Computer Engineering** from **Politecnico di Milano (PoliMi)**, Italy. Thesis Title: *"Design and Intelligent Control of an Energy-Efficient Humanoid Robot"* Advisors: *Prof. Giuseppina Gini and Prof. Miloš Žefran*
Jan 2011	He joined the **Department of Advanced Robotics, Istituto Italiano di Tecnologia (IIT)**, Genova, Italy as a **PhD Student** (Advisors: *Dr. Nikos G. Tsagarakis* and *Prof. Darwin G. Caldwell*). He is currently working on the motion control of the **COMAN robot**
Jul 2011	He was selected to participate to the **ETHZ International Summer School** *"Dynamic Walking and Running with Robots"*, in Zurich, Switzerland
Jul 2011	He was selected to participate to the **DLR International Summer School** *"On Impedance"*, jointly organized by the EU FP7 research projects **STIFF** and **VIACTORS**, in Frauenchiemsee, Bavaria, Germany
2011/2012	He was visitor at **Honda Research Institute Europe (HRI-EU)**, and at **Honda Research Institute Usa (HRI-US)** for short periods, by invitation from *Dr. Michael Gienger* and *Dr. Ambarish Goswami*, respectively
2012	He was visitor at the **Biorobotics Laboratory, École Polytechnique Fédérale de Lausanne (EPFL)** for a short period, by invitation from *Dr. Alexander Spröwitz* and *Prof. Auke J. Ijspeert*

Oct 2012	He was selected to participate to the **3rd PAVIS School** on Computer Vision, Pattern Recognition, and Image Processing *"Component Analysis Methods for Human Sensing"*, in Sestri Levante, Genova, Italy
Oct 2013	He was selected to participate to the **Xperience Summer School**, organized by the EU FP7 research projects **Xperience**, in Cala Millor, Mallorca, Spain

A.3 List of Publications

Book Chapters

2009

[Gini et al, 2009]
G. Gini, M. Folgheraiter, U. Scarfogliero, **F. Moro**
"A Biologically Founded Design and Control of a Humanoid Biped" in Humanoid Robots, Ben Choi Ed., ISBN: 978-953-7619-44-2, InTech Education and Publishing, Vienna, Austria

Journal Papers

2013

[Moro et al, 2013c]
F.L. Moro, N.G. Tsagarakis, D.G. Caldwell
"Walking in the Resonance with the COMAN Robot with Trajectories based on Human Kinematic Motion Primitives (kMPs)"
Autonomous Robots

[Moro et al, 2013b]
F.L. Moro, A. Spröwitz, A. Tuleu, M. Vespignani, N.G. Tsagarakis, D.G. Caldwell
"Horse-Like Walking, Trotting and Galloping derived from Kinematic Motion Primitives (kMPs) and their Application to Walk/Trot Transitions in a Compliant Quadruped Robot"
Biological Cybernetics, 107(3), pp. 309-320
Video: http://www.youtube.com/watch?v=zJF_-2Rbaxo

2012

[Moro et al, 2012b]
F.L. Moro, N.G. Tsagarakis, D.G. Caldwell
"On the kinematic Motion Primitives (kMPs) - theory and application"
Frontiers in Neurorobotics, 6(10), pp. 1-18

Conference Papers

2013

[Moro et al, 2013a]
F.L. Moro, M. Gienger, A. Goswami, N.G. Tsagarakis, D.G. Caldwell
"An Attractor-based Whole-Body Motion Control (WBMC) System for Humanoid Robots"
IEEE-RAS International Conference on Humanoid Robots (Humanoids), Atlanta, Georgia, USA
Video: http://www.youtube.com/watch?v=MxFuXWzi6lg

2012

[Moro et al, 2012c]
F.L. Moro, N.G. Tsagarakis, D.G. Caldwell
"The kinematic Motion Primitives (kMPs) of periodic motions, discrete motions, and motions that are a combination of discrete and periodic movements"
Cognitive Neuroscience Robotics (CNR) Workshop at the IEEE/RSJ International Conference on Intelligent Robots and Systems (IROS), Vilamoura, Algarve, Portugal

[Moro et al, 2012a]
F.L. Moro, N.G. Tsagarakis, D.G. Caldwell
"Efficient Human-Like Walking for the COmpliant huMANoid COMAN based on Kinematic Motion Primitives (kMPs)"
IEEE International Conference on Robotics and Automation (ICRA), Saint Paul, Minnesota, USA

2011

[Moro et al, 2011]
F.L. Moro, N.G. Tsagarakis, D.G. Caldwell
"A Human-like Walking for the Compliant Humanoid COMAN based on CoM Trajectory Reconstruction from Kinematic Motion Primitives"
IEEE-RAS International Conference on Humanoid Robots (Humanoids), Bled, Slovenia
Video: http://www.youtube.com/watch?v=bnlCAZLhHz0

2010

[Moro et al, 2010]
F. Moro, G. Gini, M. Žefran, A. Rodić
"Simulation for the Optimal Design of a Biped Robot: Analysis of Energy Consumption"
International Conference on Simulation, Modeling, and Programming for Autonomous Robots (SIMPAR), Darmstadt, Germany

Other Publications

2010

F.L. Moro
"Design and Intelligent Control of an Energy-Efficient Humanoid Robot"
Master's Thesis, Politecnico di Milano, Italy

F.L. Moro
"A Systematic Analysis of Energy Consumption of Bipedal Walking with the Aim of Designing a Humanoid Robot"
Master's Thesis, University of Illinois at Chicago, USA

2007

F.L. Moro, A. Giovanazzi
"Analisi e Sviluppo di un Modello per la Camminata Dinamica di un Robot Bipede"
(Analysis and Development of a Model for the Dynamic Walking of a Biped Robot)
Bachelor's Thesis, Politecnico di Milano, Italy

A.4 Patents

2013

F.L. Moro, N.G. Tsagarakis, D.G. Caldwell
"An Attractor-based Whole-Body Motion Control (WBMC) System for an Articulated Robot"
Italian Patent Application TO2013A000828

A.5 Additional Information

Guest Editor

2015

Special Issue on *"Whole-body Control for Robots in the Real World"*
International Journal of Humanoid Robotics (IJHR) - June 2015 Issue
Editors: **F.L. Moro**, M. Gienger, A. Goswami, O. Khatib, E. Yoshida

Organizer

2014

Workshop on *"Whole-body Control for Robots in the Real World"*
2014 IEEE/RSJ International Conference on Intelligent Robots and Systems (IROS)
Organizers: **F.L. Moro**, M. Gienger, O. Khatib, E. Yoshida

Invited/Seminar Talks

2013

"Torque Controlled Humanoid Robots" Workshop at the 2013 IEEE-RAS International Conference on Humanoid Robots
"An Attractor-based Whole-Body Motion Control (WBMC) System for Humanoid Robots"

2012

AMARSI meeting
"The Horse kMPs and their Application to Quadrupedal Locomotion"

AMARSI meeting
"On the kinematic Motion Primitives (kMPs) - Theory and Application"

Honda Research Institute USA
"The Kinematic Motion Primitives (kMPs) and their application to the COMAN robot"

IIT-EPFL COMAN meeting
"Kinematic Motion Primitives (kMPs) Based Walking"

Served as reviewer for

IEEE Transactions on Robotics (T-RO)
International Journal of Humanoid Robotics (IJHR)
International Journal of Advanced Robotic Systems (IJARS)
IEEE International Conference on Robotics and Automation (ICRA)
IEEE/RSJ International Conference on Intelligent Robots and Systems (IROS)
IEEE/RAS-EMBS International Conference on Biomedical Robotics and Biomechatronics (BioRob)

Contributed to the following EU projects:

WALK-MAN (Whole-body Adaptive Locomotion and Manipulation)
Role: *Communication and Divulgation Coordinator*
http://www.walk-man.eu/

AMARSI (Adaptive Modular Architectures for Rich Motor Skills)
http://www.amarsi-project.eu/

References

Abe Y, da Silva M, Popović J (2007) Multiobjective control with frictional contacts. In: ACM SIGGRAPH/Eurographics symposium on Computer animation, San Diego, California 11, 85

Atkeson CG, Hollerbach JM (1985) Kinematic features of unrestrained vertical arm movements. The Journal of Neuroscience 5(9):2318–2330 9

Ayers J, Carpenter GA, Currie S, Kinch J (1983) Which behavior does the lamprey central motor program mediate? Science 221(4617):1312–1314 9

Berenson D, Chestnutt J, Srinivasa S, Kuffner J, Kagami S (2009) Pose-Constrained Whole-Body Planning using Task Space Region Chains. In: IEEE-RAS International Conference on Humanoid Robots, Paris, France 11

Berns K, Ilg W, Deck M, Dillmann R (1998) The mammalian-like quadrupedal walking machine BISAM. In: International Workshop on Advanced Motion Control, Coimbra, Portugal 63

Billard A, Ijspeert AJ (2000) Biologically inspired neural controllers for motor control in a quadruped robot. In: International Joint Conference on Neural Networks, Come, Italy 10

Bizzi E, Cheung V, D'Avella A, Saltier P, Tresch M (2008) Combining modules for movement. Brain Research Reviews 57(1):125–133 9

Brooks R, Breazeal C, Marjanovic M, Scassellati B, Williamson M (1998) The Cog Project: Building a Humanoid Robot. In: Nehaniv C (ed) Computation for Metaphors,

Analogy and Agents, Lecture Notes in Artificial Intelligence, vol 1562, Springer-Verlag, pp 52–87 12

Brown T (1911) The Intrinsic Factors in the Act of Progression in the Mammal. Proceedings of the Royal Society of London Series B, Containing Papers of a Biological Character 84(572):308–819 9

Brown T (1912) The Factors in Rhythmic Activity of the Nervous System. Proceedings of the Royal Society of London Series B, Containing Papers of a Biological Character 85(579):278–289 9

Buehler M, Playter R, Raibert M (2005) Robots Step Outside. In: International Symposium on Adaptive Motion of Animals and Machines, Ilmenau, Germany 63

Canderle J, Caldwell DG (2000) A biologically inspired quadruped using pneumatic muscle actuators. In: International Conference on Climbing and Walking Robots, Madrid, Spain 63

Cappelletto J, Estavez P, Modina W, Fermin L, Bogado JM, Grieco JC, Fernando-Lopez G (2006) Gait synthesis and modulation for quadruped robot locomotion using a simple feed-forward network. In: International Conference on Artificial Intelligence and Soft Computing, Zakopane, Poland 10

Cappelletto J, Estevez P, Fernando-Lopez G, Grieco JC (2007) A CPG with force feedback for a statically stable quadruped gait. In: International Conference on Climbing and Walking Robots, Singapore 10

Chae KG, Park JH (2008) Trajectory optimization with GA and control for quadruped robots. Journal of Mechanical Science and Technology 23:114–123 63

Collins JJ, Richmond SA (1994) Hard-wired central pattern generators for quadrupedal locomotion. Biological Cybernetics 71:375–385 10

Collins S, Ruina A, Tedrake R, Wisse M (2005) Efficient Bipedal Robots Based on Passive-Dynamic Walkers. Science 307(5712):1082–1085 53

Corben HC, Stehle P (1960) Classical Mechanics, 2nd edn. Courier Dover Publications 87

Dallali H, Mosadeghzad M, Medrano-Cerda G, Docquier N, Kormushev P, Tsagarakis N, Li Z, Caldwell D (2013) Development of a Dynamic Simulator for a Compliant Humanoid Robot Based on a Symbolic Multibody Approach. In: International Conference on Mechatronics, Vicenza, Italy 96

D'Avella A, Lacquaniti F (2013) Control of reaching movements by muscle synergy combinations. Frontiers in Computational Neuroscience 7(42):1–7 10

D'Avella A, Saltiel P, Bizzi E (2003) Combinations of muscle synergies in the construction of a natural motor behavior. Nature neuroscience 6(3):300–308 9

De Rugy A, Sternad D (2003) Interaction between discrete and rhythmic movements: reaction time and phase of discrete movement initiation during oscillatory movements. Brain Research 994(2):160–174 42

Degallier S, Righetti L, Natale L, Nori F, Metta G, Ijspeert A (2008) A modular bio-inspired architecture for movement generation for the infant-like robot iCub. In: 2nd IEEE RAS & EMBS International Conference on Biomedical Robotics and Biomechatronics, Scottsdale, AZ, USA, pp 795 – 800 10

Dégallier Rochat S, Ijspeert A (2010) Modeling discrete and rhythmic movements through motor primitives: a review. Biological Cybernetics 103(4):319–338 10

Dégallier Rochat S, Righetti L, Gay S, Ijspeert A (2011) Towards simple control for complex, autonomous robotic applications: Combining discrete and rhythmic motor primitives. Autonomous Robots 31(2):155–181 10

Del Prete A (2013) Control of Contact Forces using Whole-Body Force and Tactile Sensors: Theory and Implementation on the iCub Humanoid Robot. PhD thesis, Istituto Italiano di Tecnologia, Italy 11

Delcomyn F (1980) Neural basis of rhythmic behavior in animals. Science 210(4469):492–498 9

Dimitrijevic M, Gerasimenko Y, Pinter M (1998) Evidence for a spinal central pattern generator in humans. Annals of the New York Academy of Sciences 860:360–376 9

Dominici N, Ivanenko YP, Cappellini G, D'Avella A, Mond V, Cicchese M, Fabiano A, Silei T, Di Paolo A, Giannini C, Poppele RE, Lacquaniti F (2011) Locomotor primitives in newborn babies and their development. Science 334(6058):997–999 9

Edsinger-Gonzales A, Weber J (2004) Domo: a Force Sensing humanoid Robot for Manipulation Research. In: IEEE-RAS International Conference on Humanoid Robots, Santa Monica, CA, USA, pp 1–19 12

Fujii A, Saito N, Nakahira K, Ishiguro A, Eggenberger P (2002) Generation of an Adaptive Controller CPG for a Quadruped Robot with Neuromodulation Mechanism. In: IEEE International Workshop on Intelligent Robots and Systems, Lausanne, Switzerland 10

Fujimoto Y (2004) Trajectory Generation of Biped Running Robot with Minimum Energy Consumption. In: IEEE International Conference on Robotics and Automation, Barcelona, Spain, pp 3803–3808 53

Fujita M, Kitano H (1998) Development of an Autonomous Quadruped Robot for Robot Entertainment. Autonomous Robots 5(1):7–18 63

Fukuoka Y, Nakamura H, Kimura H (1999) Biologically-inspired adaptive dynamic walking of the quadruped on irregular terrain. In: International Conference on Control Applications, Kohala Coast, HI, USA 10

Fukuoka Y, Kimura H, Cohen AH (2003) Adaptive Dynamic Walking of a Quadruped Robot on Irregular Terrain Based on Biological Concepts. International Journal of Robotics Research 22(2-3):187–202 10

Gienger M, Janßen H, Goerick C (2005) Task-Oriented Whole Body Motion for Humanoid Robots. In: IEEE-RAS International Conference on Humanoid Robots, Tsukuba, Japan 11

Gienger M, Goerick C, Körner E (2008) Whole body motion planning - elements for intelligent systems design. Zeitschrift Künstliche Intelligenz 4:10–15 11

Gienger M, Toussaint M, Goerick C (2010) Whole-body Motion Planning - Building Blocks for Intelligent Systems. In: Harada K, Yoshida E, Yokoi K (eds) Motion Planning for Humanoid Robots, Springer 11

Gini G, Folgheraiter M, Scarfogliero U, Moro F (2009) A Biologically Founded Design and Control of a Humanoid Biped. In: Choi B (ed) Humanoid Robotics, InTech Education and Publishing 117

Giszter SF, Mussa-Ivaldi FA, Bizzi E (1993) Convergent force fields organized in the frog's spinal cord. The Journal of Neuroscience 13(2):467–491 10, 82, 104

Golubovic D, Hu H (2003a) GA-Based Gait Generation of Sony Quadruped Robots. In: IASTED International Conference on Artificial Intelligence and Applications, Benalmadena, Spain 63

Golubovic D, Hu H (2003b) Parameter Optimisation of an Evolutionary Algorithm for On-line Gait Generation of Quadruped Robots. In: IEEE International Conference on Industrial Technology 63

Goswami A, Kallem V (2004) Rate of change of angular momentum and balance maintenance of biped robots. In: IEEE International Conference on Robotics and Automation, New Orleans, LA, USA 12, 87

Grebenstein et al M (2011) The DLR Hand Arm System. In: IEEE International Conference on Robotics and Automation, Shanghai, China, pp 3175–3182 13

Griffin TM, Kram R, Wickler SJ, Hoyt DF (2004) Biomechanical and energetic determinants of the walk trot transition in horses. The Journal of Experimental Biology 207:4215–4223 64

Grillner S (1985) Neurobiological bases of rhythmic motor acts in vertebrates. Science 228(4696):143–149 9

Grillner S (2006) Biological Pattern Generation: The Cellular and Computational Logic of Networks in Motion. Neuron 52(5):751–766 10

Hebbel M, Nistico W, Fisseler D (2007) Learning in a High Dimensional Space: Fast Omnidirectional Quadrupedal Locomotion. In: Lakemeyer G, Sklar E, Sorrenti D, Takahashi T (eds) RoboCup 2006: Robot Soccer World Cup X, Lecture Notes in Computer Science, vol 4434, Springer Berlin / Heidelberg, pp 314–321 63

Heglund NC, Taylor CR (1988) Speed, stride frequency and energy cost per stride: how do they change with body size and gait? The Journal of Experimental Biology 138:301–318 64, 72, 73

Herzog A, Righetti L, Grimminger F, Pastor P, Schaal S (2013) Experiments with a hierarchical inverse dynamics controller on a torque-controlled humanoid 11, 100

Hirose S, Fukuda Y, Yoneda K, Nagakubo A, Tsukagoshi H, Arikawa K, Endo G, Doi T, Hodoshima R (2009) Quadruped walking robots at Tokio Institute of Technology. IEEE Robotics & Automation Magazine 16(2):104–114 63

Hogan N (1985) Impedance Control: An Approach to Manipulation: Part I - Theory. Journal of Dynamic Systems, Measurement, and Control 107:1–24 96

Hogan N, Sternad D (2007) On rhythmic and discrete movements: reflections, definitions and implications for motor control. Experimental brain research 181(1):13–30 10

Hollands K, Wing A, Daffertshofer A (2007) Principal Component Analysis of Contemporary Dance Kinematics. In: 3rd IEEE EMBSS UK & RI Postgraduate Conference in Biomedical Engineering & Medical Physics, University of Southampton, UK, pp 3989–3994 9

Hollerbach MJ, Flash T (1982) Dynamic interactions between limb segments during planar arm movement. Biological Cybernetics 44(1):67–77 9

Hoyt D, Taylor R (1981) Gait and the energetics of locomotion in horses. Nature 292:239240 64

Hu H, Gu D (2005) Hybrid learning architecture for fuzzy control of quadruped walking robots. International Journal of Intelligent Systems - Soft Computing for Modeling, Simulation, and Control of Nonlinear Dynamical Systems 20(2):131–152 63

Hutter M, Remy C, Hoepflinger M, Siegwart R (2011) ScarlETH: Design and control of a planar running robot. In: IEEE/RSJ International Conference on Intelligent Robots and Systems, San Francisco, CA, USA, pp 562–567 63

Iida F, Gomez GJ, Pfeifer R (2005) Exploiting Body Dynamics for Controlling a Running Quadruped Robot. In: IEEE International Conference on Robotics and Automation, Seattle, USA 63

Ijspeert A (2008) Central pattern generators for locomotion control in animals and robots: a review. Neural Networks 21(4):642–653 10, 82

Ijspeert A, Nakanishi J, Schaal S (2002) Learning Attractor Landscapes for Learning Motor Primitives. In: Advances in Neural Information Processing Systems 15, MIT Press, pp 1547–1554 10

Inagaki K, Kobayashi H (1993) A Gait Transition for Quadruped Walking Machine. In: IEEE/RSJ International Conference on Intelligent Robots and Systems, Yokohama, Japan 64

Ishii T, Masakado S, Ishii K (2004) Locomotion of a quadruped robot using CPG. In: IEEE International Joint Conference on Neural Networks, Budapest, Hungary 10

Ivanenko YP, Poppele RE, Lacquaniti F (2004) Five basic muscle activation patterns account for muscle activity during human locomotion. The Journal of Physiology 556(1):267–282 9, 82, 103

Ivanenko YP, Cappellini G, Dominici N, Poppele RE, Lacquaniti F (2005) Coordination of Locomotion with Voluntary Movements in Humans. The Journal of Neuroscience 25(31):7238–7253 9, 82, 103

Iwata H, Sugano S (2009) Design of Human Symbiotic Robot TWENDY-ONE. In: IEEE International Conference on Robotics and Automation, Kobe, Japan, pp 580–586 13

Jafari A, Tsagarakis N, Caldwell D (2011) Exploiting Natural Dynamic for Energy Minimization Using an Actuator with Adjustable Stiffness (AwAS). In: IEEE International Conference on Robotics and Automation, Shanghai, China, pp 4632–4637 13, 53, 54

Jarquín G, Escande A, Arechavaleta G, Moulard T, Yoshida E, Parra-Vega V (2013) Real-Time Smooth Task Transitions for Hierarchical Inverse Kinematics. In: IEEE-RAS International Conference on Humanoid Robots, Atlanta, Georgia, USA 106

Kagami S, Kitagawa T, Nishiwaki K, Sugihara T, Inaba M, Inoue H (2002) A fast dynamically equilibrated walking trajectory generation method of humanoid robot. Autonomous Robots 12(1):71–82 12

Kajita S, Kanehiro F, Kaneko K, Fujiwara K, Harada K, Yokoi K, Hirukawa H (2003a) Biped walking pattern generation by using preview control of zero-moment point. In: IEEE International Conference on Robotics and Automation, Taipei, Taiwan, pp 1620–1626 12

Kajita S, Kanehiro F, Kaneko K, Fujiwara K, Harada K, Yokoi K, Hirukawa H (2003b) Resolved momentum control: humanoid motion planning based on the linear and angular momentum. In: IEEE/RSJ International Conference on Intelligent Robots and Systems, Las Vegas, NV, USA 11, 12, 93

Kajita S, Morisawa M, Harada K, Kaneko K, Kanehiro F, Fujiwara K, Hirukawa H (2006) Biped Walking Pattern Generator allowing Auxiliary ZMP Control. In: IEEE/RSJ International Conference on Intelligent Robots and Systems, Beijing, China 12

Kaynov D, Soueres P, Pierro P, Balaguer C (2009) A practical decoupled stabilizer for joint-position controlled humanoid robots. In: IEEE/RSJ International Conference on Intelligent Robots and Systems, St. Louis, MO, USA, pp 3392–3397 12

Khatib O (1987) A Unified Approach for Motion and Force Control of Robot Manipulators: The Operational Space Formulation. IEEE Journal of Robotics and Automation 3(1):43–53 11, 96, 109

Kiehn O, Butt S (2003) Physiological, Anatomical and Genetic identification of CPG Neurons in the Developing Mammalian Spinal Cord. Progress in neurobiology 70(4):347–361 9

Kim HK, Ohung W, Won D, Park S, Kim TJ, Kim SS (2008) Foot Trajectory Generation of Hydraulic Quadruped Robots on Uneven Terrain. In: IFAC World Congress, Seoul, Republic of Korea 63

Kim KY, OKwon, Yeon JS, Park JH (2006) Elliptic Trajectory Generation for Galloping Quadruped Robots. In: IEEE International Conference on Robotics and Biomimetics, Kunming, China 63

Kimura H, Shimoyama I, Miura H (1989) Dynamics in the dynamic walk of a quadruped robot. Advanced Robotics 4(3):283–301 63

Kimura H, Fukuoka Y, Cohen AH (2007) Adaptive dynamic walking of a quadruped robot on natural ground based on biological concepts. International Journal of Robotics Research 26(5):475–490 63

Kormushev P, Ugurlu B, Calinon S, Tsagarakis N, Caldwell D (2011) Bipedal walking energy minimization by reinforcement learning with evolving policy parameterization. In: IEEE/RSJ International Conference on Intelligent Robots and Systems, San Francisco, CA, USA, pp 318–324 53

Kramy DP, Orin DE (2003) Achieving Periodic Leg Trajectories to Evolve a Quadruped Gallop. In: IEEE International Conference on Robotics and Automation, Tapei, Taiwan 63

Kulic D, Ott C, Lee D, Ishikawa J, Nakamura Y (2012) Incremental Learning of Full Body Motion Primitives and their Sequencing through Human Motion Observation. The International Journal of Robotics Research 31(3):330–345 10

Kuo A (2002) Energetics of actively powered locomotion using the simplest walking model. Journal of Biomechanical Engineering 124:113–120 53

Kurazame R, Tanaka S, Yamashita M, Hasegawa T, Yoneda K (2005) Straight Legged Walking of a Biped Robot. In: IEEE/RSJ International Conference on Intelligent Robots and Systems, Edmonton, Canada, pp 337–343 53

Lacquaniti F, Ivanenko YP, Zago M (2012) Patterned control of human locomotion. The Journal of Physiology 590:2189–2199 9

Lee SH, Goswami A (2012) A Momentum-based Balance Controller for Humanoid Robots on Non-lever and Non-stationary Ground. Atonomous Robots 33(4):399–414 12, 93

Lengagne S, Vaillant J, Yoshida E, Kheddar A (2013) Generation of Whole-body Optimal Dynamic Multi-contact Motions. The International Journal of Robotics Research 32(9-10):1104–1119 11

Lin JN, Song SM (2002) Modeling Gait Transitions of Quadrupeds and Their Generalization With CMAC Neural Networks. In: IEEE International Conference on Systems, Man and Cybernetics, Yasmine Hammamet, Tunisia 64

Liu C, Chen Y, Zhang J, Chen Q (2009) CPG driven locomotion control of quadruped robot. In: IEEE International Conference on Systems, Man and Cybernetics, San Antonio, Texas, USA 10

Marder E, Bucher D (2001) Central pattern generators and the control of rhythmic movements. Current Biology 11(23):R986R996 9

Michaels C, Bongers R (1994) The dependence of discrete movements on rhythmic movements: simple RT during oscillatory tracking. Human Movement Science 13:473–493 42

Mistry M, Righetti L (2011) Operational space control of constrained and underactuated systems. In: Robotics: Science and Systems Conference, Los Angeles, CA, USA 11

Mistry M, Buchli J, Schaal S (2010) Inverse Dynamics Control of Floating Base Systems Using Orthogonal Decomposition. In: IEEE International Conference on Robotics and Automation, Anchorage, AK, USA 84, 85, 111

Mitobe K, Capi G, Nasu Y (2000) Control of walking robots based on manipulation of the zero moment point. Robotica 18(06):651–657 12

Morisawa M, Harada K, Kajita S, Nakaoka S, Fujiwara K, Kanehiro F, Kaneko K, Hirukawa H (2007) Experimentation of Humanoid Walking Allowing Immediate Modification of Foot Place Based on Analytical Solution. In: IEEE International Conference on Robotics and Automation, Rome, Italy, pp 3989–3994 12

Moro F, Gini G, Zefran M, Rodic A (2010) Simulation for the Optimal Design of a Biped Robot: Analysis of Energy Consumption. In: International Conference on Simulation,

Modeling, and Programming for Autonomous Robots, Darmstadt, Germany, pp 449–460 119

Moro FL, Tsagarakis NG, Caldwell DG (2011) A Human-like Walking for the COmpliant huMANoid COMAN based on CoM Trajectory Reconstruction from Kinematic Motion Primitives. In: IEEE-RAS International Conference on Humanoid Robots, Bled, Slovenia, pp 364–370 6, 11, 96, 100, 119

Moro FL, Tsagarakis NG, Caldwell DG (2012a) Efficient Human-like Walking for the COmpliant huMANoid COMAN based on Kinematic Motion Primitives (kMPs). In: IEEE International Conference on Robotics and Automation, Saint Paul, MN, USA, pp 2007 – 2014 6, 119

Moro FL, Tsagarakis NG, Caldwell DG (2012b) On the Kinematic Motion Primitives (kMPs): Theory and Application. Frontiers in Neurorobotics 6(10):1–18 5, 53, 118

Moro FL, Tsagarakis NG, Caldwell DG (2012c) The kinematic Motion Primitives (kMPs) of periodic motions, discrete motions, and motions that are a combination of discrete and periodic movements. In: Cognitive Neuroscience Robotics (CNR) Workshop at the IEEE/RSJ International Conference on Intelligent Robots and Systems, Vilamoura, Portugal 6, 118

Moro FL, Gienger M, Goswami A, Tsagarakis NG, Caldwell DG (2013a) An Attractor-based Whole-Body Motion Control (WBMC) System for Humanoid Robots. In: IEEE-RAS International Conference on Humanoid Robots, Atlanta, Georgia, USA, pp 42–49 5, 118

Moro FL, Spröwitz A, Tuleu A, Vespignani M, Tsagarakis NG, Ijspeert AJ, Caldwell DG (2013b) Horse-Like Walking, Trotting and Galloping derived from Kinematic Motion Primitives (kMPs) and their Application to Walk/Trot Transitions in a Compliant Quadruped Robot. Biological Cybernetics 107(3):309–320 5, 118

Moro FL, Tsagarakis NG, Caldwell DG (2013c) Walking in the Resonance with the COMAN Robot with Trajectories based on Human Kinematic Motion Primitives (kMPs). Autonomous Robots 4, 117

Mussa-Ivaldi F, Bizzi E (2000) Motor learning through the combination of primitives. Philosophical transactions of the Royal Society of London Series B, Biological sciences 335(1404):1755–1769 9

Nagasaka K, Kuroki Y, Suzuki S, Itoh Y, Yamaguchi J (2004) Integrated motion control for walking, jumping and running on a small bipedal entertainment robot. In: IEEE International Conference on Robotics and Automation, Barcelona, Spain, pp 3189–3194 12

Nakamura Y (1991) Advanced Robotics: Redundancy and Optimization. Addison-Wesley Publishing Company 11

Nichol JG, Singh SPN, Waldron KJ, Palmer III LR, Orin DE (2004) System Design of a Quadrupedal Galloping Machine. International Journal of Robotics Research 23(10-11):1013–1027 63

Orin DE, Goswami A (2008) Centroidal Momentum Matrix of a humanoid robot: Structure and properties. In: IEEE/RSJ International Conference onIntelligent Robots and Systems, Nice, France 93

Orin DE, Goswami A, Lee SH (2013) Centroidal Dynamics of a Humanoid Robot. Autonomous Robots 35(2-3):161–176 12, 92, 93, 111

Ott C, Eiberger O, Englsberger J, Roa MA, Albu-Schäffer A (2012) Hardware and Control Concept for an Experimental Bipedal Robot with Joint Torque Sensors. Journal of the Robotics Society of Japan 30(4):378–382 11, 100

Pearson K (1901) On lines and planes of closest fit to systems of points in space. Philosophical Magazine Series 6 2(11):559–572 28

Peters J, Mistry M, Udwadia F, Nakanishi J, Schaal S (2008) A unifying framework for robot control with redundant DOFs. Autonomous Robots 24(1):1–12 11

Poggio T, Bizzi E (2004) Generalization in vision and motor control. Nature 431(7010):768–774 9

Pongas D, Mistry M, Schaal S (2007) A Robust Quadruped Walking Gait for Traversing Rough Terrain. In: IEEE International Conference on Robotics and Automation, Roma, Italy 63

Popovic MB, Goswami A, Herr H (2005) Ground Reference Points in Legged Locomotion: Definitions, Biological Trajectories and Control Implications. The International Journal of Robotics Research 24(12):1013–1032 12, 87

Poulakakis I, Smith JA, Buehler M (2005) Modeling and experiments of untethered quadrupedal running with a bounding gait: the Scout II robot. International Journal of Robotics Research 24(4):239256 63

Pratt J, Chew CM, Torres A, Dilworth P, Pratt G (2001) Virtual Model Control: An Intuitive Approach for Bipedal Locomotion. The International Journal of Robotics Research 20(2):129–143 96

Raibert M (1986) Legged robots that balance. MIT Press 63

Raibert M, Blankespoor K, Nelson G, Playter R, and the BigDog Team (2008) BigDog, the roughterrain quadruped robot. In: IFAC World Congress, Seoul, Republic of Korea 63

Raibert MH (1990) Trotting, pacing and bounding by a quadruped robot. Journal of Biomechanics 23(1):8398 63

Rebula JR, Neuhaus PD, Bonnlander BV, Johnson MJ, Pratt JE (2007) A Controller for the LittleDog Quadruped Walking on Rough Terrain. In: IEEE International Conference on Robotics and Automation, Roma, Italy 63

Righetti L, Ijspeert AJ (2008) Pattern generators with sensory feedback for the control of quadruped locomotion. In: IEEE International Conference on Robotics and Automation, Pasadena, CA, USA 10

Righetti L, Buchli J, Mistry M, Schaal S (2011) Inverse dynamics control of floating-base robots with external constraints: A unified view. In: IEEE International Conference on Robotics and Automation, Shanghai, China 11, 84, 85, 111

Ronsse R, Sternad D, Lefèvre P (2009) A computational model for rhythmic and discrete movements in uni- and bimanual coordination. Neural Computation 21(5):1335–1370 10

Rutishauser S, Sproewitz A, Righetti L, Ijspeert AJ (2008) Passive compliant quadruped robot using central pattern generators for locomotion control. In: IEEE International Conference on Biomedical Robotics and Biomechatronics, Scottsdale, AZ, USA 10

Saab L, Ramos OE, Keith F, Mansard N, Soueres P, Fourquet JY (2013) Dynamic Whole-Body Motion Generation Under Rigid Contacts and Other Unilateral Constraints. IEEE Transactions on Robotics 29(2):346–362 11

Sakakibara Y, Kan K, Hosoda Y, Hattori M, Fujie M (1990) Foot trajectory for a quadruped walking machine. In: IEEE International Workshop on Intelligent Robots and Systems, Ibaraki, Japan 63

Santello M, Flanders M, Soechting J (1998) Postural Hand Synergies for Tool Use. The Journal of Neuroscience 18(23):10,105–10,115 9

Schaal S (2007) The New Robotics-towards human-centered machines. Human Frontier Science Program 1(2):115–126 10

Schaal S, Sternad D, Osu R, Kawato M (2004) Rhythmic arm movement is not discrete. Nature Neuroscience 7(10):1136–1143 10

Semini C, Tsagarakis NG, Guglielmino E, Focchi M, Cannella F, Caldwell DG (2011) Design of HyQ a hydraulically and electrically actuated quadruped robot. Proceedings of the Institution of Mechanical Engineers, Part I: Journal of Systems and Control Engineering 225(1):831–849 63

Sentis L (2007) Synthesis and Control of Whole-Body Behavior in Humanoid Systems. PhD thesis, Stanford University, CA, USA 11, 96, 109

Sentis L (2010) Compliant Control of Whole-Body Multi-Contact Behaviors in Humanoid Robots. In: Harada K, Yoshida E, Yokoi K (eds) Motion Planning for Humanoid Robots, Springer 11, 96, 105, 109

Sentis L, Khatib H (2005) Synthesis of Whole-Body Behaviors through Hierarchical Control of Behavioral Primitives. International Journal of Humanoid Robotics 2(4):505–518 11

Sentis L, Khatib H (2006) A Whole-Body Control Framework for Humanoids Operating in Human Environments. In: IEEE International Conference on Robotics and Automation, Orlando, FL , USA 11

Sentis L, Khatib H (2010) Compliant Control of Multicontact and Center-of-Mass Behaviors in Humanoid Robots. IEEE Transactions on Robotics 26(3):483–501 11

Sheridan T (1966) Three Models of Preview Control. IEEE Transactions on Human Factors in Electronics (2):91–102 12

Silva FM, Machado JAT (1999) Energy Analysis During Biped Walking. In: IEEE International Conference on Robotics and Automation, Detroit, MI, USA, pp 59–64 53

Soechting J, Lacquaniti F (1981) Invariant characteristics of a pointing movement in man. The Journal of Neuroscience 1(7):710–720 9

Son Y, Kamano T, Yasuno T, Suzuki T, Harada H (2006) Generation of adaptive gait patterns for quadruped robot with CPG network including motor dynamic model. Electrical Engineering in Japan 155(1):35–43 10

Spröwitz A, Tuleu A, Vespignani M, Ajallooeian M, Badri E, Ijspeert AJ (2013) Towards Dynamic Trot Gait Locomotion—Design, Control, and Experiments with Cheetah-cub, a Compliant Quadruped Robot. The International Journal of Robotics Research 32(8):932–950 63, 64, 67

Stephens BJ, Atkeson CG (2010) Dynamic Balance Force Control for Compliant Humanoid Robots. In: IEEE/RSJ International Conference on Intelligent Robots and Systems, Taipei, Taiwan 11, 100

Sternad D (2008) Towards a unified theory of rhythmic and discrete movements - behavoral, modeling and imaging results. In: Fuchs A, Jirsa V (eds) Coordination: Neural, Behavioral and Social Dynamics, Understanding Complex Systems, vol 17, Springer Berlin / Heidelberg, pp 105–133 10

Sternad D, Dean W, Schaal S (2000) Interaction of rhythmic and discrete pattern generators in single joint movements. Human Movement Science 19:627–665 42

Sugihara T (2009) Standing stabilizability and stepping maneuver in planar bipedalism based on the best COM-ZMP regulator. In: IEEE International Conference on Robotics and Automation, Kobe, Japan, pp 1966–1971 12

Sugimoto N, Morimoto J, Hyon S, Kawato M (2012) The eMOSAIC model for humanoid robot control. Human Frontier Science Program 29-30:8–19 10

Torres-Jara E (2005) Obrero: a Platform for Sensitive Manipulation. In: IEEE-RAS International Conference on Humanoid Robots, Tsukuba, Japan, pp 327–332 13

Toussaint M, Gienger M, Goerick C (2007) Optimization of sequential attractor-based movement for compact behaviour generation. In: IEEE-RAS International Conference on Humanoid Robots, Pittsburgh, PA, USA 11

Tresch M, Saltiel P, Bizzi E (1999) The construction of movement by the spinal cord. Nature Neuroscience 2(2):162–167 9

Tsagarakis N, Becchi F, Singlair M, Metta G, Caldwell D, Sandini G (2007a) Lower Body Realization of the Baby Humanoid 'iCub'. In: IEEE/RSJ International Conference on Intelligent Robots and Systems, San Diego, CA, USA, pp 3616–3622 13

Tsagarakis N, Metta G, Sandini G, Vernon D, Beira R, Becchi F, Righetti L, Victor J, Ijspeert A, Carrozza M, Caldwell D (2007b) iCub: the Design and Realization of an Open Humanoid Platform for Cognitive and Neuroscience Research. Advanced Robotics 21(10):1151–1175 13

Tsagarakis N, Laffranchi M, Vanderborght B, Caldwell D (2009) A Compact Soft Actuator Unit for Small Scale Human Friendly Robots. In: IEEE International Conference on Robotics and Automation, Kobe, Japan, pp 4356–4362 14, 16, 23

Tsagarakis N, Li Z, Saglia J, Caldwell D (2011) The Design of the Lower Body of the Compliant Humanoid Robot cCub. In: IEEE International Conference on Robotics and Automation, Shanghai, China, pp 2035–2040 13

Tsagarakis NG, Morfey S, Medrano Cerda G, Li Z, Caldwell DG (2013) Compliant humanoid COMAN: Optimal joint stiffness tuning for modal frequency. In: IEEE International Conference on Robotics and Automation, Karlsruhe, Germany 13, 96, 100

Tsujita K, Toui H, Tsuchiya K (2005) Dynamic turning control of a quadruped locomotion robot using oscillators. Advanced Robotics 19(10):1115–1133 63

Ugurlu B, Kawamura A (2010) Eulerian ZMP resolution based bipedal walking: Discussions on the intrinsic angular momentum rate change about center of mass. In: IEEE International Conference on Robotics and Automation, Anchorage, AK, USA 12, 93

Ugurlu B, Saglia J, Tsagarakis N, Caldwell DG (2012) Hopping at the Resonance Frequency: A Trajectory Generation Technique for Bipedal Robots with Elastic Joints. In: IEEE International Conference on Robotics and Automation, Saint Paul, MN, USA 13

Van Mourik A, Beek P (2004) Discrete and cyclical movements: unified dynamics or separate control. Acta Psychologica 117(2):121–138 10

Vanderborght B, Verrelst B, Van Ham R, Van Damme M, Lefeber D, Duran B, Beyl P (2006) Exploiting Natural Dynamics to Reduce Energy Consumption by Controlling the Compliance of Soft Actuators. International Journal of Robotics Research 25(4):343–358 13, 53, 54

Vilensky JA, Libii JN, Moore AM (1991) Trot-gallop gait transitions in quadrupeds. Physiology & Behavior 50(4):835–842 64

Vukobratovic M, Borovac B (2004) Zero-Moment Point - Thirty five years of its life. International Journal of Humanoid Robotics 1(1):153–173 12, 87

Wensing PM, Orin DE (2013) Generation of Dynamic Humanoid Behaviors Through Task-Space Control with Conic Optimization. In: IEEE International Conference on Robotics and Automation, Karlsruhe, Germany 11, 85

Wensing PM, Hammam GB, Dariush B, Orin DE (2013) Optimizing Foot Centers of Pressure through Force Distribution in a Humanoid Robot. International Journal of Humanoid Robotics 10(3):1–21 12, 93

Wilson DM (1961) The central nervous control of flight in a locust. The Journal of Experimental Biology 38(47):471–490 9

Witte H, Hackert R, Ilg W, Biltzinger J, Schillinger N, Biedermann F, Jergas M, Preuschoft H, Fischer MS (2003) Quadrupedal Mammals as Paragons for Walking Machines. In: Proc AMAM - Adaptive Motion in Animals and Machines 10

Yamasaki F, Hosoda K, Asada M (2002) An Energy Consumption Based Control for Humanoid Walking. In: IEEE/RSJ International Conference on Intelligent Robots and Systems, Lausanne, Switzerland, pp 2473–2477 53

Zhang X, Zheng H, Guan X, Chifeng Z, Zhao L (2005) A biological inspired quadruped robot: structure and control. In: IEEE International Conference on Robotics and Biomimetics, Hong Kong, China 63